The Structure and Spectra of Molecular Ions

A thesis submitted in partial fulfilment of the requirements for the degree of Doctor of Philosophy

by

Alan Nigel Hughes

School of Electrical and Electronic Engineering

Newcastle University

July 2013

Abstract

I give a review of the theory of the hydrogen molecular ion H_2^+ and its isotopomers D_2^+ and HD^+ including the direct analytical solution and the standard adiabatic approximation. I discuss dissociation limits for homonuclear and heteronuclear species; the effect of an external electric field; non adiabatic calculations, relativistic and radiative effects; and spectroscopic measurements of H_2^+ and D_2^+ with a comparison of theoretical to experimental values. I give a detailed description of the fast ion-beam spectrometer as used for both laser-beam and microwave spectroscopy and describe the challenges involved in making high resolution spectroscopic measurements.

An account is given of theory, experimental details and measurements of transition frequencies and intensities of the forbidden rotational transition (v = 19, N = 1) - (v = 19, N = 0) in the ground electronic state ($X^2\sum_g^+$, also represented as $1s\sigma_g$) of H_2^+. Theory has predicted that the transition has measurable intensity due to the Fermi contact hyperfine interaction causing a breaking of electronic g/u symmetry resulting in the mixing of ***ortho-para*** states. The measurements were made in both single and double resonance using a fast ion beam/microwave spectrometer at a transition frequency of 14961.7 ± 1.1 MHz, in agreement with the theoretical prediction of 14960 ± 3 MHz. An account is also given of a further search that was conducted for a second forbidden rotational transition (v = 0, N = 1) - (v = 0, N = 0) in the first excited electronic state ($2p\sigma_u$) of H_2^+. A discussion is given on the possibility of making further observations of forbidden rotational transitions and the experimental difficulties involved; and of adapting the experimental techniques used in order to observe the recently discovered (v = 1, N = 0) in the first excited electronic state ($2p\sigma_u$) of H_2^+.

To Carrie, with love.

Acknowledgements

My deepest thanks go to my supervisor Dr Iain R. McNab for his unending patience, help and continued support over many years; for his skill as an educator, mentor and scientist; and for his enthusiasm and understanding which has always been an inspiration to me. Thank you also to Dr Patrick Briddon for his continued help and support throughout my studies.

I wish to thank all the past members of the McNab group who have helped and supported me, in particular Andrew Critchley, Faye Slade (née Kemp), Simon Cox and Peter Kreynin.

I am grateful also to the past members of staff of the Physics Department at Newcastle University including the highly skilled engineering and electronics technicians

I extend my gratitude also to The British Mass Spectrometry Society for funding my research with a John Beynon scholarship; to Seneca College of Applied Arts and Technology, Toronto, Canada for their assistance during the latter stages of my study.

Finally I must thank my wife Carrie, for her unswerving love, patience and continued support, without which I could not have completed my studies.

Table of Contents

List of Figures

List of Tables

Introduction

The first chapter contains a review of the theory and experiment of H_2^+ and its isotopomers D_2^+ and HD^+ including the direct analytical solution and the standard adiabatic approximation. I discuss dissociation limits for homonuclear and heteronuclear species; adiabatic and non-adiabatic calculations, variational and non-variational calculations and include relativistic and radiative effects. I describe the effect of an external electric field from a theoretical consideration but this is also described in chapter 4 with particular relevance to the use of an electric field dissociation lens for dissociating selected levels as a means of monitoring transitions. In chapter 1 I also describe spectroscopic measurements of H_2^+ and D_2^+ and give a comparison of theoretical versus experimental values.

In chapter 2 I describe in great detail the fast ion-beam spectrometer used during this research for both laser beam spectroscopy and microwave spectroscopy. I also describe the infrared laser and optics set-up; how the instrument is controlled and data is collected; how mass spectrometry, kinetic energy spectroscopy and frequency spectroscopy are performed and how calibration of various parameters is achieved along with a discussion of stability, sensitivity and dynamic range. In the final section of chapter 2 I describe how the instrument was modified for microwave spectroscopy and electric field dissociation; this is also described in chapter 4 with a particular emphasis on how these techniques were used to observe a pure rotation transition in H_2^+. For this reason some information in chapter 2 is duplicated in chapter 4 but this is required in both chapters for the benefit of the reader. Some of the detail in chapter 2 was published as an instrumental review (R. Abusen, S. G. Cox, A. D. J. Critchley, A. N. Hughes, F. Kemp, I. R. McNab*,* et al*.*, "Coaxial ion beam/infrared laser beam spectrometer for investigating infrared spectra of doubly positively charged molecules (molecular dications)," *Review of Scientific Instruments,* vol. 73, p. 241, 2002) and a spectroscopy review (A. N. Hughes, F. Kemp, P. S. Kreynin, I. R. McNab, and S. Spoor, "Recent research developments in Ion Beam Spectroscopy," Solicited review for "Recent Research Developments in Chemical Physics, Vol-4", vol. 4, pp. 359-377, 2003).

Chapter 3 describes in detail the theory of g/u symmetry-breaking and the history and application to H_2^+. Parts of this chapter were published as "Energy shifts and forbidden transitions in H_2^+ due to electronic g/u symmetry breaking," A. D. J. Critchley, A. N. Hughes, I. R. McNab, and R. E. Moss, Molecular Physics, vol. 101, pp. 651-661, 2003.

Chapter 4 is an account of the experimental methods used to measure the “forbidden” (19,1)-(19,0) pure rotation transition in the ground electronic state ($1s\sigma_g$) of H_2^+ using both single- and double-resonance microwave spectroscopy techniques; and electric field dissociation. The electric field dissociation lens and its operation are described in some depth as are the experimental methods employed for microwave spectroscopy. Microwave propagation is discussed along with an analysis of the $TE_{m,n}$ mode structure which could be propagated under certain circumstances. A full account is given of the search for a second “forbidden” pure rotation transition between the $v = 0$, $N = 1$ and $v = 0$, $N = 0$ levels in the $2p\sigma_u$ electronic state of H_2^+. Parts of this chapter were published as "Energy shifts and forbidden transitions in H_2^+ due to electronic g/u symmetry breaking," A. D. J. Critchley, A. N. Hughes, I. R. McNab, and R. E. Moss, Molecular Physics, vol. 101, pp. 651-661, 2003.

Chapter 5 is a discussion of the potential future developments in the spectroscopy of electronic g/u symmetry breaking transitions. I describe methods which could be employed to detect the recently discovered $v = 1$, $N = 0$ level in the $2p\sigma_u$ electronic state of H_2^+ with a consideration of the experimental challenges this would pose and how they might be overcome. I also discuss the possibility of observing electronic g/u symmetry breaking transitions in the microwave region for other ions including $^3He_2^+$; and propose further experiments involving H_2^+ and D_2^+.

Chapter 1: Introduction to the Theory of H_2^+

1.1 H_2^+

‘The two most common things in the Universe are Hydrogen and Stupidity’

- Harlan Ellison (1934)

Molecular hydrogen is the simplest and most abundant molecule in the universe. Atomic hydrogen is the only atom for which exact quantum mechanical solutions can be found for its energy levels and wavefunctions and has therefore played a central role in the development of theories of atomic structure. H_2^+ plays a similar central role in theories of molecular structure, as it is (within the Born-Oppenheimer approximation) a system with exact quantum mechanical solutions

1.1.1 *The Simplest Molecule*

In what follows I give a brief introduction to the theory of the hydrogen molecular ion, together with a review of the literature pertaining to spectroscopic measurements and highly accurate ab-initio calculations that have been, in part, developed as a response to the measurements. For details of earlier work, including details of accurate theoretical approaches, we direct the reader to the following reviews:

(1) Edward Teller and H.L. Sahlin gave a detailed review of the Born-Oppenheimer solution for H_2^+ in “Chapter 2: The hydrogen molecular ion and the general theory of electron structure”, in Physical Chemistry: An Advanced Treatise (H Eyring Ed.) Volume 5, **1970** (New York, Academic) pp35-124. [1]

(2) Alan Carrington and Richard A. Kennedy reviewed theory and experiment in Gas Phase Ion Chemistry, vol 3 Ions and Light Ed M.T. Bowers (London: Academic) pp 393-442 **1983**. [2]

(3) Alan Carrington, Iain .R. McNab and Christine A. Montgomerie reviewed theory and experiment up to 1989 in "*Spectroscopy of the hydrogen molecular ion*", J. Phys. B: A.t Mol. Opt. Phys. 22 (**1989**) 3351-3586. [3]

(4) Christine A. Leach (nee Montgomerie) and Richard E. Moss reviewed theory and experiment up to 1995 in "Spectroscopy and quantum mechanics of the hydrogen molecular cation: a test of molecular quantum mechanics", Annu. Rev. Phys. Chem., 1995, 46, 55-82.[4]

(5) The most recent (slightly specialised) review article is by Hilico *et al.* [5]

The hydrogen molecular ion is the simplest of all ionic systems and along with its isotopic relations HD^+ and D_2^+ played a major part in the development of molecular quantum mechanics. It can be regarded as an ideal model for the formulation of many different methods and approximations since the absence of inter-electron interactions allows other aspects of molecular structure theory to be studied in detail. As was pointed out by Wing [6], if theory can be sufficiently improved, accurate measurements of the spectrum of HD^+ should allow the proton/deuteron mass ratios to be determined to a higher accuracy than they are presently known. This aim has been part of the recent renaissance in both experimental [7-14]; and theoretical determinations of the HD^+ spectrum [15-24], but has not yet been realised. Similarly, accurate measurements and calculations for H_2^+ should enable the proton/electron mass ratio to be measured with great accuracy [Korobov et al., [13] and references therein].

The structure and dynamics of H_2^+ has been studied for many years and is now well understood – probably more so than any other molecule. However despite many theoretical studies, and its physical properties being well understood, it is a more difficult candidate to study experimentally than theoretically because

although it has a large binding energy and is therefore thermodynamically stable, it is very reactive, particularly towards molecular hydrogen. Thus any experimental approach which relies on direct ionisation of H_2 requires that the H_2^+ ions are rapidly separated from the neutral parent.

However, there are other difficulties which must be overcome for the experimental studies of such species. One such difficulty is that since H_2^+ and D_2^+ are homonuclear they do not possess electric dipole moments and so they do not exhibit fully allowed electric-dipole vibrational or rotational spectra. For this reason, the mixed isotope species HD^+ has been studied far more extensively than its homonuclear relatives. However, HD^+ is only of tangential relevance to the work described in this thesis, and so its interesting properties are only briefly touched upon. Studies of electronic spectra of H_2^+ would be possible if suitable excited electronic states existed but its lowest excited electronic state is repulsive and the higher excited states lie more than 88×10^3 cm^{-1} (i.e. about 11 eV) above the ground state – i.e. in the far-vacuum ultra-violet. Moreover, because the potential minimum of the ground state occurs at a very small internuclear distance compared with those calculated for the higher excited states there is only a small degree of overlap of wavefunctions thus the Franck-Condon factors for transitions between these states are poor resulting in very low transition intensities.

The hydrogen molecular ion, H_2^+, (also called the hydrogen molecule ion or, more precisely, the hydrogen molecular cation) is the simplest molecule, consisting of two protons bound together by a single electron. The hydrogen molecular ion is one example of the three-body problem in quantum mechanics (others are the He atom and the negative ion of hydrogen, H^-, but these are cases where electron correlation dominates the difficulty of solution). The solutions of the quantum mechanical problem for H_2^+ are sometimes known as the “one electron two-centre problem”, and this problem is exactly soluble for the special case where the nuclei are fixed in space - this is an example of the Born-Oppenheimer approximation – separation of electronic and nuclear motion. To put the theoretical framework in place and develop notation used

later we now develop the Born-Oppenheimer and standard Adiabatic approximations, closely following reference [3].

1.1.2 *Direct Analytical Solution*

For a system of point charges the complete non-relativistic Hamiltonian in the laboratory frame may be written as:

$$\mathcal{H} = \sum_i \frac{-\hbar^2 \nabla_i^2}{2m_i} - \sum_i \sum_{j>i} \frac{z_i z_j e^2}{4\pi\varepsilon_0 r_{ij}} \tag{1}$$

Where $\hbar = h/2\pi$ and h is Planck's constant, $\nabla_i^2 = \left(\frac{\partial^2}{\partial x^2} + \frac{\partial^2}{\partial y^2} + \frac{\partial^2}{\partial z^2}\right)$, m_i is the mass of the i^{th} particle, $z_i e$ is its charge, r_{ij} is the separation between particles i and j, e is the charge on the electron and ε_0 is the permeability of free space.

The usual first step in solution is to separate out the translational motion – this may be achieved by any transformation of variables that places the new origin within the moving framework, and different authors have chosen different molecule-based origins, according to the nature of the problem they were interested in [see for example [25] and below]; the different choices partition the Hamiltonian in different ways, some of which are more appropriate for considering particular aspects of the structure. Interestingly, Moss and Valenzano [26] state "There does not seem to be a way to write down a fully relativistic equation for a molecule, even as small as H_2^+…. Even separating off overall translational motion seems impossible relativistically."

We follow Carrington et al. [3] in transforming to the geometric centre of the nuclei from the laboratory frame (illustrated in figure 1.1). Other common choices of origin are (1) at the centre of mass of the molecule, (2) at the centre of mass of the nuclei, and (3) at one nuclei or the other; no matter which choice is followed the centre of mass motion of the molecule can be factored out of the Hamiltonian that results.

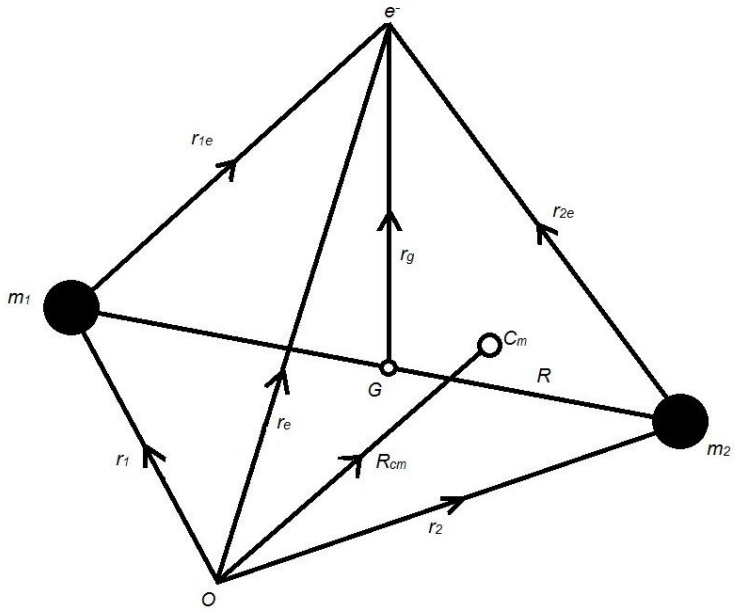

Figure 1.1

Electron and nuclear coordinates used in the transformation of the origin from the laboratory frame to the geometric centre of the nuclei. The basis vectors in the geometric centre of the nuclei are the internuclear vector ***R,*** the position of the centre of mass relative to the space-fixed origin $\boldsymbol{R_{cm}}$ and the position of the electron relative to the geometric centre of the nuclei $\boldsymbol{r_g}$.

The transformation is written in matrix form as:

$$\begin{bmatrix} \boldsymbol{r_g} \\ \boldsymbol{R} \\ \boldsymbol{R_{cm}} \end{bmatrix} = \begin{bmatrix} -1/2 & -1/2 & 1 \\ -1 & 1 & 0 \\ m_1/M & m_2/M & m_e/M \end{bmatrix} \begin{bmatrix} \boldsymbol{r_1} \\ \boldsymbol{r_2} \\ \boldsymbol{r_e} \end{bmatrix} \tag{2}$$

With inverse transform:

$$\begin{bmatrix} \boldsymbol{r_1} \\ \boldsymbol{r_2} \\ \boldsymbol{r_e} \end{bmatrix} = \begin{bmatrix} -m_e/M & -\left(m_2 + \frac{1}{2}m_e\right)/M & 1 \\ -m_e/M & \left(m_1 + \frac{1}{2}m_e\right)/M & 1 \\ (m_1 + m_2)/M & \frac{1}{2}(m_1 - m_2)/M & 1 \end{bmatrix} \begin{bmatrix} \boldsymbol{r_g} \\ \boldsymbol{R} \\ \boldsymbol{R_{cm}} \end{bmatrix} \tag{2.1}$$

where $M = m_1 + m_2 + m_e$.

The electrostatic potential energy, *V*, is unchanged because it depends on the relative positions of the particles,

$$V = \frac{e^2}{4\pi\varepsilon_0}\left[\frac{1}{R} - \frac{1}{r_{1e}} - \frac{1}{r_{2e}}\right] \tag{3}$$

The kinetic energy operator becomes:

$$T = -\hbar^2\left[\frac{\nabla_g^2}{2m_e} + \frac{\nabla_R^2}{2\mu} + \frac{\nabla_g^2}{8\mu} + \frac{\nabla_g \cdot \nabla_R}{2\mu_a} + \frac{\nabla_{cm}^2}{2M}\right] \tag{4}$$

where $1/\mu = (1/m_1) + (1/m_2)$ and $1/\mu_a = (1/m_1) - (1/m_2)$ – which is zero for homonuclear species. The ∇_{cm}^2 term accounts for the centre of mass motion, and may be separated off, leaving for the internal motions of the molecule the Schrödinger equation,

$$\left\{-\hbar^2\left[\frac{\nabla_g^2}{2m_e} + \frac{\nabla_R^2}{2\mu} + \frac{\nabla_g^2}{8\mu} + \frac{\nabla_g \cdot \nabla_R}{2\mu_a}\right] + V\right\}\psi_{mol} = E_{int}\psi_{mol} \tag{5}$$

The term in braces is equivalent to $\mathcal{H}_{int}$. Soon, we will develop the approximate solutions known as Born Oppenheimer solution (clamped nuclei) and what Carrington et al. called the “standard adiabatic” solution. However, equation (5) can be solved without making any further approximations by constructing a variational wavefunction and adjusting the parameters to minimise the energy. We will return to variational solutions in section 1.16 when we consider non-adiabatic calculations and relativistic and radiative corrections.

The Born Oppenheimer solution is usually taken to be the solution of the Schrödinger equation for the motion of the electron in the electrostatic field of the clamped nuclei (what we refer to as the standard adiabatic solution has also been considered to be a Born-Oppenheimer solution by some authors, because the notion of potential energy curves is retained). This yields the electronic clamped nuclei equation,

$$\left(\frac{-\hbar^2\nabla_g^2}{2m_e} + V\right)\varphi_t = E_t\varphi_t \tag{6}$$

where φ_t and E_t are labelled according to the electronic state ***t***. Use of the natural symmetry for the motions (prolate spheroidal coordinates) enables (6) to be separated, giving three one-dimensional differential equations, which may be solved exactly, by which we mean a series solution is developed in terms of popular functions, whose terms can be computed to any desired accuracy [27] [28].

The prolate spheroidal coordinates, ξ, η, and χ, are defined by

$$\begin{aligned} \xi &= (r_{1e} + r_{2e})/R \quad \text{with} \quad 1 \le \xi < \infty \\ \eta &= (r_{1e} - r_{2e})/R \quad \text{with} \quad -1 \le \eta \le 1 \end{aligned} \tag{7}$$

and χ is the rotation of the electron about the internuclear (z) axis ($0 \le \chi < 2\pi$). In the prolate spheroidal coordinate system (6) is transformed to (now working in atomic units),

$$\left[\frac{\partial}{\partial\xi}(\xi^2-1)\frac{\partial}{\partial\xi} + \frac{\partial}{\partial\eta}(1-\eta^2)\frac{\partial}{\partial\eta} + \left(\frac{1}{(\xi^2-1)} + \frac{1}{(1-\eta^2)}\right)\frac{\partial^2}{\partial\chi^2} + 2R\xi - p^2(\xi^2-\eta^2)\right]\varphi_t = 0 \tag{8}$$

where $\varphi_t = \varphi(R,\xi,\eta,\chi)$ and $p^2 = -\frac{1}{2}\left[E_t(R) - \left(\frac{1}{R}\right)\right]R^2$. The wavefunction is parametrically dependent upon *R*, which means that the equations must be solved for a fixed value of *R*, with many such calculations defining a potential energy curve. The apparent complexity of the equation masks the simplicity of separation; by making the substitution

$$\varphi_t(R,\xi,\eta,\chi) = L(R,\xi)M(R,\eta)N(\chi) \tag{9}$$

we obtain three separated equations, with separation constants Λ^2 and *A*:

$$\left(\frac{\partial^2}{\partial\chi^2} + \Lambda^2\right)N = 0 \tag{10}$$

$$\left(\frac{\partial}{\partial\xi}(\xi^2-1)\frac{\partial}{\partial\xi} + A - \frac{\Lambda^2}{(\xi^2-1)} + 2R\xi - p^2\xi^2\right)L = 0 \tag{11}$$

$$\left(\frac{\partial}{\partial\eta}(1-\eta^2)\frac{\partial}{\partial\eta} - A - \frac{\Lambda^2}{(1-\eta^2)} + p^2\eta^2\right)M = 0 \tag{12}$$

Solving the χ equation analytically gives

$$N(\chi) = exp(i\Lambda\chi)/(2\pi)^{1/2} \tag{13}$$

where Λ takes values 0, ±1, ±2, … Λ may be identified as the projection of the orbital angular momentum of the electron on the internuclear axis, and within the BO approximation wavefunctions are doubly degenerate for Λ>0 – higher order interactions may lift this degeneracy, giving rise to “Λ-doubling” [29]. Jaffé [27] solved the ξ equation with the expansion:

$$L(R,\xi) = (\xi^2-1)^{\Lambda/2}(\xi+1)^{\sigma}\exp(-p\xi)\sum_{n=0}^{\infty} g_n(R)[(\xi-1)/(\xi+1)]^n$$

(14)

where $\sigma = (R/p) - \Lambda - 1$ and $g_n(R)$ are to be determined. In the united atom limit (12) becomes the defining equation for the associated Legendre functions [1] and therefore the η equation is naturally solved with an expansion over associated Legendre functions:

$$M(R,\eta) = \sum_{s=0}^{\infty} f_s(R) P_{\Lambda+s}^{\Lambda}(\eta)$$

(15)

Where $f_s(R)$ must be determined. The two equations may be solved in many ways. Hunter and Pritchard [30], [31] substituted these expansions in (11) and (12) to yield recursion relations that can be expressed as a matrix eigenvalue equation. The overall solution is achieved for a given R value by requiring that A simultaneously satisfies both (14) and (15).

The solution of the clamped-nuclei equation defines the electronic potential energy curves, $U(R) = E_t(R)$, in which all couplings between nuclear and electronic motion have been neglected. The total binding energy recovered for H_2^+ in the Born-Oppenheimer approximation is (at equilibrium) approximately 25,000 cm^{-1}.

The radial Schrödinger equation for the nuclear motion is

$$\left(-\frac{d^2}{dR^2} + \frac{2\mu}{\hbar^2}(U(R) - E_{vN}) + \frac{N(N+1)}{R^2}\right)\chi_{vN}(R) = 0$$

(16)

and its vibration-rotation eigenfunctions and eigenenergies may be found by any suitable method, for example Numerov-Cooley integration [32], as implemented in the program LEVEL by R.J. Leroy [33].

1.1.3 *The Standard Adiabatic Approximation*

The standard adiabatic approximation is developed by expanding possible solutions for the full internal Hamiltonian (5) as a series over the Born-Oppenheimer solutions (φ_t) [34] ; this is often called a “Born expansion”. That is, we write

$$\psi_{mol}(\boldsymbol{R}, \boldsymbol{r_g}) = \sum_t F_t(\boldsymbol{R})\phi_t(\boldsymbol{R}, \boldsymbol{r}_g) \tag{17}$$

Substituting (17) into (5) we find a set of coupled differential equations for the functions F_t ($\boldsymbol{R}$)

$$\mathcal{H}_{int} \sum_t F_t(\boldsymbol{R})\varphi_t(\boldsymbol{R}, \boldsymbol{r_g}) = E_{int} \sum_t F_t(\boldsymbol{R})\, \varphi_t(\boldsymbol{R}, \boldsymbol{r}_g) \tag{18}$$

Premultiplying by $\varphi_s^*(\boldsymbol{R}, \boldsymbol{r_g})$ and integrating over the electronic coordinate $\boldsymbol{r}_g$ gives

$$E_s(R)F_s(\boldsymbol{R}) + \sum_t \int \varphi_s^*(\boldsymbol{R}, \boldsymbol{r}_g)\left(-\frac{\nabla_R^2}{2\mu} - \frac{\nabla_g^2}{8\mu} - \frac{\nabla_g \cdot \nabla_R}{2\mu_a}\right) F_t(\mathbf{R})\varphi_t(\boldsymbol{R}, \boldsymbol{r}_g)\mathrm{d}\boldsymbol{r}_g = E_{int}F_s(\boldsymbol{R}) \tag{19}$$

The nuclei are treated as point charges, and so the functions φ_t ($\boldsymbol{R}$, $\boldsymbol{r}_g$) are either symmetric or antisymmetric under exchange of nuclei and electron inversion through the geometric centre of the nuclei. Using these symmetry operations allows us to rewrite (19) in the form

$$\left[E_s(\boldsymbol{R}) - \frac{\nabla_{\boldsymbol{R}}^2}{2\mu} - \int \varphi_s^*(\boldsymbol{R},\boldsymbol{r}_g)\left(\frac{\nabla_g^2}{8\mu} + \frac{\nabla_R^2}{2\mu}\right)\varphi_s(\boldsymbol{R},\boldsymbol{r}_g)\mathrm{d}\boldsymbol{r}_g\right]F_s(\boldsymbol{R}) + \sum_{t\neq s}\left[\int \varphi_s^*(\boldsymbol{R},\boldsymbol{r}_g)\left(-\frac{\nabla_g^2}{8\mu} - \frac{\nabla_R^2}{2\mu} - \frac{\nabla_g\cdot\nabla_R}{2\mu_a}\right)\varphi_t(\boldsymbol{R},\boldsymbol{r}_g)\mathrm{d}\boldsymbol{r}_g + \int \varphi_s^*(\boldsymbol{R},\boldsymbol{r}_g)\left(-\frac{\nabla_R}{\mu} - \frac{\nabla_g}{2\mu_a}\right)\varphi_t(\boldsymbol{R},\boldsymbol{r}_g)\mathrm{d}\boldsymbol{r}_g\cdot\nabla_R\right]F_t(\boldsymbol{R}) = E_{int}F_s(\boldsymbol{R})$$

(20)

This is an infinite set of coupled differential equations. The standard adiabatic approximation consists of retaining only diagonal couplings:

$$\left(E_s(\boldsymbol{R}) - \int \varphi_s^*(\boldsymbol{R},\boldsymbol{r}_g)\frac{\nabla_g^2}{8\mu}\varphi_s(\boldsymbol{R},\boldsymbol{r}_g)\mathrm{d}\boldsymbol{r}_g - \int \varphi_s^*(\boldsymbol{R},\boldsymbol{r}_g)\frac{\nabla_R^2}{2\mu}\varphi_s(\boldsymbol{R},\boldsymbol{r}_g)\mathrm{d}\boldsymbol{r}_g - \frac{\nabla_R^2}{2\mu}\right)F_s^{AD}(\boldsymbol{R}) = E_{int}^{AD}F_s^{AD}(\boldsymbol{R})$$

(21)

and thereby defines an effective potential

$$U(\boldsymbol{R}) = E_s(\boldsymbol{R}) - \int \varphi_s^*(\boldsymbol{R},\boldsymbol{r}_g)\frac{\nabla_g^2}{8\mu}\varphi_s(\boldsymbol{R},\boldsymbol{r}_g)\mathrm{d}\boldsymbol{r}_g - \int \varphi_s^*(\boldsymbol{R},\boldsymbol{r}_g)\frac{\nabla_R^2}{2\mu}\varphi_s(\boldsymbol{R},\boldsymbol{r}_g)\mathrm{d}\boldsymbol{r}_g$$

(22)

which may again be substituted into (16) to obtain vibration-rotation wavefunctions (χ_{vN}) and energies (E_{vN}). The standard adiabatic correction therefore consists of retaining the diagonal corrections, improving the clamped nuclei approximation while still effectively separating the electronic and nuclear motions. The adiabatic corrections do not couple together different electronic states.

The magnitude of the standard adiabatic corrections at equilibrium is approximately 35 cm^{-1} for the first term in equation (22) and approximately 25 cm^{-1} for the second term in equation (22). The variation as a function of bond length is marked, and so different vibrational levels are affected in different degrees by the terms.

1.1.4 *Dissociation Limits for Homonuclear and Heteronuclear Species*

The first published calculations of vibration-rotation levels from v = 0 to dissociation in the ground states of H_2^+ , D_2^+ and HD^+ were by Hunter et al. [35]

1.1.4.1 *Dissociation Limits for Homonuclear Species*

For the homonuclear species, the ground (1sσ) and first excited (2pσ) electronic states are degenerate at long range and far away in energy from the next sets of excited states, enabling most properties of the homonuclear ions to be calculated without taking into account couplings with the higher electronic states.

However, in the form given above, the adiabatic potentials do not correctly correlate with the atomic dissociation limits of H^+ + H(1s) because the reduced mass at large *R* does not pass to the value for a proton and an electron and therefore gives an incorrect energy for the hydrogen atom. This difficulty can be overcome for the homonuclear ions by a slight reformulation which Leach and Moss call the “partitioned adiabatic” approach [Leach and Moss, [4] and references therein].

Because the expectation values of $(1/2)\nabla_R^2$ and $(1/8)\nabla_g^2$ are equal in the limit R tends to infinity (17), the adiabatic correction may be made to vanish at dissociation by rewriting the adiabatic Hamiltonian as

$$\mathcal{H}_{B0} + (1/\mu)\mathcal{H}_{\mathrm{ad}} = \left[\mathcal{H}_{B0} - (1/4\mu)\nabla_g^2\right] - (1/\mu)\left[(1/2)\nabla_R^2 - (1/8)\nabla_g^2\right] \tag{23}$$

The electron kinetic energy term now involves the electron reduced mass $[1+(1/2\mu)]^{-1}$ = m/(m+1), which is appropriate to a one-electron atom with nucleus of mass m.

Despite the satisfactory nature of this correction properties calculated using the standard adiabatic approximation and the partitioned adiabatic approximation are found not to differ appreciably.

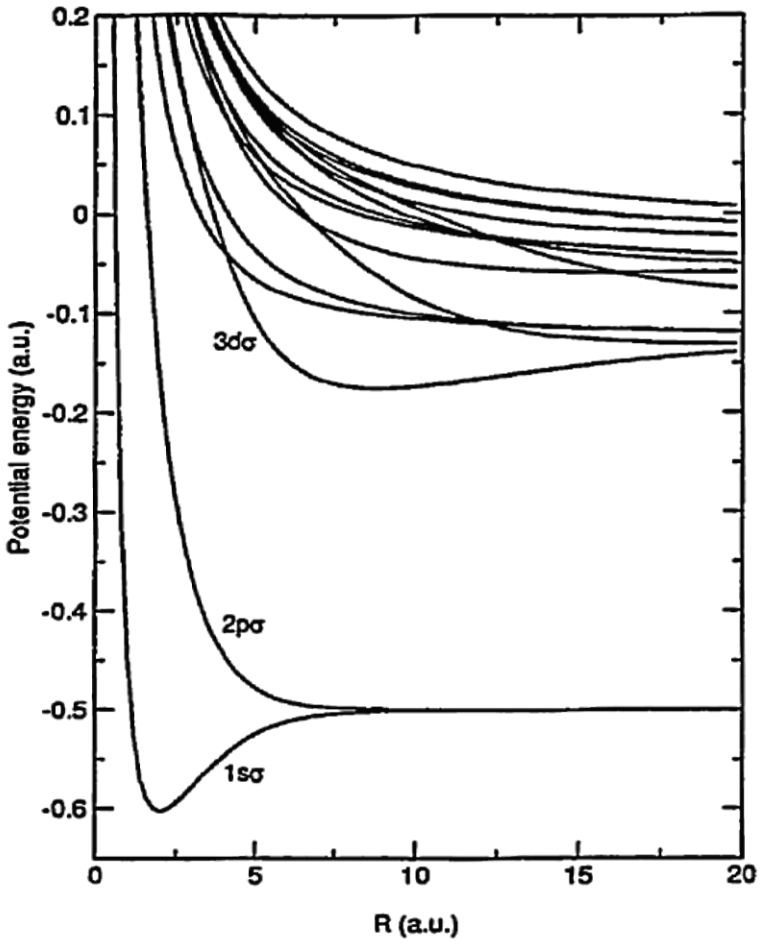

Figure 1.2

Lowest potential energy curves corresponding to Σ electronic states of the bare H_2^+ molecular ion vs internuclear separation R. The Coulomb repulsion between protons is included. The levels are labelled by united-atom-limit quantum numbers. *(Reproduced with permission from Zufar Mulyukov, "Part I. Break up of the hydrogen molecular ion by an electric field", PhD thesis, University of Southern California, 2000)*

As first noted by Coulson [36], the 2pσ electronic state is not entirely repulsive, but contains a shallow minimum induced by charge / induced-dipole interaction – despite the nature of the interaction responsible for the minimum it is usually named a van der Waals' minimum. This shallow well supports several vibration-

rotation levels, and has been critical in successful ion beam measurements of H_2^+ and D_2^+, including those explained in chapter 4, its existence allows spectra to be measured whose transitions terminate in these levels. Figure 1.3 shows the van der Waals minimum with vibration-rotation energy levels of D_2^+ superimposed.

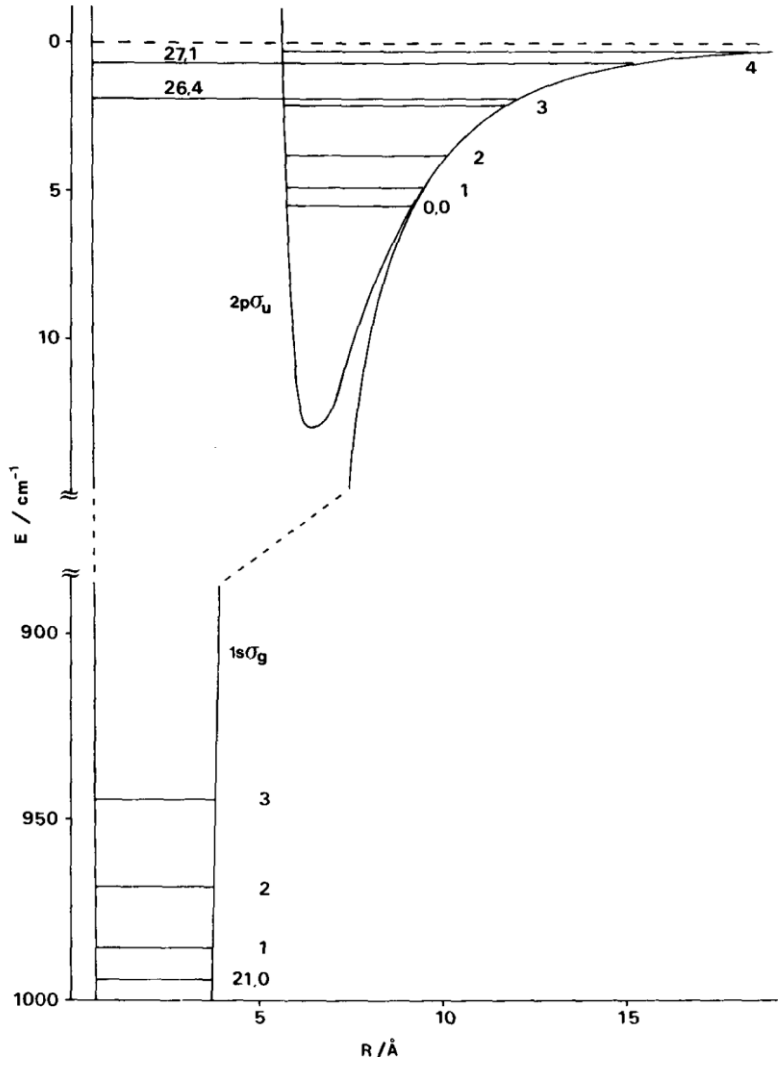

Figure 1.3

Adiabatic potential energy curves for the D_2^+ $1s\sigma_g$ and $2p\sigma_u$ states showing some of the vibration-rotation levels of the van der Waals' minimum in the region of the dissociation limit. (*Reprinted from Molecular Physics, Vol. 67, No. 4, Alan Carrington, Iain R. McNab, and Christine A. Montgomerie, "Electronic spectrum ($2p\sigma_u$-$1s\sigma_g$) of the D_2^+ ion", Pages 711-738, Copyright (1989), with permission from Taylor and Francis Group)*

1.1.4.2 *Dissociation Limits for Heteronuclear Species*

For heteronuclear species such as HD^+, DT^+ and HT^+ $\nabla_g \cdot \nabla_{\boldsymbol{R}}/2\mu_a$ is nonzero ($1/\mu_a = 0$ for the homonuclear molecules) and couples together electronic states – principally the ground (1sσ) and first excited (2pσ) electronic states which are degenerate at long range for the homonuclear ions. For heteronuclear species there are two possible dissociation limits. For HD^+ at long range these correlate with H^+ + D(1s) for the ground electronic state (1sσ) and H(1s) + D^+ for the first excited (2pσ) electronic state. They differ in energy by 29.8 cm^{-1} because the 1s atomic energies for H and D are different – the difference arises from the different reduced masses for H and D. The potential energy curves for HD^+ close to dissociation are shown in figure 1.4. As for the homonuclear case, the van-der Waals minimum in the 2pσ state supports vibration rotation levels, but as these now exist in the continuum of the 1sσ state they can predissociate to H^+ + D(1s) and therefore are best described as Feschbach resonance [37]. Their predissociation lifetimes are calculated to be short, which leads to calculated linewidths of several cm^{-1}, making them unsuitable for detection by high resolution spectroscopic techniques. In principal, these states should be observable in scattering experiments, but to our knowledge no such observations have been made.

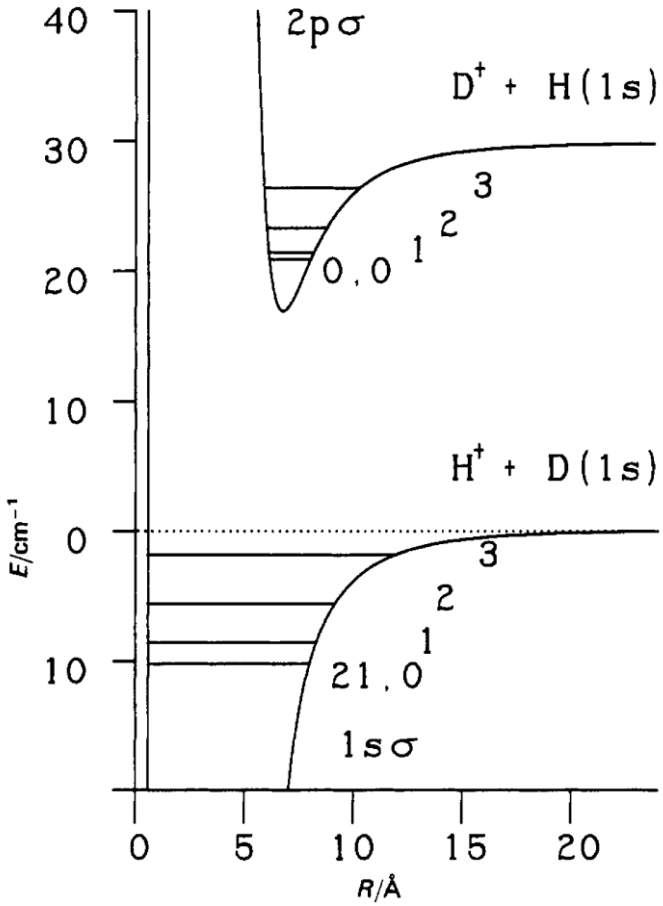

Figure 1.4

Portions of the potential-energy curves for the lsσ and 2pσ electronic states of HD^+ showing the non-degenerate dissociation limits. The $v = 22$, $N = 0$, 1 levels of the ground state have been omitted for clarity. Molecules in vibration-rotation levels of the van der Waals minimum in the 2pσ state can predissociate to the lower dissociation limit. (*Reprinted from Journal of the Chemical Society, Faraday Transactions, Vol. 86, No. 11, Alan Carrington and Iain R. McNab, "Spectroscopy of the H...H$^+$ and D...D$^+$ Charge/Induced-dipole Complexes", Pages 1957-1962, Copyright (1990) with permission from R.S.C. Publishing)*

The standard adiabatic approximation fails to discriminate between the two dissociation limits for HD^+, leading to serious errors in vibration-rotation energies calculated near dissociation; there are modified adiabatic treatments (essentially relying upon a different partitioning of the Hamiltonian) which do correctly account for HD^+ close to dissociation. Spectra of HD^+ were measured by Wing et al. [6] and Carrington and co-workers [38-43]; the theory necessary to take account of the non-degenerate dissociation limits was considered by

Wolniewicz and Poll [44-46] and in a different approach by Moss and his co-workers [25], and more recently by Hilico and his co-workers [15].

1.1.4.3 *HD^+ Close to Dissociation*

We do not consider further calculations and measurements of HD^+, other than to note that Carrington et al., in a series of papers [39, 47-49] [43] examined the structure of energy levels and electron distributions close to the first dissociation limit of HD^+ in detail. Transition frequencies were successfully reproduced by the transformed Hamiltonian theory of Moss and his co-workers. Analysis of hyperfine structure showed that within the ground electronic state, close to the lowest energy dissociation limit, the $1s\sigma$ electronic wavefunction is highly asymmetric; the electron is almost entirely associated with the deuteron. This asymmetry was demonstrated through measurements of the Fermi contact interactions, which essentially depend upon the electron density at the nucleus. The observed hyperfine structure in transitions to levels close to dissociation was widely split, showing that the hyperfine structures in the two levels considered (far from, and close to dissociation) were radically different.

Correctly accounting for the different dissociation limits of HD^+ was crucial in providing theoretical estimates of measured transition frequencies in HD^+ which were obtained close to the first dissociation limit. The work of Richard Moss and his co-workers was essential to the prediction and interpretation of the spectra obtained by Carrington and co-workers, and his calculations remain as a benchmark for other workers (see for example Karr et al. [18, 22]).

1.1.4.4 *H_2^+ - Asymmetry Induced by Hyperfine Interaction*

Above we saw that an electronic asymmetry is introduced into the solutions of the Schrödinger equation for HD^+ which arises in a simple and natural way from the difference in nuclear masses. Carrington et al. [50] made measurements of microwave electronic transitions in H_2^+ close to the first dissociation limit. They

were surprised to find there was a splitting in two of the observed transitions; a 6.0 MHz splitting in the (0, 2)-(19, 1) transition and a 7.6 MHz splitting in the (0, 0)-(19, 1) transition. These splittings were explained as arising from an asymmetry in the Hamiltonian induced by nuclear hyperfine interactions, specifically the Fermi contact interactions between the electron and proton nuclear spins. Herzberg states [51] "*in the presence of nuclear spin the selection rule symmetric ↮ antisymmetric no longer holds absolutely*, although it is still very strict."

Considering the strongest interactions first, Carrington et al. [50] used a symmetric coupling scheme whereby the two nuclear spins in H_2^+, ($I_1 = I_2 = 1/2$), couple to produce the total nuclear spin, $I = I_1 + I_2$, of 0 or 1. For H_2^+ the ground state, $1s\sigma_g$, rotational levels with even-N correspond to $I = 0$ (*para*-H_2^+), but odd-N levels correspond to $I = 1$ (*ortho*-H_2^+). For the $2p\sigma_u$ state this is reversed: even N correspond to $I = 1$ (*ortho*-H_2^+); odd N levels correspond to $I = 0$ (*para*-H_2^+). All the vibration-rotation levels with $I = 1$ should therefore be split by nuclear hyperfine interaction; that is odd-N levels of the ground state and even-N levels of the excited-state.

The experimental observations were consistent with the above analysis as they did not observe splitting of the line arising from the $2p\sigma_u$ (0, 1) - $1s\sigma_g$ (19, 0) transition. An example of the nuclear hyperfine splittings is shown in the nuclear hyperfine energy level diagram of figure 1.5, which shows that there are only two electric dipole allowed components of the $2p\sigma_u$ (0, 2) - $1s\sigma_g$ (19, 1) transition.

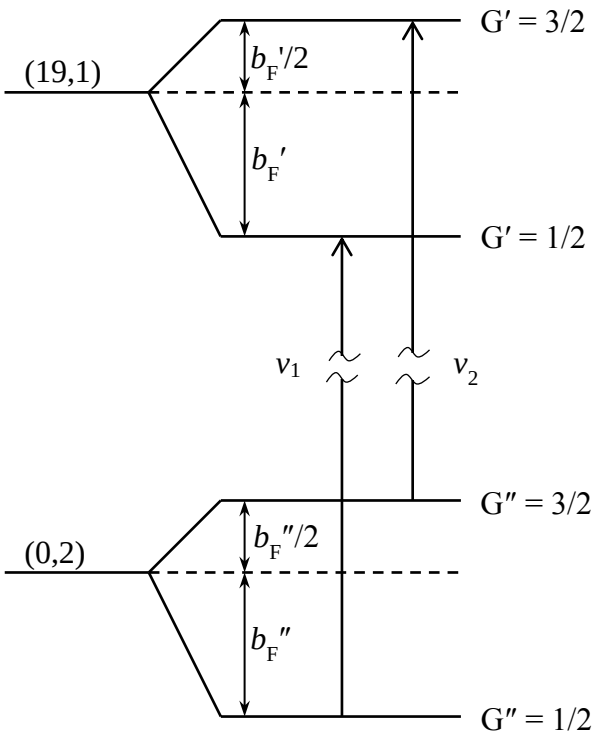

Figure 1.5

Nuclear hyperfine energy level diagram for the $2p\sigma_u$ (0, 2) - $1s\sigma_g$ (19, 1) transition of H_2^+; the two electric dipole allowed components of the transition are indicated. (*Reprinted from Journal of the Chemical Society, Faraday Transactions, Vol. 89, No. 4, Alan Carrington, Christine A. Leach, Richard E. Moss, Timothy C. Steimle, Mark R. Viant and Yvonne D. West, "Microwave Electronic Spectroscopy, Electric Field Dissociation and Photofragmentation of the H_2^+ ion", Pages 603-614, Copyright (1993) with permission from R.S.C. Publishing)*

As can be seen, if the Fermi contact interactions in 19,1 and 0,2 were the same, then ν_1 and ν_2 would be degenerate and no splitting would be observed. The surprising observation was that they are ***not*** the same – the hyperfine interactions are different implying an asymmetry is present which is greater for one level than for another. We will consider this in greater detail in chapters three and four.

1.1.5 *The Effect of an External Electric Field*

The effect of external electric and magnetic fields upon the energy levels of H_2^+ is of intrinsic interest, but is important to us because we use static electric fields as a method of dissociating upper levels of H_2^+ with sensitive discrimination between energy levels that are close in energy. In addition to the use of static electric fields, more recent experiments have studied ultrafast fragmentation and desorption using ultrafast laser techniques. See for example the studies of the dissociation of H_2^+ using high power infrared pulses carried out by Peng et al. [52] and by Paramonov and Kuhn [53], and of HD^+ by Kiess et al. [54]. An example of the use of femtosecond laser pulses in surface physics is that of Fuschel et al. [55] to cause the ultrafast desorption of H_2 and D_2 from ruthenium surfaces.

Perturbative calculations of the effect of low electric field strengths upon energy levels of H_2^+ were published by both Hiskes (1961) [56] and Wind (1966) [57]. Carrington et al. [50], West, [58] and Leach et al. [59] considered in detail the different dissociation rates of states close to the dissociation limit, when using an electric field lens of the type which was used at Newcastle, and which is described in chapter 4. The most accurate calculations of this type are those of Leach et al. [59], which take into account multiple dissociation channels within the context of scattering theory. Zufar Mulyukov (2000) [60] calculated the induced shifts and widths of the first few electronic Σ levels of H_2^+ in the presence of a dc and low frequency ac field over a range of internuclear separations; and also the frequency profile of the rate for dissociation of H_2^+ by one photon in the presence of a strong dc field.

Hiskes's calculations were made in the centre of nuclear mass coordinate system, which may be defined by the transformation,

$$\begin{bmatrix} \boldsymbol{r}_c \\ \boldsymbol{R} \\ \boldsymbol{R}_{cm} \end{bmatrix} = \begin{bmatrix} -m_1/M_n & -m_2/M_n & 1 \\ -1 & 1 & 0 \\ m_1/M & m_2/M & m_e/M \end{bmatrix} \begin{bmatrix} r_1 \\ r_2 \\ r_e \end{bmatrix}$$

or its inverse

$$\begin{bmatrix} r_1 \\ r_2 \\ r_e \end{bmatrix} = \begin{bmatrix} -m_e/M & -m_2/M_n & 1 \\ -m_e/M & m_1/M_n & 0 \\ M_n/M & 0 & 1 \end{bmatrix} \begin{bmatrix} \boldsymbol{r}_c \\ \boldsymbol{R} \\ \boldsymbol{R}_{cm} \end{bmatrix}$$

(23)

where the total mass is M (= $m_1 + m_2 + m_e$) and the nuclear mass M_n (= $m_1 + m_2$). Vector $\boldsymbol{r_c}$ gives the position of the electron relative to the centre of nuclear mass. Adding electric field $\boldsymbol{F}$ to the Hamiltonian adds the Stark-term

$$V_2 = -e\boldsymbol{F} \cdot (\boldsymbol{r_1} + \boldsymbol{r_2} - \boldsymbol{r_e})$$

(24)

to the potential energy, and in a different context matrix elements of this term are commonly evaluated during calculation of spectroscopic absorption intensities where it is used to represent the electric field intensity of incident radiation. Specifying $\boldsymbol{F}$ to be in the space-fixed z direction, then after transforming Hamiltonian (l) and the new electric field term, V_2, to centre of nuclear mass coordinates and removing the term for centre-of-mass translation, the Hamiltonian becomes

$$-\frac{\hbar^2}{2}\left[\frac{\nabla_c^2}{m_e} + \frac{\nabla_R^2}{\mu} + \frac{\nabla_c^2}{M_n}\right] + V + eF_z\left[\left(1 + \frac{m_e}{M}\right)z_c - \left(\frac{m_2 - m_1}{M_n}\right)z_R\right]$$

(25)

where z_c and z_R are the z-components of vectors $\boldsymbol{r}_c$ and $\boldsymbol{R}$. The terms in z_c therefore describe the effect of the electric field on the electron, while the term in z_R describes the effect on the nuclei and is zero for homonuclear ions. As before the Born-Oppenheimer and adiabatic Hamiltonians may be derived, but now including new field terms. For clamped nuclei with the electric field parallel to the internuclear axis (which approximation automatically excludes molecular rotation), the Hamiltonian becomes

$$-\frac{\hbar^2}{2m_e}\nabla_c^2 + eF_z z_c\left(1 + \frac{m_e}{M}\right) + V$$

(26)

and this was the Hamiltonian used by Hiskes. The electric field couples together electronic states, and it is a good approximation to consider only the $1s\sigma_g$ and $2p\sigma_u$ states which are degenerate at dissociation. Hiskes therefore diagonalised the Hamiltonian for clamped nuclei with only these two lowest electronic states. The diagonalisation results in the situation which is illustrated in figure 1.6 for HD^+ which has the added interest of exhibiting asymmetry due to the difference in nuclear mass. Asymptotically, at large $\boldsymbol{R}$, for H_2^+ we have

$$E(1s\sigma) = U_{1s\sigma_g} - 1/2e\boldsymbol{F}\cdot\boldsymbol{R}(1+m/M)$$

$$E(2p\sigma) = U_{2p\sigma_u} + 1/2e\boldsymbol{F}\cdot\boldsymbol{R}(1+m/M) \qquad (27)$$

These limits are a consequence of the clamped nuclei approximation, and correspond to a single hydrogen ion (H^+) being accelerated in the direction of the field (decreasing energy) or in opposition to the field (increasing energy).

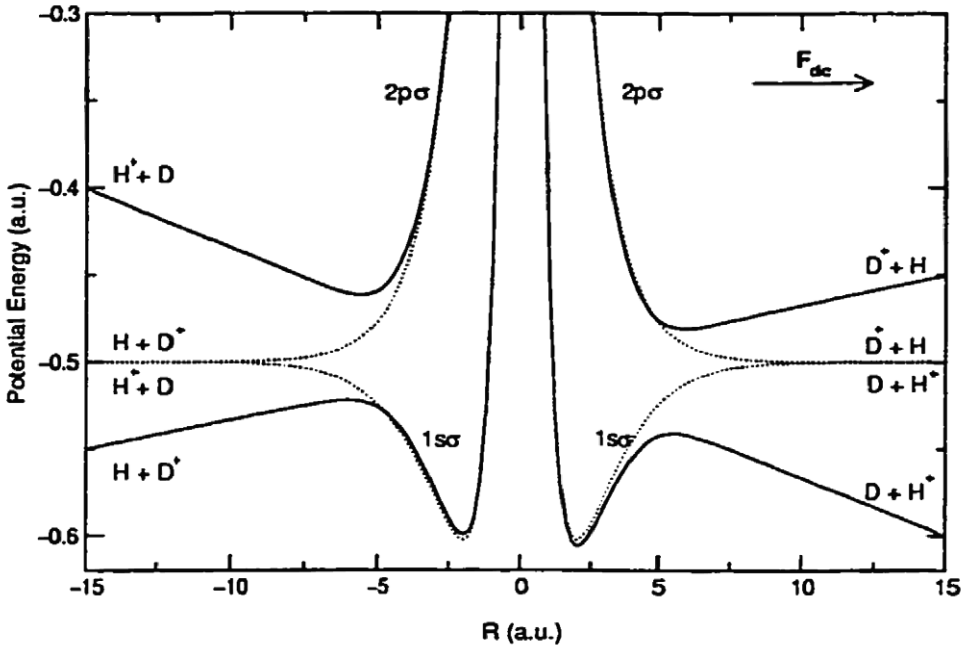

Figure 1.6

The 1sσ and 2pσ potentials for nuclear motion of HD^+ when dressed by a dc field F_{de} of strength 0.01 a.u. ($\approx 5 \times 10^9$ Vm^{-1}) , with the internuclear line oriented parallel (positive *R*) or antiparallel (negative *R*) to F_{de}. The broken lines are the undressed potential curves; the 3.7 meV separation of the undressed dissociation limits is not visible.

(Reproduced with permission from Zufar Mulyukov, "Part I. Break up of the hydrogen molecular ion by an electric field," PhD thesis, University of Southern California, 2000)

Within this clamped nuclei approximation, the potential curves may be used to calculate vibration-rotation levels and their lifetimes. This is a single channel theory, and ignores the coupling of M_N levels induced by the field. Nevertheless, the single channel theory gave useful results; Hiskes calculated that an electric field of just 10^5 V cm^{-1} was sufficient to dissociate v =18, N = 0 of H_2^+ (with dissociation energy of 25.5 cm^{-1}) in 10^{-8} s. When the barrier height dressed by the electric field is below the energy of a level in the absence of a field, then the energy level will dissociate classically and the vibrational period forms an upper bound on the lifetime (approximately 10^{-14} s). Hiskes found that the electric fields required for above barrier dissociation were about twice those required for tunnelling in 10^{-8} s. Although the requirement that the electric field be along the internuclear axis excludes molecular rotation from the Hamiltonian, Hiskes included rotation classically by considering an angle between the molecule and the electric field; a similar approach was used by Wind [57]. For a given vibrational level Hiskes found that high-N states were dissociated more readily than low-N states.

The effect of molecular rotation was investigated by Carrington et al. [50] in a perturbation approach that generated adiabatic potential energy curves. A single adiabatic potential was selected and its vibration-rotation levels obtained by solving the radial Schrödinger equation using LeRoy's program LEVEL [33]. Because the method ignored non-adiabatic couplings, infinite lifetimes are found for levels in the 2pσ state, which are known from experiment to dissociate in moderate fields [50].

Leach et al. [59] undertook calculations to simulate the effect of an electric field lens on a beam of H_2^+ ions, and the subsequent detection of fragment H^+ ions following passage through an energy selective electrostatic analyser (ESA).

They followed the approach of Carrington et al. to include the rotation of the molecule, but instead of calculating results for a single channel, they performed multichannel calculations using a scattering theory approach which does include non-adiabatic couplings. The principal finding was that fields of 40 kV cm^{-1} could dissociate levels up to 25 cm^{-1} below the 1sσ dissociation limit.

1.1.6 *Non-adiabatic Calculations, Relativistic and Radiative Effects*

In this section we give a brief, essentially non-mathematical discussion of non-adiabatic calculations, and the calculated magnitude of relativistic and radiative effects. In order to achieve ultimate theoretical accuracy, all three need to be taken into account, and these are currently very active areas of research; the group which is making the greatest contribution is that of Hilico.

1.1.6.1 *Non Adiabatic Calculations*

In order to achieve calculations of accuracy comparable to, or better than spectroscopic measurements, non-adiabatic calculations are necessary. Many authors have developed non-adiabatic approaches, and illustrated their technique by calculations on the hydrogen molecular ion, but we do not report calculations unless spectroscopic accuracy has been hoped for or achieved.

Non adiabatic calculations may be divided into variational solutions, and non-variational solutions, in which we include *partly* variational calculations.

Of the non-variational non-adiabatic solutions, two have proved historically to give the most accurate agreement with experiment: the variation-perturbation treatment of Wolniewicz and Poll [44-46, 61] , and the transformed Hamiltonian theory of Moss and his co-workers [see Leach and Moss, and references therein, [4]].

The calculations of Wolniewicz and Poll first used a “two state” approximation to allow for the non-degenerate dissociation limits of HD^+, and then improved upon this with perturbation theory [see Carrington and Kennedy review for details [2]]. A complete description of the two-state approach appears in [62] and even without the further refinements of Wolniewicz and Poll, the two-state approximation proved to be useful for calculating hyperfine constants for HD^+ in good agreement with experimental measurements.

The approach of Moss and Sadler [25, 63] was to use a succession of unitary transformations of the full non-adiabatic Hamiltonian. This is similar in nature to, and inspired by, the Foldy-Wouthesson transformations of the Dirac equation [64, 65]. The effect of successive transformations was to re-partition terms from the kinetic energy operator into the potential energy terms of the Hamiltonian. This was particularly successful in accounting for the properties of HD^+, where the asymmetry due to the two different isotopes becomes an asymmetry in the potential energy term achieved by introducing an asymmetric “effective nuclear charge” which is greater for the deuteron than for the proton. A surmountable difficulty of this theory is that wavefunctions are not produced, and that expectation values of operators need to be calculated in a somewhat indirect manner, see Moss et al. [66-69]. This approach was first [70] suggested by Hutson [71]. A particular success of Moss’s approach is that it is easily applicable to states of high rotational angular momentum – as will be seen, variational solutions are normally restricted to solutions with rather low total angular momentum.

1.1.6.2 *Variational Solutions for the Hydrogen Molecule Ion*

Variational solutions for the hydrogen molecule ion are now more common than ever before, due to the availability of increased computer power and storage. Typically, trial variational wavefunctions are constructed to take advantage of the known solutions of the Born-Oppenheimer and standard adiabatic solutions. It has been suggested that the Born-Oppenheimer wavefunctions, which are easily calculable, could themselves be used as a complete basis for a

variational calculation [Jeremy Frey, private communication to Iain McNab, 1985, [70]], but to our knowledge this approach has not yet been successfully implemented.

To use the full non-adiabatic Hamiltonian [2] in calculations requires that the differential operators be expressed in terms of internal coordinates of the system. There are many suitable sets of internal coordinates; the mathematical transformations to particular coordinates can be achieved by means of several transformations similar in nature to those given in [2]; both the matrix elements and their explicit derivations are given by Carrington and Kennedy (1984 [2]) for prolate spheroidal coordinates. Determining the “best” coordinates to use to calculate particular properties remains an active area of research.

The earliest accurate variational solutions for H_2^+ were made by Bishop and Cheung [72]. Such solutions are fully non-adiabatic which makes the interpretation of the resulting wavefunctions non-obvious. Bishop and Cheung [73] analysed their variational solution by projecting their wavefunction onto “natural orbitals” and found that the variational wavefunction separated naturally into electronic and nuclear motions, which they compared with Born-Oppenheimer solutions.

Hilico and his co-workers, in a series of papers [15, 18, 74, 75], have re-introduced the use of perimetric coordinates as being particularly well-suited for studies of the hydrogen molecular cation. Perimetric coordinates were first used in such a study by Rebane and Filinsky, (1997) [76] but they published only results of their method, not the method itself. The perimetric (derived from the word perimeter) coordinates x, y, z for H_2^+ may be defined by

$$x = r_1 + r_2 - R;$$

$$y = r_1 - r_2 + R;$$

$$z = -r_1 + r_2 + R:$$

(this is *equation* (22) of reference [15] by Hilico et al.), where r_1 and r_2 and R are the inter-particle distances (the perimeters of the triangle formed by the three particles).

The main idea of Hilico was to develop a variational approach that included only the formally exact symmetries of the system, and then to arrange a representation that was “strongly coupled” – in essence this means that the description gives well behaved matrices that are amenable to diagonalisation. It should be noted that the use of quantum numbers by Hilico and his co-workers is somewhat vague: “In our different papers, the notation may sometimes differ. Nevertheless, the "angular momentum" L or J is always the total angular momentum [of the molecule, excluding nuclear spins]” [Hilico, private communication to Iain McNab, 2013].

The ultimate aim of Hilico is to calculate transition frequencies to sub ppb accuracy, including full relativistic and radiative corrections. He, along with Jean-Philippe Karr, Vladimir Korobov and many co-workers (such as Carbonell, Lazauskas, Delande, Roth, Koelemeij and Kiliç; and more recently Bielsa, Douillet, and Gutierrez) are approaching this in a wonderful series of papers, which we do not attempt to précis here. [11-13, 20, 22, 74, 75].

1.1.6.3 *Relativistic and Radiative Corrections*

The relativistic corrections are significant at the level of accuracy with which spectroscopic measurements have been made and must be included. The relativistic correction allows for the use of the Schrödinger equation rather than the Dirac equation and has been solved by using a zero-order non-relativistic Hamiltonian and applying first order perturbation theory. The relativistic correction is of the order of the square of the fine structure constant (α^2). Moss and Gonzalves give the perturbation operator as:

$$\mathcal{H}' = \alpha^2\{-(1/2)[E_t(R) + (1/r_1) + (1/r_2)]^2 + (\pi/2)[\delta(r_1) + \delta(r_2)]\} \quad (28)$$

Howells and Kennedy [77] tabulated the correction against bond length for the $1s\sigma_g$ and $2p\sigma_u$ states of H_2^+, D_2^+ (using adiabatic wavefunctions) and HD^+ (using full coupled-states wavefunctions). The tabulated results are given in full in papers by Moss and his colleagues in ref. [78] for H_2^+, ref. [79] for D_2^+, and in

ref. [80] for HD^+. For v=0, N=0 of H_2^+, the relativistic correction, given by Moss and Valenzano [26], is -1.5921 cm^{-1}.

The radiative correction for the Hydrogen atom is called the Lamb shift. There are analogous contributions to final energies in H_2^+ which have their origins in quantum electrodynamics. As for the relativistic correction, the radiative correction may be calculated perturbatively and added to the adiabatic potentials. The perturbation depends on the Bethe logarithm, and Kolos et al., tabulated values for the Bethe logarithm for values up to six Bohr [81]. The principal contribution to the radiative correction is the self-energy of an electron in its own field. The radiative correction is of the order of the cube of the fine structure constant (α^3) [82]. The tabulated results are given in full by [78] (for H_2^+), [79] (for D_2^+) and [80] for HD^+. For v=0, N=0 of D_2^+, the radiative correction is -0.0816 cm^{-1} [79].

The radiative correction for the $2p\sigma_u$ electronic state has been assumed to be zero [4].

1.1.6.4 *Hyperfine Structure*

Most calculations of hyperfine parameters have used first-order perturbation theory and standard adiabatic wavefunctions (or full two-state wavefunctions for HD^+).

Such calculations have proved adequate to reproduce spectra obtained close to dissociation for H_2^+ and D_2^+ in the infrared and microwave regions of the spectrum. The hyperfine Hamiltonian is considered in chapter 2 in reference to electronic g/u symmetry breaking.

The objective behind the driving force to obtain more and more calculations of hyperfine parameters has been the desire to match with theory the accuracy of the measurements by Dehmelt and Jefferts [83] (see the next section).

Non-adiabatic effects were included in hyperfine calculations for H_2^+ by Babb and Dalgarno [84]. Their calculation of the Fermi-contact constants for v=4-8,

N=1) was within 600 kHz of the experimental results. More recently, Korobov, Hilico and Karr [13, 20] have attempted to improve on this accuracy. To do so they have evaluated hyperfine interactions including relativistic and radiative effects to order of α^6, and in some cases to α^7).

Korobov et al. reproduce the measured Fermi-contact constants to within 10 kHz. They comment that "The remaining discrepancy is somewhat larger than expected from comparison with the hydrogen atom, and further theoretical work to improve the hfs [hyperfine structure] intervals is needed." They are presently working on a numerical approach to compute the relativistic Bethe logarithms [22]. They examined several effects that might have an impact on the Fermi contact interaction, including g/u symmetry breaking (which was not thought to be responsible for the remaining discrepancy).

1.2 Spectroscopic Measurements of Hydrogen Molecular Ions

It is not our purpose to review in detail the experimental techniques used to study hydrogen molecular ions, but a brief introduction to some work is given. In what follows we give a list of the experimentally determined transition frequencies for H_2^+ (table 1.1) and D_2^+ (table 1.2) with references to the original work, together with brief descriptions of the experiments used. We have not included transition frequencies that were determined *indirectly* from measurements of the Rydberg spectroscopy of molecular hydrogen and its isotopes.

1.2.1 *Ion-trap Spectroscopy of H_2^+*

The first spectroscopic measurements of a hydrogen molecular ion were in an ion trap. The ion-trap measurements were made to very high precision.

Dehmelt (Nobel prize for physics in 1989) and his co-workers [83, 85, 86] measured magnetic-dipole allowed transitions between hyperfine and spin-rotation components in the v = 4-8, N = 1 and 2 levels of H_2^+. H_2^+ ions were held in an ion trap, and radiofrequency transitions detected by changes in photodissociation rates. The long residence times of the ions in the radiation

field applied to the trap resulted in high spectroscopic resolution – typical linewidths were between 200 and 750 Hz. Analysis of the spectra yielded values for the Fermi contact interaction (b_F), electron-nuclear dipolar interaction (t), electron-spin-nuclear-rotation interaction (γ) and nuclear-spin-nuclear-rotation interaction (f). The high spectroscopic resolution achieved in these experiments is a consequence of the long residence time of the ions in the radiation field applied to the ion trap. The coupling scheme they used (as shown in figure 1.7) is $\boldsymbol{I} + \boldsymbol{S} = \boldsymbol{F_2}$ and $\boldsymbol{N} + \boldsymbol{F_2} = \boldsymbol{F}$. This is in contrast to the scheme described for the present work (see chapter 3) which is $\boldsymbol{I_1} + \boldsymbol{I_2} = \boldsymbol{I}$ and $\boldsymbol{I} + \boldsymbol{S} = \boldsymbol{G}$.

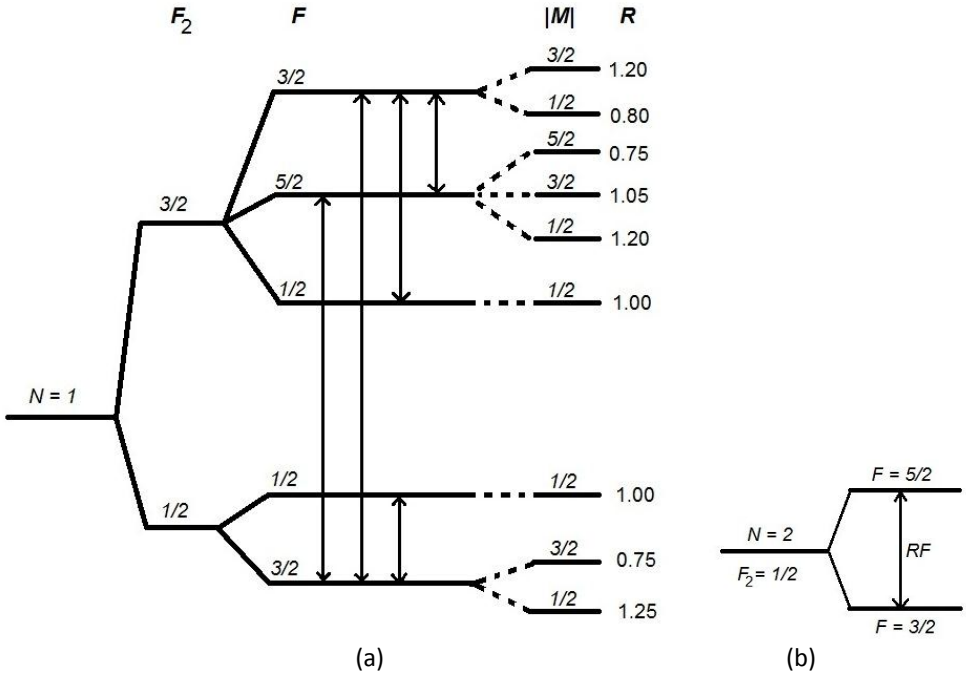

Figure 1.7

(a) Proton hyperfine, spin-rotation and Zeeman splitting of the $N = 1$ rotational levels of H_2^+, and observed radiofrequency transitions. (b) Spin-rotation splitting of the $N = 2$ rotational levels of H_2^+, and observed radiofrequency transition. (*Redrawn after Journal of Physics B: Atomic, Molecular and Optical Physics, Vol. 22, Alan Carrington, Iain R. McNab and Christine A. Montgomerie, "Spectroscopy of the hydrogen molecular ion", Pages 3551-3586, 1989)*

1.2.2 *Ion-beam Spectroscopy of H_2^+ and D_2^+*

Carrington et al. made observations of microwave transitions in H_2^+ [87] and D_2^+ [88] using ion beam methods in 1989. These were electronic transitions between high-lying vibration-rotation levels of the $1s\sigma_g$ ground state and the $2p\sigma_u$ first excited electronic state; these were the (19,1)–(0,2) transitions in H_2^+ and the (26,4)-(0,3) and (1,0)-(27,1) transitions in D_2^+. They went on to measure another 10 transitions in the electronic spectrum of D_2^+ [89], and re-measured the two previously recorded transitions. Their methods were similar in all cases; ions were created with electron impact and mass analysed using a magnet sector and transitions were induced using either a carbon dioxide laser for infrared transitions or a microwave synthesiser for microwave transitions. In many of their experiments the ions were then passed through an electric field dissociation lens (EFDL) and the fragment protons monitored as a means of detecting the transition. They found that the EFDL was an excellent method of selecting the state of interest and continued to use this method successfully for studies of H_2^+, D_2^+ and HD^+. In 1993 they measured seven microwave transitions in D_2^+ [90], observing an unexpected hyperfine splitting of the (0,3)-(27,2) transition which was interpreted in terms of g/u symmetry breaking caused by the deuteron Fermi contact interaction. They also measured three hyperfine resolved electronic transitions in H_2^+ [50] from the ground state $v = 19$ to the first excited state $v = 0$ levels having made detailed calculations (which included the rotation of the molecule) of the electric field strengths required to dissociate particular vibration-rotation levels in the $1s\sigma_g$ ground state. These were later re-measured along with the observation of the $2p\sigma_u$ $v = 0$ $N = 2$ - $1s\sigma_g$ $v = 18$ $N = 3$ transition [91]; this latter transition showed a characteristic structure which was interpreted in terms of hyperfine, fine and electronic g/u symmetry-breaking effects. Following this the theory of electronic g/u symmetry-breaking was studied in greater detail by Bunker and Moss [92] who calculated transition moments and Einstein A-factors for “forbidden” electric dipole rotation and rotation-vibration transitions in H_2^+. This led to the work reported in later chapters [93] of the first, and only to-date, direct measurement of a pure rotation

transition in H_2^+; this was the N = 1←0 transition in the v =19 level of the ground electronic state.

The results of the above measurements are compared to theoretical predictions for the transition frequencies in tables 1.1 and 1.2. In both tables the values of |Experimental – Theory| are given in the final column and it can be seen that in all cases where both experimental and theoretical values are available that excellent agreement has been achieved between theory and observation, to within less than 2 MHz for H_2^+; and similarly close agreement has been achieved for D_2^+. In those cases where the coupling scheme Jefferts et al. is used (i.e. $\boldsymbol{I} + \boldsymbol{S} = \boldsymbol{F_2}$ and $\boldsymbol{N} + \boldsymbol{F_2} = \boldsymbol{F}$) then F_2' and F_2'' may be read instead of G′ and G″.

v',N'	G′ (F_2')	F′	v'',N''	G″(F_2'')	F″	H_2^+ Exp. (E) freq. (MHz)	± (MHz)	Ref	Theory (T) freq. (MHz)	± (MHz)	Ref	|E-T| MHz
4,1	3/2	3/2	4,1	3/2	5/2	5.721	0.015	[86]	5.697	0.002	[94]	0.02
4,1	3/2	3/2	4,1	3/2	1/2	74.027	0.015		74.104	0.002		0.08
4,1	1/2	3/2	4,1	1/2	1/2	15.371	0.015		15.298	0.002		0.07
4,1	3/2	5/2	4,1	1/2	3/2	1270.550	0.015		1271.253	0.002		0.70
4,1	3/2	3/2	4,1	1/2	3/2	1276.271	0.015		1276.950	0.002		0.68
4,2	1/2	5/2	4,2	1/2	3/2	81.121	0.015		81.084	0.002		0.04
5,1	3/2	3/2	5,1	3/2	5/2	5.258	0.015		5.235	0.002		0.02
5,1	3/2	3/2	5,1	3/2	1/2	68.933	0.015		69.006	0.002		0.07
5,1	1/2	3/2	5,1	1/2	1/2	14.381	0.015		14.312	0.002		0.07
5,1	3/2	5/2	5,1	1/2	3/2	1243.251	0.015		1243.972	0.002		0.72
5,1	3/2	3/2	5,1	1/2	3/2	1248.509	0.015		1249.207	0.002		0.70
5,2	1/2	5/2	5,2	1/2	3/2	75.601	0.015		75.566	0.002		0.03
6,1	3/2	3/2	6,1	3/2	5/2	4.817	0.015		4.795	0.002		0.02
6,1	3/2	3/2	6,1	3/2	1/2	63.989	0.015		64.057	0.002		0.07
6,1	1/2	3/2	6,1	1/2	1/2	13.413	0.015		13.347	0.002		0.07
6,1	3/2	5/2	6,1	1/2	3/2	1218.154	0.015		1218.895	0.002		0.74
6,1	3/2	3/2	6,1	1/2	3/2	1222.971	0.015		1223.690	0.002		0.72
6,2	1/2	5/2	6,2	1/2	3/2	70.231	0.015		70.198	0.002		0.03
7,1	3/2	3/2	7,1	3/2	5/2	4.395	0.015		4.374	0.002		0.02
7,1	3/2	3/2	7,1	3/2	1/2	59.164	0.015		59.227	0.002		0.06
7,1	1/2	3/2	7,1	1/2	1/2	12.461	0.015		12.398	0.002		0.06
7,1	3/2	5/2	7,1	1/2	3/2	1195.156	0.015		1195.917	0.002		0.76
7,1	3/2	3/2	7,1	1/2	3/2	1199.551	0.015		1200.291	0.002		0.74
7,2	1/2	5/2	7,2	1/2	3/2	64.977	0.015		64.855	0.002		0.12
8,1	3/2	3/2	8,1	3/2	5/2	3.989	0.015		3.969	0.002		0.02
8,1	3/2	3/2	8,1	3/2	1/2	54.425	0.015		54.483	0.002		0.06
8,1	1/2	3/2	8,1	1/2	1/2	11.517	0.015		11.458	0.002		0.06
8,1	3/2	5/2	8,1	1/2	3/2	1174.169	0.015		1174.953	0.002		0.78
8,1	3/2	3/2	8,1	1/2	3/2	1178.159	0.015		1178.922	0.002		0.76
8,2	1/2	5/2	8,2	1/2	3/2	59.804	0.015		59.774	0.002		0.03
0,2	3/2		19,1	3/2		17610.300	0.5	[50, 87]	17609	1.0	[95, 96]	1.3
0,2	1/2		19,1	1/2		17604.300	0.5					
0,1	1/2		19,0	1/2		52894.600	0.5	[50]	52893	1.0		1.6
0,0	3/2		19,1	3/2		96431.800	0.5		96431	1.0		0.8
0,0	1/2		19,1	1/2		96424.200	0.5					
0,2	1/2		19,1	1/2		17604.400	0.5	[91]	17603	3.0	[97]	1.4
0,2	3/2		19,1	3/2		17610.400	0.5		17609	3.0		1.4
0,1	1/2		19,0	1/2		52894.600	0.5		52893	3.0		1.6
0,0	1/2		19,1	1/2		96424.200	0.5		96423	3.0		1.2
0,0	3/2		19,1	3/2		96431.800	0.5		96431	3.0		0.8
0,2			18,3			156632.80	0.5		156632	3.0		0.8
19,1			19,0			14961.700	1.1	[93]	14960	3.0	[98]	1.7

Table 1.1

Comparison of experimental (E) and theoretical (T) (where available – see column 13) transition frequencies for H_2^+ in the ground electronic state ($1s\sigma_g$) and for transitions between the ground and first excited electronic states ($2p\sigma_u$ - $1s\sigma_g$).

v',N'	G′	v'',N''	G″	D_2^+ Exp. (E) Freq.(MHz)	± (MHz)	Ref	Theory (T) freq.(MHz)	± (MHz)	Ref	|E-T| (MHz)
26,4		0,3		11929.0	0.5	[88]	12471.0		[89]	542
1,0		27,1		11145.0	0.5		11032.0			113
0,2		21,3		28222492.0		[89]	28222941.7			449.7
0,1		21,2		28925115.6			28925535.3			419.7
0,0		21,1		29402535.0			29402954.8			419.8
0,1		21,0		29667641.5			29668091.2			449.7
0,2		21,1		29452240.6			29452630.4			389.8
0,3		21,2		29005100.2			29005549.9			449.7
0,4		21,3		28327329.4			28327779.1			449.7
1,1		21,2		29069165.8			29069585.5			419.7
1,0		21,1		29558577.0			29558996.7			419.7
1,1		21,0		29811751.8			29812141.5			389.7
0,3		26,4		11928.7	0.5		11991.7			63
1,0		27,1		11146.3	0.5		11152.3			6
1,0		27,1		11144.0	3.0	[90]	11144.0			0
26,4		0,3		11928.8	1.2		11930.0			1.2
1,1		27,0		25755.0	5.0		25759.0			4
0,2		26,3		48061.8	0.5		48061.0			0.8
27,2	1/2	0,3	1/2	64288.3	0.5					
27,2	3/2	0,3	3/2	64289.5	0.5					
27,2	5/2	0,3	5/2	64291.1	0.5		64290.0			1.1
27,1		0,2		95222.0	0.5		95222.0			0
0,1		26,2		109672.8	0.5		109673.0			0.2
1,0		27,1		11138.1	0.4	[99]	11145.0	3.0	[79]	6.9
26,4		0,3		11928.0	0.3		11927.0	3.0		1
1,1		27,0		25755.4	0.4		25759.0	3.0		3.6
0,2		26,3		48064.3	0.4		48064.0	3.0		0.3
27,2		0,3		64290.9	0.1		64290.0	3.0		0.9
27,2	5/2	0,3	3/2	64289.2	0.1		64288.4	3.0	[97]	0.8
27,2	3/2	0,3	1/2	64289.8	0.1		64288.9	3.0		0.9
27,1		0,2		95222.5	0.1		95221.0	3.0	[79]	1.5
0,1		26,2		109672.8	0.1		109675.0	3.0		2.2
27,0		0,1		118296.7	0.4		118296.0	3.0		0.7
27,2		0,1		144299.0	0.6		144299.0	3.0		0
27,2	5/2	0,1	3/2	144297.4	0.6		144297.4	3.0	[97]	0
27,2	3/2	0,1	1/2	144297.9	0.6		144298.0	3.0		0.1
27,1		0,0		144895.2	0.4		144895.0	3.0	[79]	0.2
0,4		26,3		152896.5	0.5		152899.0	3.0		2.5
0,0		26,1		162165.2	0.6		162169.0	3.0		3.8
0,3		26,2		189681.0	5.0		189684.0	3.0		3
0,2		26,1		211847.0	5.0		211842.0	3.0		5
0,1		26,0		215484.0	5.0		215479.0	3.0		5

Table 1.2

Comparison of experimental (E) and theoretical (T) (where available – see column 11) transition frequencies for D_2^+ showing the source of the experimental and theoretical results and the associated uncertainties.

1.3 Discussion

In this chapter I have given a review of the theory and experiment of the hydrogen molecular ion H_2^+ and its isotopomers D_2^+ and HD^+. I have given comparisons of theoretical and experimental results for H_2^+ and D_2^+ with an emphasis on ion-beam spectroscopy in the infrared and microwave regions. In the next chapter I will describe in detail the ion-beam instrument I used for both laser and microwave spectroscopy including the instrumental requirements and the challenges these presented along with a full description of how these challenges were overcome.

Chapter 2: Fast Ion Beam Spectrometer

In this chapter is given a full description of the Newcastle Fast Ion Beam Spectrometer, including a description of its use for the measurement of the infra-red spectra of doubly-charged molecules. Such measurements were not part of the author's experimental studies, but were carefully considered in arriving at a theoretical description of the available instrumental signal to noise ratio (section 2.6.3). The majority of this chapter was published in two articles [100, 101]; and many of the figures presented are taken directly from review of Scientific Instruments, 73, 241-254 (2002) to which a number of people contributed. They are Ramadan Abusen, Simon G. Cox, Andrew D. J. Critchley, Alan N. Hughes, Fay Kemp, Iain R. McNab, Ralph C. Shiell and Fiona E. Smith.

2.1 Apparatus Description

2.1.1 *Overview*

The Newcastle fast ion beam spectrometer was constructed for the study of infrared and microwave spectra of molecules with a single or double positive charge (molecular cations and dications respectively). The spectroscopic transitions were recorded indirectly by means of observing a change in the fragmentation rate of the molecular cation / dication when a transition was in resonance. In this chapter is a description of the design and performance of the spectrometer, with particular emphasis on the sensitivity achieved – the experimental signal to noise ratio. The operation and calibration of the spectrometer are discussed, and it is shown that the maximum possible signal to noise ratio that could be achieved in this type of experiment was achieved.

2.1.2 *Principle of Indirect Detection of Transitions*

Ion beam spectroscopy has a number of advantages over spectroscopy in discharges and ion traps [102] (see for example [103] and references therein). The detection sequence used for the ions that we wished to investigate is summarised in figure 2.1, using the molecular dications of DCl^{2+} as an example. Both initial and final states dissociate with a characteristic (and different) kinetic energy release, on a characteristic (and different) time scale. When a transition is at resonance, population transfer occurs from a long-lived to a short-lived state and manifests itself as an increase in the number of fragments. By monitoring the production of fragment ions as a function of laser frequency a spectrum is obtained. In order to make some use of the kinetic energy information stored in the fragment kinetic energy we chose to use an electrostatic analyser (ESA) as a method of selecting fragment ions for detection. The final design of our spectrometer has the following advantages:

a) the species of interest is known unambiguously by its mass/charge ratio making isotope studies particularly simple compared with discharge spectroscopy,
b) very high sensitivity; in a well devised experiment 100% quantum efficiency is approached - single photon absorption can be detected,
c) the ability to accurately determine quantum resolved lifetimes,
d) the ion beam energy is variable and permits the use of fixed frequency lasers and Doppler scanning techniques to achieve broad frequency coverage,
e) the high kinetic energy release from the Coulomb explosion means that the ESA passes the fragments of interest on a background of fragments arising only from spontaneous dissociation of the molecular dication,
f) kinetic energy analysis can help to lead to an unambiguous knowledge of the electronic state of the molecular dication that is being probed (resolution is insufficient to measure the vibrational state),
g) once a transition has been located, the experimental parameters can be varied to optimize the signal to noise ratio of the spectrum,

h) ionisation is a vertical process and the molecular dications are formed vibrationally hot, enabling the spectroscopy of states other than the ground vibrational state, to be examined,

i) the ability to directly determine transition moments in favourable cases

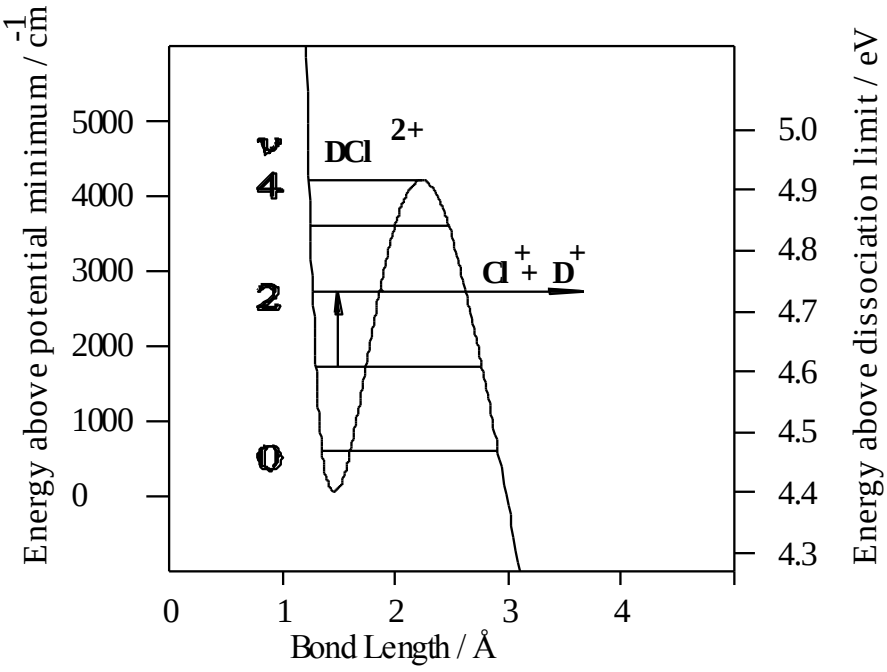

Figure 2.1

A potential energy curve for a kinetically stable, thermodynamically unstable molecular dication (DCl_2^+). The low lying vibrational states may have lifetimes of years, while the uppermost vibrational states may fragment in picoseconds. The principle of spectroscopic measurements on dications is illustrated; at resonance an infrared laser beam causes a vibrational transition which results in population transfer from a long-lived state of the molecular dication to a short lived state. The resulting increase in fragmentation is monitored as a function of laser frequency and enables a spectrum to be detected; the fragmentation is a 'Coulomb explosion' that releases considerable kinetic energy (4.73 eV/molecule for v=2 of DCl^{2+}) (*Reprinted from Review of Scientific Instruments, Vol. 73, No. 2, Ramadan Abusen, Simon G. Cox, Andrew D. J. Critchley, Alan N. Hughes, Faye Kemp, Iain R. McNab, Ralph C. Shiell, and Fiona E. Smith, "Coaxial ion beam/infrared laser beam spectrometer for investigating infrared spectra of doubly positively charged molecules (molecular dications)", Pages 241-254, Copyright (2002), with permission from A.I.P. Publishing LLC.)*

2.1.3 *Overview of the Spectrometer*

An overview of the ion beam spectrometer is shown in figures 2.2 (a basic description of its operation is given in the figure caption). The spectrometer is a “reverse geometry double focusing mass spectrometer”, that is the ions emerging from the source slit are focused by a magnetic sector into the object plane of an electrostatic analyser. It was desirable for the focus to occur within the interaction region so that a coincident focus with the laser or microwave beam could be achieved; a 90^0 electrostatic analyser was therefore used rather than an analyser with a magic angle. Figure 2.2 shows the apparatus in the configuration used for laser spectroscopy; section 2.7 describes the modifications required to use the instrument for microwave spectroscopy with electric field dissociation with figure 2.6 showing the apparatus in the configuration used for microwave spectroscopy and electric field dissociation.

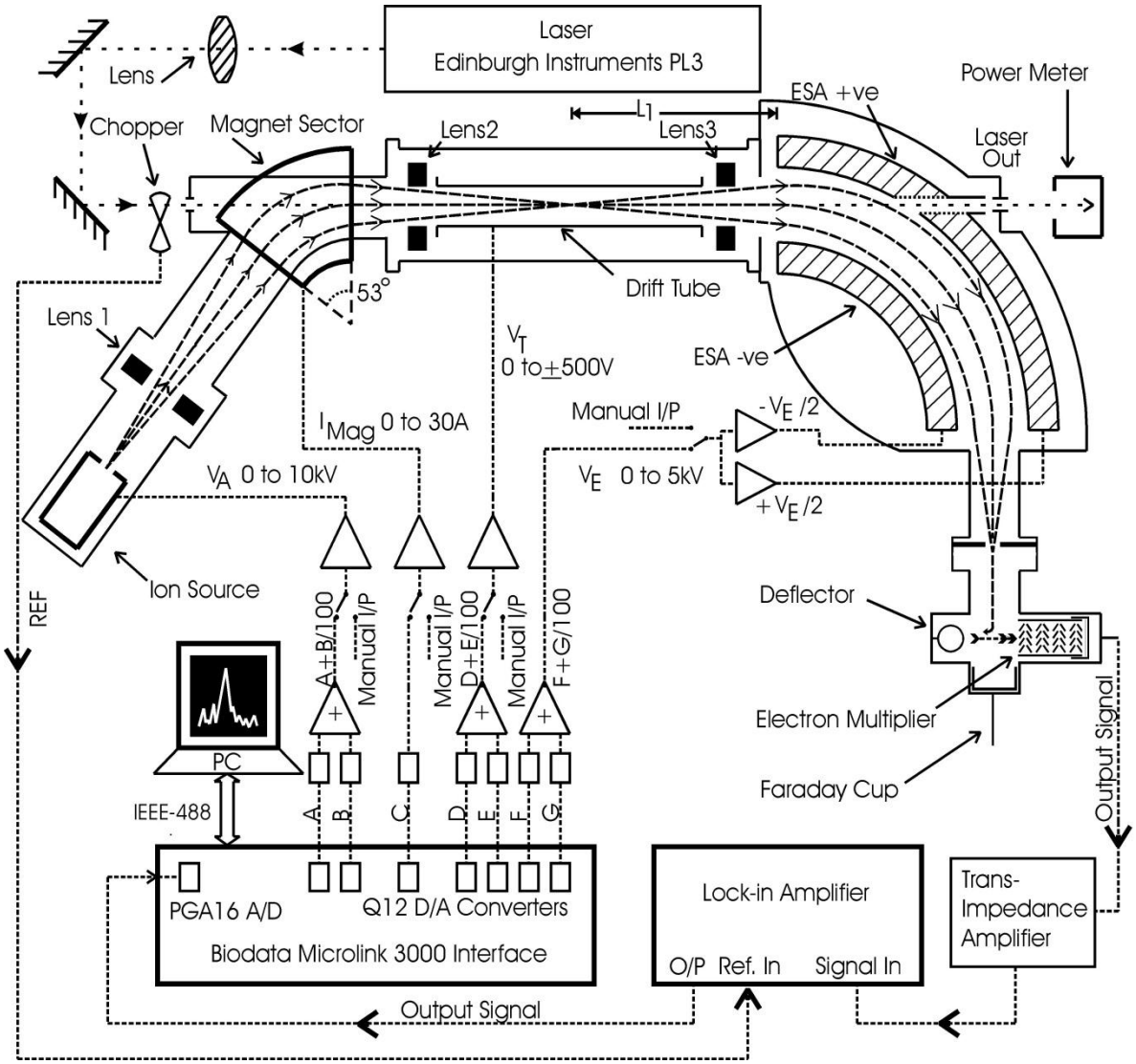

Figure 2.2

A schematic diagram of the instrument in the configuration used for laser spectroscopy. Molecular dications are created in the ion source by electron impact ionization. An ion beam is extracted from the source by a potential gradient and accelerated by 1 to 10 kV (set either manually or by two channels of the D/A unit, see text for details) towards an electrostatic lens. This lens, combined with a magnetic analyser and a second electrostatic lens, focuses the ion beam into an interaction region according to its mass to charge ratio. The interaction region contains a Faraday cage constructed from a stainless steel mesh (hereafter called the drift tube). A co-axial laser beam is introduced into the mass spectrometer through antireflection coated zinc selenide windows and is brought to a coincident focus with the ion beam within the drift tube. The drift tube voltage is scanned by a single 12-bit D/A. Inside the drift tube spectroscopic transitions may occur which result in an increase in fragmentation of the molecular ion. Fragments which arise in the drift tube are selected according to their kinetic energy / charge ratio using the electrostatic analyser and detected with an off-axis electron multiplier /

deflector system. The resulting signal is processed by lock in amplification, measured using a 12-bit A/D and then stored on a computer as a function of drift tube voltage (and hence of effective laser frequency for the laser frequency used). (*Reprinted from Review of Scientific Instruments, Vol. 73, No. 2, Ramadan Abusen, Simon G. Cox, Andrew D. J. Critchley, Alan N. Hughes, Faye Kemp, Iain R. McNab, Ralph C. Shiell, and Fiona E. Smith, "Coaxial ion beam/infrared laser beam spectrometer for investigating infrared spectra of doubly positively charged molecules (molecular dications)", Pages 241-254, Copyright (2002), with permission from A.I.P. Publishing LLC.)*

2.2 The Mass Spectrometer

In this section is given a detailed description of the main components of the spectrometer - that is the vacuum system, ion source, ion lenses, magnetic and electrostatic analysers, the interaction region and the detector; paying particular attention to the fragmentation properties of molecular cations / dications in relation to kinetic energy selection and measurement by the electrostatic analyser.

2.2.1 *Vacuum System*

The vacuum system is constructed using stainless steel chambers and conflat flanges and pumping is achieved using diffusion and rotary pumps [104]. The working pressure in the source housing is approximately 10^{-6} to10^{-5} Torr. After their formation in the ion source ions are rapidly extracted into the analyser region which is usually maintained at a pressure 10^{-8} Torr. The flight tube between the source and the magnet is pumped by a small diffusion pump which allows a high degree of differential pumping to take place between the source and analyser regions.

2.2.2 *Ion Source*

The molecular ions are created by electron impact ionisation of a precursor gas in a Vacuum Generators in-line ion source (for a description see [43]); the ion source has a 1mm x 9mm rectangular exit slit oriented to give a line source of ions in the z-plane [105]. As ions leave the source the full potential drop from

the source potential, V_A, to the potential of the rest of the apparatus, 0 V, is experienced by the ions. Extraction of the ions from the ion source is optimized using a repeller electrode, with a potential set from $0.92V_A$ to $1.1V_A$, but penetration of the earth's potential through the ion source exit slit also contributes. A consequence of the repeller potential and earth field penetration into the ion source is that the ion beam potential is not the same as the source potential (calibration of beam potential is discussed below). In order to design the ion optics following the ion source I modelled the ion source using SIMION [106] and found the maximum ion extraction efficiency was obtained when a near-parallel beam of ions passes through the lens aperture and the source exit slit. For the purposes of ion optical design, this corresponded to a source image placed at infinity.

2.2.3 *Ion Lens One*

The efficient use of a magnetic sector requires the ion beam to enter the magnet perpendicular to the centre radius of the magnet and central to the entrance aperture. In order to achieve this Ion lens 1 was constructed; it is an electrostatic lens positioned between the ion source and the magnetic analyser and it consists of a pair of y and z deflection plates separated by an earth plate [105], mounted on ceramic rods. The gap between opposing plates is 2 cm and each plate can be individually set at potentials from 0 to -5 kV and this is scaled with the source potential. In practice it was found that potentials of magnitude greater than 500 V were normally sufficient to achieve satisfactory transmission to the magnet.

2.2.4 *Magnet*

Our magnet, from a VG MM16F mass spectrometer, was used to achieve mass/charge separation and primary focusing of the parent ion beam. The magnet has a 53° transmission angle with a centre radius of 16 cm and a maximum field strength of 9×10^2 Gauss (0.09 Tesla). To enable unimpeded transmission of the laser beam through the magnet flight tube the separation of the magnet pole pieces was widened to 2 cm and a new flight tube was

manufactured with an aperture of 1.8 cm. The magnetic sector selects the ions of interest according to their mass-to-charge ratios

$$\frac{m}{q} = \frac{B^2 r_m{}^2}{2V_B},$$

where B is the magnetic field of the analyser, r_m is the radius of the analyser and V_B is the electric potential of the ion beam.

2.2.5 *Electrostatic Analyser (ESA)*

The second analyser about whose primary focusing abilities the ion optics were designed was an electrostatic analyser (ESA). In order to energy select and refocus a line object (in the z plane [105]) the ESA used in our experiment is a cylindrical plate analyser. The potential difference between the plates of a cylindrical analyser creates a central force for charged particles; angular momentum is necessarily conserved under such a force. The main function of the ESA is to separate out the fragment ions from the main ion beam according to their kinetic energy/charge ratio. A secondary function is to permit kinetic energy analysis of the parent and fragment ion beams.

The ESA consists of two polished 90° radially concentric cylindrical metal plates spaced 1 cm apart and with a centre radius, r_E, of 21.5 cm; the plates were obtained from an AEI MS10 mass spectrometer. The outer plate has a 1 cm diameter hole bored out of it on the beam axis to act as a conduit for the laser beam; to minimize earth field penetration a 10 cm long metal pipe was fitted to the outer wall of the plate. These modifications do not appear to have affected the resolution of the ESA.

Application of Gauss's law to the ESA shows that the electric field E_{ESA} at the centre radius r_E is given by:

$$E_{ESA} = \frac{V_E}{r_E \ln\left(\frac{r_2}{r_1}\right)} = \frac{V_E}{1.0002 \times 10^{-2}} \approx \frac{V_E}{r_2 - r_1} = \frac{V_E}{1.0000 \times 10^{-2}} Vm^{-1}, \qquad (1)$$

where r_1 and r_2 are the radii of curvature of the inner surfaces of the plates of the ESA and V_E the electric potential difference between them. The field is well approximated by that due to a pair of parallel plates (rhs of eqn 1).

Neglecting the small non-zero potential at the entrance slit for plates with equal and opposite voltages it can be seen that ions with kinetic energy *KE* and charge *q* will follow a circular trajectory of radius r_E if centripetal and electrostatic forces are equal: $qE_{ESA} = mv^2 / r_E$. For selective transmission of ions by a given analyser (r_E) it can be seen that the important characteristic of the ions is the kinetic energy:charge ratio;

$$E_{ESA} r_E / 2 = mv^2 / 2q = KE / q.$$

In our experiment the fragment ions arise in the drift tube with trajectories that are only slightly modified (for example by the Coulomb explosion in the case of molecular dications) from that of the parent beam. The fragment beam is therefore initially focused in the interaction region where it acts as the source (S) of ions to be transmitted by the ESA.

To a first-order approximation a source, S, placed a distance L_1 from the entrance aperture of the ESA (with centre radius r_E) and subtending angle φ to the entrance aperture is imaged by the ESA at a distance L_2 from the exit aperture where [107]:

$$L_2 = \left(\frac{r_E^2}{2\sin^2\sqrt{2}\varphi} + \frac{L_1 r_E \cot\sqrt{2}\varphi}{\sqrt{2}} - \frac{r_E^2 \cot^2\sqrt{2}\varphi}{2} \right) \Bigg/ \left(L_1 - \frac{r_E \cot\sqrt{2}\varphi}{\sqrt{2}} \right)$$

Our detector slit is 9 cm from the exit aperture of the ESA, and here the image of a source S at distance L_1 = 6 cm from the entrance aperture is refocused. Thus the fragment ion beam should form a focus at position S. In practice it was found that a mismatch between the true fragment ion source position (the focus

of the parent ion beam) and the theoretical fragment ion source position (6 cm in front of the entrance to the ESA) of up to 50 cm only degrades the spectrometer signal/noise for measured infra-red transitions by a factor of 2. The transmission of fragments by the ESA depends upon the fragmentation process; what follows is a derivation of the relationships needed to determine the centre of mass fragmentation energy from the measured kinetic energies of the fragments.

The kinetic energy of fragment ions is changed by scanning a potential applied to the drift tube (see below) and the voltage applied to the ESA must also therefore be scanned to enable continuous transmission of the fragment ions. The Coulomb explosion of the dications results in fragment ions that also have a centre of mass kinetic energy. By understanding the kinetics of the fragmentation process (see for example [108]) the instrument could be used to determine this centre of mass kinetic energy release and by scanning the ESA appropriately.

Consider the Coulomb explosion of a molecular ion

$$m_p^{+q_p} \rightarrow m_1^{+q_1} + m_2^{+q_2}$$

where m_p is the mass of the parent ion with charge $+q$ (=2e for a dication), m_1 and m_2 the masses of fragment ions 1 and 2 and internal energy Δ is released as kinetic energy of the two fragments in the Coulomb explosion. If the ion beam had been accelerated to a beam potential of V_B volts and the drift tube is at a potential V_T, then fragmentation in the drift tube occurs at a total beam potential of V_B - V_T volts, yielding a parent velocity of

$$v_p = \sqrt{2q_p(V_B - V_T) / m_p}$$

Momentum is conserved and in the centre of mass frame of the parent ion the kinetic energies of each fragment ion are therefore,

$$KE_{1,2}^{CofM} = \frac{\mu\Delta}{m_{1,2}}$$

where $\mu = \frac{m_1 m_2}{m_1 + m_2}$, yielding fragment velocities in the centre of mass of

$$v_{1,2}^{CofM} = \frac{\sqrt{2\mu\Delta}}{m_{1,2}}$$

The lab-frame velocities of the fragments within the drift tube are given, using Galilean relativity (see for example [109]), by the sum of the lab-frame parent ion velocity and the fragment ion centre of mass velocity:

$$v_{1,2}^{inDT} = \left[\frac{2q_p(V_B - V_T)}{m_p}\right]^{\frac{1}{2}} + \left[\frac{2\mu\Delta}{m_{1,2}^{\ 2}}\right]^{\frac{1}{2}} \cos\theta\,,$$

where θ is the angle between the fragment velocity and the parent velocity. Our signal detection relies upon collecting fragment ions from the drift tube. The solid angle subtended by the fragment beam to the entrance of the ESA depends upon the size of the off axis velocity component and so for maximum sensitivity it is better to collect the more massive fragment (Cl^+ in the case of DCl^{2+}) resulting from the dissociation. The acceptance angle of the ESA causes θ to be constrained to nearly 0 and 180 degrees (forward and backward relative to the parent beam).

On leaving the drift tube the fragment ions gain (or lose) kinetic energy due to re-acceleration to earth potential and their new kinetic energy becomes

$$KE_{1,2} = \frac{1}{2} m_{1,2} \left(v_{1,2}^{inDT}\right)^2 + q_{1,2} V_T$$

$$KE_{1,2} = \frac{1}{2} m_{1,2} \left\{ \frac{2q_p(V_B - V_T)}{m_p} + \frac{2\mu\Delta}{m_{1,2}^2}\cos^2\theta + 2\left(\frac{2q_p(V_B - V_T)}{m_p} \frac{2\mu\Delta}{m_{1,2}^{\ 2}} \right)^{\frac{1}{2}} \cos\theta \right\} + q_{1,2} V_T\,.$$

Where $q_{1,2}$ is the charge of the fragment under consideration. The third term in brackets leads to a separation in lab frame kinetic energy between forward (cos θ=1) and backward (cos θ=-1) scattered fragments of

$$2\left(\frac{2q_p\left(V_B - V_T\right)\ 2\mu\Delta}{m_p}\right)^{\frac{1}{2}}$$

Equating centripetal and electrostatic forces yields the field required to pass fragments through the electrostatic analyser as

$$E = \frac{2KE_{1,2}}{q_{1,2}r_E} =$$

$$\frac{2}{q_{1,2}r_E}\left[\frac{1}{2}m_{1,2}\left\{\frac{2q_p\left(V_B - V_T\right)}{m_p} + \frac{2\mu\Delta}{m_{1,2}^2}\cos^2\theta + 2\left(\frac{2q_p\left(V_B - V_T\right)}{m_p}\frac{2\mu\Delta}{m_{1,2}{}^2}\right)^{\frac{1}{2}}\cos\theta\right\} + q_{1,2}V_T\right]$$

The centre of mass kinetic energy release can be found from the measured separation in electric potential, V_E^{fb} , between forward and backward scattered fragments as

$$\Delta = \frac{m_p}{\mu q_p\left(V_B - V_{DT}\right)}\left[\frac{q_{1,2}V_E^{fb}}{8\ln\left(\frac{r_2}{r_1}\right)}\right]^2 \approx \frac{m_p}{\mu q_p\left(V_B - V_{DT}\right)}\left[\frac{q_{1,2}V_E^{fb}r_E}{8\left(r_2 - r_1\right)}\right]^2.$$

The kinetic energy resolution of the ESA (which is used for measuring the centre-of-mass kinetic energy release) is $\Delta E/E$ and for a particular value of ΔE is greater at lower total energy E. For the fragmentation of DCl^{2+} into D^+ and Cl^+ the D^+ fragment had only $2E/37$ of the initial beam energy while the Cl^+ fragment has $35E/37$, it was therefore preferable to measure D^+ fragments if kinetic energy releases were to be measured. Conversely, for measuring spectra obtained by drift tube scans it was preferable to monitor Cl^+ fragments, as more were collected. Further details of ion beam transport properties are now discussed.

2.2.6 *Interaction Region*

To improve the ion transport from the source to the detector, the interaction region contains entrance and exit lenses. The drift tube is placed between the

two lenses and in order for the absorption of a photon to be detected, the absorption must occur within the drift tube.

The drift tube was constructed from a mesh of non-magnetic stainless steel wound around and braised onto two metal rings of 4 cm diameter and supported between lens 2 and lens 3. The principal purpose of the drift tube is to enable Doppler tuning. Doppler tuning is achieved by applying a sweep voltage to the drift tube of up to $\pm$ 500 V. This has the effect of accelerating or decelerating the ion beam and leads to a change in the effective frequency experienced by the ions. The effective frequency is given by the relativistic Doppler equation (see for example [110]),

$$\frac{\nu_{ion}}{\nu_{laser}} = \left(\frac{1 \mp \frac{u}{c}}{1 \pm \frac{u}{c}} \right)^{1/2},$$

Where ν_{ion} is the frequency experienced by the ion beam, ν_{laser} is the frequency of the laser beam, u is the speed of the ion beam and c is the speed of light. The upper signs refer to the laser beam and ion beam co-propagating (parallel), whereas the lower signs refer to the beams counter-propagating (anti-parallel). The transmission of the ion beam into the drift tube, and of fragment ions from the drift tube, is maximised using ion lenses.

The ion source, the magnet and the ESA have characteristic focusing properties, which formed the initial focusing elements around which the ion optics were designed. The ion optics were designed to transmit the desired molecular dications to the interaction region, focus them in coincidence with the laser beam, and efficiently transmit the fragment ions through the ESA to the detector.

Ion lens 2 is an Einzel lens positioned between the magnetic analyser and the drift tube. The function of lens 2 is to augment the focusing and deflection of the magnetic analyser. It consists of a pair of y and z direction half-plates. The y-plates deflect the ion beam, with a maximum potential difference across the lens of 1 kV (at 10 kV source potential); y-focusing is provided by the magnet.

The z-plates deflect the ion beam and focus it at the centre of the drift tube; each plate is separately supplied with a potential of 0 to -10 kV (at 10 kV source potential).

Ion lens 3 is a mirror image of ion lens 2. It is positioned between the drift tube and the electrostatic analyser. Although lens 3 is a mirror image of lens 2, different voltages are provided to lens 3 in order to maximise transmission of photo fragment ions (which have a different mass to charge ratio to the parent ions) through the ESA. When used, the Electric Field Dissociation Lens (EFDL – for details see later) is attached to the magnet-side of Lens 3.

2.2.7 *Detector*

Due to the wide range of ion currents which need to be measured with this spectrometer, from an intense parent beam of singly charged ions to the smaller fragment beam from a molecular dication, a detector containing both a Faraday cup and an electron multiplier arrangement was used. This is a commercial “off-axis” detector system taken from a VG ZAB 1F mass spectrometer. The Faraday cup is on-axis with the ion beam and is used to monitor the parent ions. The fragment ions are monitored with an off-axis electron multiplier (Thorn 119 EM) working in conjunction with a negatively biased aluminium deflector plate. The total gain achievable with the electron multiplier system is typically 10^5.

2.3 Infrared Laser and Optics

Spectroscopy is achieved by the interaction of our ion beam with a suitable radiation source. For the experiments described here that source was an infrared laser beam, and there follows a description of the properties of the laser and the optics used to bring it into coincidence with the ion beam.

2.3.1 *Infrared Laser*

An Edinburgh Instruments PL3 continuous wave infrared laser was used as the light source in the spectrometer. The PL3 uses either CO or CO_2 (naturally occurring or isotopically substituted) as the lasing medium but in all studies at Newcastle was used only with CO_2. The PL3 is line tuneable and with CO_2 lases over the 880-1090 cm^{-1} range. Adjacent lines are typically separated by 1 to 2 cm^{-1}. In order to achieve large output powers a larger than standard bore laser tube was used (internal diameter 2.5 cm); typical output powers with CO_2 were between 2 and 20 W constant wave. The large bore tube causes the laser to work in a combination of TEM_{01} and TEM_{10} rather than TEM_{00} but this was not important for our purpose. The laser power transmitted to the spectrometer could be lowered with a beam attenuator constructed from graduated reflectivity germanium. Output powers were measured with a thermoelectric detector (Coherent Model 201 or Photon Control 25-S). The laser line in use was monitored using a spectrum analyser (Optical Engineering Model 16-A CO_2).

At the output coupler of the laser the beam was 7.5 mm in diameter with a divergence of 3.5 mrad (full angle). Different longitudinal modes were separated by 84 MHz, the linewidth of infrared CO_2 transitions at 300 K is 5 GHz (0.2 cm^{-1}) and the linewidth of the laser was set by the diffraction grating response to 1 MHz ($3x10^{-5}$ $cm^{-1)}$ [38].

2.3.2 *Laser Beam Steering and Focusing*

The laser beam was required to pass between the two zinc selenide entry and exit windows, 170 cm apart, and to be brought to a focus in the centre of the drift tube. The zinc selenide entry and exit windows were anti-reflection coated rather than set at Brewster's angle. Beam focusing was achieved using a ZnSe lens (anti-reflection coated on both sides) of 0.916 m focal length placed at distance 1.35 m from the output coupler and 0.45 m from the magnet-end window. Beam steering was accomplished by solid molybdenum mirrors, which have the advantage of high durability and a high reflectivity (>98%) at 10.6 μm.

2.4 Instrument Control and Data Collection

The spectrometer was controlled by setting voltages at an instrument control panel (modified from a standard VG ZAB 1F console) and via a personal computer. All static instrument settings could be manually controlled. When a spectrum was recorded relevant parameters were set from a computer program written in FORTRAN on an IBM compatible PC. Part [58] of the control code was written by Y. D. West in her PhD thesis at the University of Southampton in 1995; part [111] was written by C. Le Sech, and part [112] by R.C. Shiell in his PhD thesis at the University of Newcastle upon Tyne in 1995. Further code was added [113] by Andrew D.J. Critchley in 1999 to control the microwave equipment required for the work described in chapter 4. The production, steering and focusing of the ion beam for this work; along with signal optimisation and processing were controlled by Alan N. Hughes.

DC voltages to control the instrument are derived from an external interface (Biodata Microlink 3000) controlled via an IEEE-488 bus (a schematic of the modules involved in instrument control and data acquisition is given in figure 2.2).

Control voltages of 0 to 10 V were amplified as required by the control electronics and transmitted to the spectrometer. The main components of the spectrometer were the ion source (requiring the acceleration voltage V_A and all optimizing potentials), the magnet (requiring current I_B), ion lenses 1, 2 and 3, the drift tube (requiring potential V_T), ESA plates (requiring potentials $\pm V_E$) and the detector (requiring a deflector and multiplier potential). The instrument control is now discussed in some detail.

2.4.1 *Instrument Control*

The currents and voltages which operated the mass spectrometer were amplified from 0 to 10 V control voltages. Most of these control voltages had to be set and scanned in fixed ratios which were set by analogue electronics. Those voltages required in a particular data recording mode were set with either one or two 12 bit Digital to Analogue Converters (hereafter DACs); due to the

fine control required in the control of the source potential (V_A) and the magnet current (I_B) two 12 bit DACs are used to emulate one 18 bit DAC (as shown in figure 2.2). An integer value was found for the required number of bits (from 0...4095) to obtain exactly, or just below, the voltage required. The remainder (if any) is multiplied by 100 and the closest number of bits found for this voltage. Each integer was sent to its respective DAC channel and the outputs added with that from the second channel divided by 100. This allows 409600 steps across the output range, an equivalent resolution of ~18 bits. In principle this should allow a voltage resolution of 0.04 V on 10,000 V, but in reality the linearity of the amplifier and noise pick-up (see below) reduced this to 1 V resolution for the source potential, V_A.

The potential required on ESA plates of radii r_1 and r_2 to transmit an ion of kinetic energy to charge ratio, $KE_{1,2}/q_{1,2}$, along a circular trajectory of radius r_E is given by equation (1).

The ESA therefore transmits fragment ions of mass $m_{1,2}$ and kinetic energy/charge ratio $KE_{1,2}$ / $q_{1,2}$ when the settings of V_A and V_T satisfy

$$\frac{KE_{1,2}}{q_{1,2}} = \frac{2m_{1,2}}{M}(V_A - V_T) + V_T .$$

Thus, it follows that the potentials applied to each of the ESA plates must be

$$V_E \approx \pm\left(\frac{2m_{1,2}}{M}(V_A - V_T) + V_T\right)\frac{(r_2 - r_1)}{r_E};$$

when either V_A or V_T are scanned this ratio was maintained by analogue electronics with the ratio $m_{1,2}$ /M set by a voltage division using a ten turn potentiometer.

The potentials to the ion lenses were set manually by ten turn potentiometers using the lens control unit which housed eight 0 to -10 kV high voltage amplifiers (Applied Kilovolts HP10N). The voltages applied to the plates were scaled in proportion to the source voltage. In lens one the maximum voltage available to each plate was -V_A. In lenses 2 and 3 the maximum voltage available to the y (deflection) plates was ±V_A/20, and the maximum voltage

available to each z (focus and deflection) plate was $-V_A$. The potentials to the ESA plates were derived from two opposite polarity high voltage amplifiers (Applied Kilovolts HP2.5N and HP2.5P). In principle the potentials to lens 3 should have been scaled by V_T as well as V_A, but no noticeable detuning of the fragment beam occurred over a drift tube scan of 500 V.

2.4.2 *Data Acquisition*

Spectral absorption intensities were measured by monitoring the ion fragments that were selected with the ESA. These were detected with an off-axis Thorn 119EM windowless 17 stage venetian blind electron multiplier, working in conjunction with a negatively biased deflector plate. The collector control unit determined the potential of the deflector and the voltage drop, and therefore the gain, of the electron multiplier. A gain of 4×10^4 for a beam current of 3.8×10^{-10} A was typical. The signal current from the electron multiplier was converted to a signal voltage by a preamplifier (Brookdeal 5002) and the signal voltage was processed by a lock in amplifier (Stanford Research SR530). Amplitude modulation of the laser beam (and hence signal) was accomplished with an optical chopper (Stanford Research SR540) which was typically run at 333 Hz to avoid harmonics of the mains frequency (50 Hz).

2.4.3 *Data Types*

Three types of spectra were routinely recorded, mass spectra, kinetic energy spectra and frequency spectra. These are now described.

a. Mass Spectra.

Mass spectra were obtained in one of two ways. Either the ion source potential (and therefore the kinetic energy of the ions) was scanned in conjunction with the ESA (set to transmit parent ions) at a fixed magnetic field or the magnetic field was scanned while the ion source potential and ESA potential (set to transmit parent ions) remain fixed.

b. Kinetic Energy Spectra.

The kinetic energy of fragment or parent ions was measured by scanning the ESA voltage with the source potential, drift tube potential and the magnet current fixed; this could be accomplished with or without a spectroscopic transition in resonance. With a spectroscopic transition in resonance the signal was taken from the lock-in amplifier and the kinetic energy spectrum obtained gave information on the upper dissociation channel involved in the transition. Without a spectroscopic transition in resonance the kinetic energy spectrum resulted from fragments due to predissociating energy levels and collision induced dissociation. Measurement of a fragment kinetic energy release was best achieved by observing both the forward and backward scattered fragments due to dissociation and setting the zero centre-of-mass kinetic energy release mid-way between them.

c. Frequency Spectra using laser excitation

If the radiation was supplied using a laser, frequency spectroscopy was achieved by applying a scanning voltage to the drift tube with the ion source and magnet set to transmit the parent ion beam to the drift tube and the ESA set to transmit fragments from the drift tube to the detector. As the drift tube voltage was scanned, analogue electronics (see above) maintained the necessary ESA voltage for transmission of the fragment ions. With V_A set to 6000 V and a laser excitation at 1000 cm^{-1} a drift tube scan of 500 V corresponded to a scan of 0.035 cm^{-1} for DCl^{2+} ions.

2.5 Molecular Properties, Mass Spectrometry, Kinetic Energy Spectroscopy and Frequency Spectroscopy

I now consider the properties of molecular dications and their measurement by kinetic energy spectroscopy and frequency spectroscopy. I first consider how the measurement technique constrained which molecular states could be measured and then I discuss the spectroscopic resolution and sensitivity that could be achieved for mass spectrometry and kinetic energy and frequency spectroscopy.

2.5.1 *Molecular Properties*

Consider the possibilities shown in figure 2.3, below, for the fate of an AB^{2+} ion in a quasibound state (v'',N'') in conjunction with a photon with frequency equal to that of a resonant transition between the initial state and a second state (v',N').

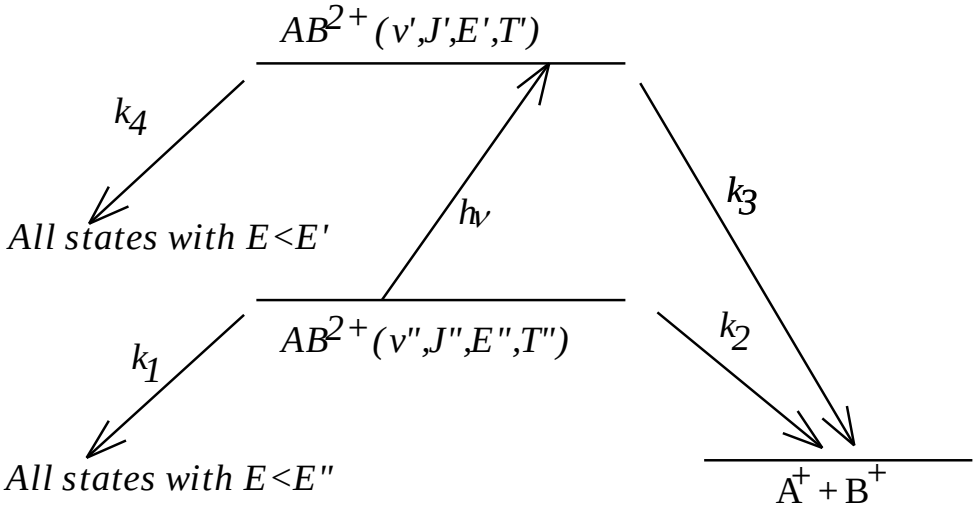

Figure 2.3

Possible outcomes for dication AB^{2+} illustrating the rate processes that need to be taken into account in assessing which transitions will be accessible to the experiment. k_1 and k_4 are the total rates of spontaneous transition to the manifold of states with energies below that of the initial state and second state respectively and k_2 and k_3 are the corresponding total rates of spontaneous and induced dissociation into the ionic fragments (assuming only a single open channel). (*Reprinted from Review of Scientific Instruments, Vol. 73, No. 2, Ramadan Abusen, Simon G. Cox, Andrew D. J. Critchley, Alan N. Hughes, Faye Kemp, Iain R. McNab, Ralph C. Shiell, and Fiona E. Smith, "Coaxial ion beam/infrared laser beam spectrometer for investigating infrared spectra of doubly positively charged molecules (molecular dications)", Pages 241-254, Copyright (2002), with permission from A.I.P. Publishing LLC.)*

In order for the transition of interest to be observed, the initial state must survive long enough to interact with the laser beam. Its lifetime (T'') against both radiative decay and dissociation must therefore be greater than the total time of flight from the source to the interaction region, a distance of l = 1.5 m. The

limitation on the lifetime of the initial state for ions of mass m and charge q, accelerated to a beam potential, V_B, becomes:

$$T'' = \frac{1}{k_1 + k_2} > l\sqrt{\frac{m_p}{2q_p V_B}}$$

Assuming the ions were extracted from the ion source in a time of the order of 1 μs, for the case of DCl^{2+} ions the smallest typical source potential of 1 kV restricts the total limiting lifetime of the initial state to be greater than 13 μs.

Once transferred to the final state, spontaneous or induced dissociation (determined by k_3), and not decay (determined by k_4), must have occurred before the end of the drift tube (at distance 0.3 m away) was reached. For spontaneous dissociation the limiting case for any dissociation was where the source potential was 1 kV, resulting in $1/k_4$<0.85 μs. An estimate of which levels might be probed in this fashion can be made by assuming it will be those with a natural dissociation lifetime of $1/k_4$<10 μs. Significant relaxation of the upper level to the manifold of lower states must not have taken place within the drift tube restricting $1/k_3$>4.4 μs.

A further restriction on those observable transitions comes from the natural energy width associated with all states of finite lifetime. When this is much larger than the energy scanning range of a particular scan the change in the number of fragment ions produced, and therefore the transition itself, would not be recorded. For instances where the upper level lifetimes were so short as to yield natural linewidths in excess of 500 MHz or so, it was not possible for us to observe a transition by a voltage scan. Such lines could be observed by observing photodissociation yields at more widely spaced frequencies, by measuring relative photodissociation rates at several combinations of laser line and beam potential (see for example Carrington et al. [114]).

For the relativistic Doppler equation when v<<c, a scan from an initial to a final source potential, $V_{B,1}$ to $V_{B,2}$ covers a frequency range

$\Delta\nu = \frac{\nu_0}{c}\sqrt{\frac{2q_p}{m_p}}.\left(\sqrt{V_{B,1}} - \sqrt{V_{B,2}}\right)$,which for DCl^{2+} ions gave a maximum scanning range of $\pm$0.13 cm^{-1} about each laser line. Using the energy-time uncertainty principle, this limits the total rate of decay from the upper state to,

$$\frac{1}{k_3 + k_4} > 3.62 \times 10^{-11}\ s\,,$$

giving the total lifetime limit on upper states observable to be >36ps.

2.5.2 *Mass/Charge Resolution of the Magnetic Sector*

Barber's rule [115] shows that the ion beam is focused by the magnetic analyser to a point that lies along a straight line joining the centre of the analyser radius and the object focal point; this assumes the ion beam is monoenergetic and is valid to first order. In a conventional mass spectrometer a second slit is placed at the natural focus of the magnet.

The resolving power of the magnet is the reciprocal of the minimum Δm/m that can be resolved. Our apparatus used a source exit slit of 1 mm width and the only apertures that restricted the beam that emerged from the magnet were of 8 mm width and were in lens 2 and lens 3 - neither of which was at the natural focus of the magnet. Consequently the instrument had a very low mass resolving power (experimentally found to be 70). The extremely large "slits" were used to maximize transmission of the ion and laser beams, and as described below the instrument was not always used in the optimum geometry for the ion beam focusing properties.

2.5.3 *Kinetic Energy Resolution of the ESA*

The kinetic energy release on dissociation of the excited state is characteristic of the molecule and its internal energy. Our resolution was not sufficient to distinguish vibrational or rotational states in a kinetic energy spectrum. For DCl^{2+} the maximum resolution that was achieved (monitoring D^+) was a lab frame kinetic energy resolution of ΔE/E=15/850. The centre of mass kinetic energy release was obtained by the transformation given above and is

quadratic - small kinetic energy releases can be measured more accurately than large kinetic energy releases, as may be seen from the centre of mass kinetic energy release scale on figure 2.4 below. The major problem with such a spectrum is where to measure the kinetic energy release on the line shapes; two possible values are shown in figure 2.4, corresponding to line centre (4.9 eV energy release) and half-way down the outside edge (6.0 eV energy release). The best way to determine the kinetic energy release would be to make a monte-carlo simulation of the apparatus.

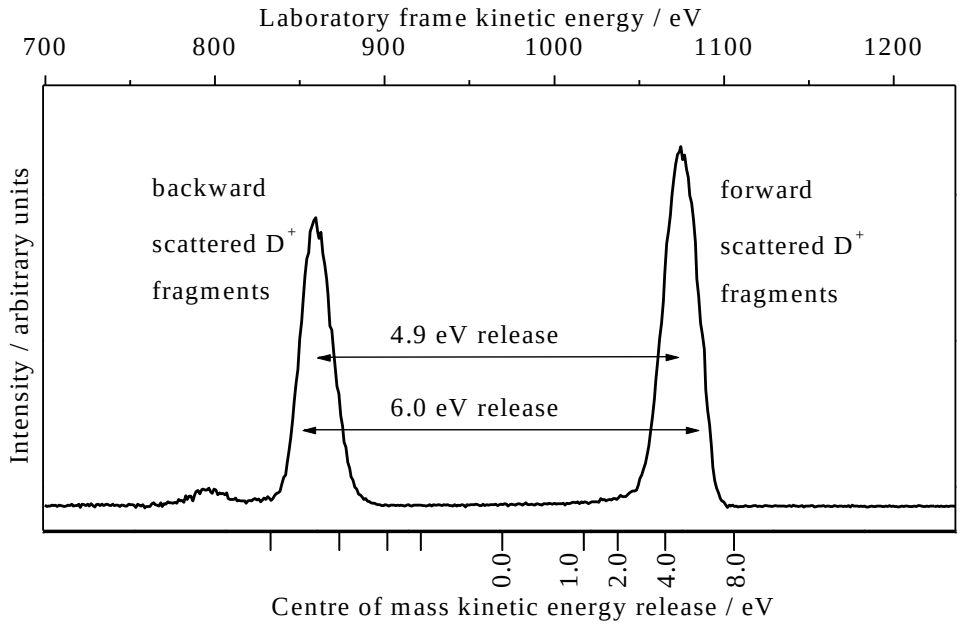

Figure 2.4

A typical ESA spectrum for D^+ ions which arise from the upper state of a resonant transition in $D^{35}Cl^{2+}$. Forward and backward scattered D^+ fragments are seen; the transformation from lab frame kinetic energy to centre of mass kinetic energy release is illustrated by the upper and lower scales. (*Reprinted from Review of Scientific Instruments, Vol. 73, No. 2, Ramadan Abusen, Simon G. Cox, Andrew D. J. Critchley, Alan N. Hughes, Faye Kemp, Iain R. McNab, Ralph C. Shiell, and Fiona E. Smith, "Coaxial ion beam/infrared laser beam spectrometer for investigating infrared spectra of doubly positively charged molecules (molecular dications)", Pages 241-254, Copyright (2002), with permission from A.I.P. Publishing LLC.)*

2.5.4 *Frequency Resolution of the Spectrometer*

The Doppler linewidth of the ion beam represents the most important factor in determining the resolution of the experiment. However, in a fast ion beam, a narrowing of the linewidth takes place (S.L. Kauffman [116]). This is known as “kinematic compression” or “velocity bunching”; if two ions having the same mass, but differing velocities, are accelerated by an applied potential then the spread in the final velocities along the direction of acceleration (and hence the Doppler width) is much reduced. In our experiment the Doppler linewidth was governed by the energy spread of the ions emerging from the ion source and by fluctuations in the accelerating potential rather than the thermal velocity spread in the ion beam. The kinetic energy spread in the ion beam extracted from the ion source could be as much as 2 to 10 V for the source that was employed.

The width of a collinear resonance can be expressed as

$$\Delta\nu_{ion} \approx \nu_{laser}\left(\frac{q}{2mc^2}\right)^{1/2}\frac{\Delta V}{V_B^{1/2}},$$

Where ΔV is the energy spread in volts and V_B is the beam potential. Therefore the higher the beam potential, the narrower will be the Doppler width. This has the effect of yielding spectra of high resolution. For $D^{37}Cl^{2+}$ at V_B = 5000 V a spread in ion energies of 5 V yields a Doppler width of 11 MHz at 1000 cm^{-1} excitation; similarly for H_2^+ at V_B = 2000 V a spread in ion energies of 5 V yields a Doppler width of 0.03 MHz at 0.56 cm^{-1} (17 GHz)

Another factor which influences the linewidth is the divergence, $\Delta\theta$, between the ion and laser beams. In a collinear geometry the maximum width due to the divergence would be

$$\Delta\nu_{ion} \approx \nu_{laser}\left(\frac{qV_B}{2mc^2}\right)^{1/2}(\Delta\theta)^2.$$

A careful alignment of the laser beam was necessary in order for it to enter and leave the spectrometer through the two zinc selenide windows. This ensured that the laser beam was kept to within a few milliradians of the ion beam axis. The maximum divergence of the ion beam in the interaction region is

determined by the entrance and exit apertures of the drift tube in which the interactions take place and the distance between them. In our experiments with DCl^{2+} this gave a worst case divergence of 0.025 radians and a corresponding Doppler width of 7 MHz at 5000 V beam potential and 1000 cm^{-1} excitation.

2.5.5 *Example - Infra-red Spectra of DCl^{2+}*

Part of the spectrum of DCl^{2+} is shown in figure 2.5. With the ion source and ion optics used the frequency coverage that could be obtained using Doppler tuning about the individual lines of the CO_2 laser was about 50% of the range from 880 cm^{-1} to 1090 cm^{-1} for $D^{35}Cl^{2+}$. Typically data was recorded using drift tube scans of ±500 V at source potentials stepped in 1000 V increments from 500 V to 9,500 V. The infrared spectrum that is shown in figure 2.5 was obtained using a drift tube scan of 300 V.

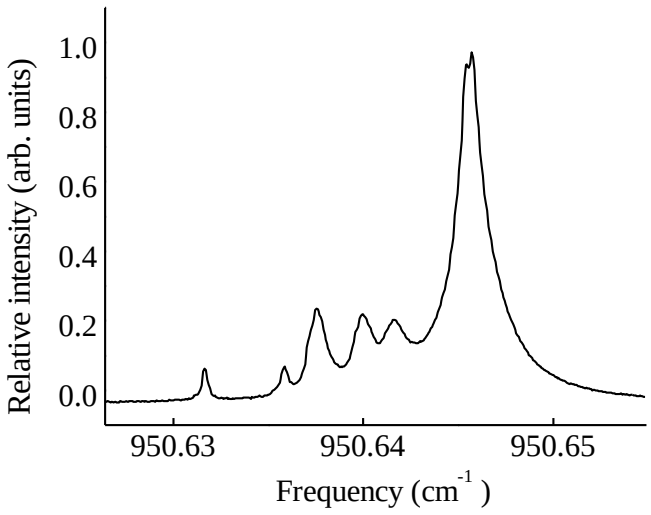

Figure 2.5

Part of the infrared spectrum of $D^{35}Cl^{2+}$. The spectrum shown was recorded by scanning the drift tube by 300 V at a source potential of 3,050 V using the $^{12}CO_2$ laser line P(12) at 951.1923 cm^{-1}. The structure observed is a single fine structure component of the ν=2←1 vibration-rotation band; the six lines are due to resolved ^{35}Cl (**I**=3/2) nuclear hyperfine structure. (*Reprinted from Review of Scientific Instruments, Vol. 73, No. 2, Ramadan Abusen, Simon G. Cox, Andrew D. J. Critchley, Alan N. Hughes, Faye Kemp, Iain R. McNab, Ralph C. Shiell, and Fiona E. Smith, "Coaxial ion beam/infrared laser beam spectrometer for investigating infrared spectra of doubly positively charged molecules (molecular dications)", Pages 241-254, Copyright (2002), with permission from A.I.P. Publishing LLC.)*

2.6 Calibration, Stability of Operation, Sensitivity and Dynamic Range.

I now discuss the calibration of the beam voltage, which translated directly to the final accuracy of absolute frequency measurements using infrared laser excitation. I also consider the long term stability of the instrument, the spectroscopic sensitivity that was achieved, and the dynamic range of the signals that were detected.

2.6.1 *Beam Potential Calibration*

In commercial reverse geometry double focusing mass spectrometers, the beam potential, V_B, is crudely set by the acceleration potential applied to the ion source, V_A, and then adjusted with a fine control until the maximum beam current is transmitted by the electrostatic analyser which has been set to pass the parent ions at the desired beam energy (that is $V_B = V_A \pm \delta V$). In our apparatus the resolution of the ESA was deliberately degraded by using 1 cm entrance slits in order to maximize transmission of the ion beam and this method was not accurate.

The ion beam potential was therefore assumed to be determined by the source potential (that is $V_B = V_A$). The true beam potential of the ion beam, V_B, is slightly less than the potential sent to the source as a result of penetration by the earth's field into the ion source, but is also affected by the potential applied to the repeller plate (which may be positive or negative), the potential due to the electron beam passing down the axis of the ion source and contact potentials between different metals within the ion source. The true beam potential, V_B, therefore depends upon a variety of source parameters, and I consider it to be equal to V_A ±50 V; this represents a semi-random uncertainty in beam potential of ±50 V which corresponds to uncertainties in absolute infrared transition frequencies of about 0.003 cm^{-1} (90 MHz) at a beam potential of 5000 V. This was the limiting uncertainty on infrared measurements. However, where it was possible to record lines on a single voltage scan (as in hyperfine resolved transitions), the frequency separations between lines are determined to the accuracy with which they can be fitted, that is to about 2 MHz.

The source voltage, V_A, was supplied by a high voltage amplifier (Wallis 10 kV). Calibration of the source voltage showed that the greatest difficulty in setting the voltage arose from amplified 50 Hz pick up, rather than from the digital resolution of the signal. This was in spite of “common mode” amplification of the signal. As it was unnecessary to sweep the source voltage rapidly the 50 Hz pick up was eliminated by placing a high capacitance across the feedback resistor of the input stage of the amplifier. This reduced the noise level below 1V at 10 kV which was below the limit at which effects on the frequency spectrum were observable. The source voltage was calibrated directly using a digital meter. The other potentials which needed to be calibrated in the experiment were the drift tube potential and the ESA potential difference, which I now discuss.

a. Drift Tube Potential

The drift tube potential was set by a high voltage (times-fifty) amplifier; the input voltage to which was supplied either from a potentiometer, or from a 12 bit DAC. The final potential of up to ± 500 V was monitored directly using a digital voltmeter and could be set accurately to 0.1 V at 500 V (12 bit resolution), with good linearity.

b. ESA Potential Difference

The 0 to 10V ESA control potential was set either from a potentiometer, or from a 12 bit DAC. The 0 to ± 2.5 kV ESA potentials were monitored using a permanently connected potential divider which provided a 0-10 V output that was used to monitor either the potential supplied to each plate separately, or the difference between them, using a 5 digit display digital voltmeter. The display was calibrated directly using a 5 digit 0 to 1000 V dc digital voltmeter.

2.6.2 *Stability in Operation*

It was found that the ion beam spectrometer, once tuned up, was stable for two to three days, after which a noticeable (>10%) drop in fragment beam current was experienced. This was critical to the success of our microwave measurements, described in chapter 4. However, the principle limitation on the length of our infrared experiments was the power stability of the PL3 laser which lases on a single longitudinal mode and which, when used with only passive stabilisation, had output power fluctuations as great as 50% over a period of a few hours; this did not normally represent a problem as most of our spectroscopic scans were achieved within 20 minutes or so. If longer times were required for recording spectra active power stabilization of the PL3 laser could be provided from an optogalvanic feedback system (EI209 laser stabilizer) which provided an amplitude stability of about 1%. The PL3 laser has a frequency stability of 1 MHz or 3.34×10^{-5} cm^{-1} over a 10 minute period.

2.6.3 *Signal to Noise Ratio*

At high laser powers our infrared spectral lines were saturated. The PL3 laser was capable of producing output powers in excess of 20 W but for DCl^{2+} high laser powers led to saturation and broadening of the transitions and were therefore counter-productive in measuring relative line intensities. Laser powers of 5 mW were sufficient, in most cases, to provide a satisfactory level of absorption leading to S/N of 300 or 400 on strong lines. I now consider separately the noise and the signal and show, using a combination of measured and calculated parameters, that for the DCl^{2+} spectrum the maximum possible signal/noise ratio for this type of experiment was achieved.

a. Noise

There were a number of contributions to the noise levels in this experiment that could be categorized as either short-term or long-term noise effects. The long term noise effects were dealt with under the heading of stability above and are not important on the timescale of a typical infrared spectral recording (about 20 minutes). Short term noise effects were due to interference from external

electromagnetic signals and to the properties of the signal itself. The most important short term noise effect is the shot noise of the fragment ion beam (as magnified by the electron multiplier) which is the limiting noise background that cannot be reduced.

The shot noise current is given by the usual formula [117] as

$$I^{noise} = \sqrt{2eI^{background}\Delta f},$$

where Δf is the bandwidth of the measurement electronics (and is equal to the reciprocal of the measurement time), e is the electron charge and the relevant currents are proportional to the number of charge carriers per second

($I = N(s^{-1})e$). More usefully the shot noise measured as ions per second,

N^{noise} s^{-1}, is therefore determined from the off-resonance fragmentation rate,

$N^{background}$ s^{-1} as:

$$N^{noise} = \sqrt{2N^{background}\Delta f},$$

and $N^{background}$ s^{-1} is the off-resonance number of fragments per second.

The fragment ion beam was monitored using an electron multiplier; which increased the signal by, G the gain of the multiplier. The resultant shot noise of this amplified signal had increased by about $1.05G$ (the factor of 1.05 comes from the behaviour of the electron multiplier). The current from the electron multiplier was passed through a transimpedance amplifier that provided a voltage level proportional to the fragment ion beam current, but the signal level was so great that the thermal noise of the amplifier was negligible in comparison with the shot noise. Electromagnetic interference could contribute to the noise levels on the signal, but these effects were largely avoided by using careful screening and lock-in-amplification.

The noise in a spectrum allowed an absolute value to be put on the total number of fragments detected, provided the background number of fragments per unit time and the measurement bandwidth were known. As both the noise and the signal were processed by the same electronics they underwent

essentially the same gain. The background number of fragments per unit time could either be measured directly or calculated from the properties of the ion and a knowledge of the total ion beam current.

b. Signal

The intrinsic intensity of a ro-vibrational transition (a measure of its strength that is unrelated to the populations of the relevant levels) is given by:

$$I(v', J'; v'', J'') = \sum_{M', M''} \left| \langle v', J', M' | d(R) | v'', J'', M'' \rangle \right|^2$$

Where $d(R)$ is the electric dipole moment of the molecule in the electronic state in question and depends upon the internuclear separation, R. While $d(R)$ is identically zero for homonuclear molecules at all R (provided hyperfine effects are ignored) this function can be calculated ab-initio for all polar molecules, and such a calculation was been made for DCl^{2+} by McNab and Bennett [118]. $I(\nu',J';\nu'',J'')$ is directly related to the integrated intensity (the area beneath a spectral line) [119] and can be compared to the total excitation rate of a two-level molecule when illuminated by low intensity broadband light. For incident spectral energy density (energy per unit volume per unit frequency range) of $\rho(\nu)$, the transition rate per molecule per state is [119].

$$R = I(\nu', J'; \nu'', J'')\rho(\nu)\frac{2\pi^2}{3\varepsilon_o h^2} \quad s^{-1}$$

This leads to an excitation rate (total number of molecules that are excited per second per unit volume) given by

$$\frac{dN}{dt} = \left(\frac{N_l}{g_l} - \frac{N_u}{g_u} \right) I(v', J'; v'', J'')\rho(\nu)\frac{2\pi^2}{3\varepsilon_0 h^2}$$

Where N_l and N_u are the initial numbers of molecules per unit volume in the lower and upper states (with degeneracies g_l and g_u).

A full calculation of the expected signal (total number of signal ions collected due to a transition) in a general case would be quite involved and would require the following steps

1. The number of fragment ions formed at each position in the drift tube would be calculated, together with the probability of their being transmitted through the ESA to the detector (this requires a knowledge of the fragmentation rate, ion beam velocity and density as a function of position in the drift tube and subsequent focusing conditions between the drift tube and the ESA).

2. To calculate the number of fragment ions formed at each position in the drift tube would require a calculation of the decay rate from the final state as a function of drift tube position. A full calculation of coupled rate equations including decay from both initial and final states and population oscillation between them would be necessary if the reciprocal of the transition rate were close to the time of flight through the drift tube, as this leads to observable Rabi oscillations [103]. This in turn would require a knowledge of the spectral energy density $\rho(\nu)$ at each position in the drift tube (that is of the laser beam power and profile), and the population density difference $\left(\frac{N_l}{g_l} - \frac{N_u}{g_u}\right)$ at each position in the drift tube and the overlap between them.

For the case of DCl^{2+} such a detailed calculation was not necessary as the upper state (which dissociates quickly) was assumed to start with no population and any excitation from the (much longer lived) lower state to the upper state resulted in fragmentation. The following formula can therefore be used to describe the total number of fragments detected per second when parent molecules in the drift tube were irradiated for a time t_{dt} (given by the length of the drift tube divided by the velocity of the parent ions),

$$\frac{dN(t_{dt})}{dt} = C.F.\left(\frac{N_l}{g_l}\right) I(\nu', J'; \nu'', J'')\rho(\nu)\frac{2\pi^2}{3\varepsilon_0 h^2} t_{dt},$$

The relevant volume is the overlap between the ion beam and laser beam within the drift tube, but it appears on both sides of the equation and does not

contribute to the final result. $\left(\frac{N_l}{g_l}\right)$ is the number of molecules in each lower state per second (directly determined by the parent ion current) which are irradiated by the laser beam for a time t_{dt}. F is a form factor which describes the average effect of merging the ion beams and laser beams (=1 in the ideal case) and C represents the average collection efficiency for fragments formed in the drift tube.

c. Signal to Noise Ratio

The ratio of the on-resonance signal rate (that is number of fragments formed per second due to the laser beam) to the off-resonance shot noise rate provides a (dimensionless) value for the instrumental signal to noise of a particular transition in this experiment. As expected this depends upon the residence time of parent molecules in the drift tube, the parent and background fragment ion beam currents and the square root of the measurement time (the reciprocal of the square root of the measurement bandwidth, $\sqrt{1/\Delta f}$):

$$\frac{Signal}{Noise}(t_{dt}) = \frac{C.F.\left(\frac{N_l}{g_l}\right) I(v', J'; v'', J'')\rho(\nu)\frac{2\pi^2}{3\varepsilon_0 h^2} t_{dt}}{1.05\sqrt{2N^{background}\Delta f}}.$$

This expression relies on two assumptions: that the transition does not saturate (the molecules in the upper state are assumed to dissociate faster than any population can build up in that state) and that the overlap between ion and laser beams can adequately be described by the simple number F. In reality the signal maximum is given by the number of ions present in both upper and lower states at the beginning of the measurement, and no increase in transition rate can overcome this.

d. *Comparison of Calculated and Measured Signal to Noise Ratio for One Transition*

Using the above expression I now compare a measured signal in the DCl^{2+} spectrum with the *ab-initio* calculations of the properties of DCl^{2+} (McNab and Bennett, 1996) [118]. The transition I compare is assigned as the $D^{37}Cl^{2+}$ transition R(17) of the $\nu=2\leftarrow1$ of the $X^3\Sigma^-$ state (F. E Smith, PhD T thesis, 2000) [120]. The experimental measurement gave a signal (area under peak) to noise ratio of 589. The area under the peak is the total number of signal fragments collected. This was accomplished using a beam of $D^{37}Cl^{2+}$ of $1.3\text{x}10^{-10}$ Amps against a background off-resonance fragment current of 10^{-13} Amps (that is $N_{background} = 3.12 \text{ x } 10^5 s^{-1}$) using a laser power of 0.03 W and a measurement bandwidth of 4 Hz (this bandwidth is for each drift tube voltage, 512 measurements were taken across the spectrum with a resulting frequency separation between each measurement of 2 MHz; this is exactly equivalent to making a single measurement across the same total frequency range using a white light source with the same spectral energy density). The upper state tunnelling lifetime was calculated to be $1.5\text{x}10^{-9}$ s, compared with the residence time in the drift tube of $t_{dt} = 2.5\text{x}10^{-6}$ s (the spectrum was taken at a beam potential of 5835 V, which corresponds to a velocity of $2.4\text{x}10^5$ ms^{-1} for $D^{37}Cl^{2+}$; the drift tube was of length 60 cm) and all $D^{37}Cl^{2+}$ ions excited into the upper state while resident in the drift tube therefore dissociated almost immediately after excitation.

The collection efficiency C is determined by the degree of divergence of fragments from the parent beam. Taking the case of DCl^{2+} fragmenting at the start of the drift tube (a worst case for collection efficiency) the fragment must then travel 60 cm to the entrance of the ESA which has a 1 cm aperture. If the divergence were more than 1.0^o over this distance then the fragment ion would not enter the ESA and would not be detected. The worst case fragment divergence is when the fragment velocity (Centre of mass) is perpendicular to that of the parent beam (Lab frame), that is

$$\varphi_{divergence} = \tan^{-1}\left(\frac{v_{Cl^+(CofM)}}{v_{DCl^{2+}(Lab)}}\right),$$

For Cl^+ fragments with a kinetic energy release of 4.5 eV from $D^{37}Cl^{2+}$ the worst case divergence angle, φ, =1.1^0 and almost all fragments will be collected (that is $C \approx 1$ for Cl^+ fragments from DCl^{2+}). It is assumed that the ion and laser beams are perfectly and uniformly merged with uniform densities of photons and ions across the whole drift tube, that F =1 (this is incorrect as both are actually focused in coincidence, but it is a reasonable first approximation).

The number of lower state molecules entering the drift tube per second was calculated from the *measured* ion beam current as follows; the only vibrational levels that have a significant fraction of their population able to survive the trip in the parent ion beam to the drift tube are the v = 0 and v = 1 levels of the $X^3\Sigma^-$ state. The initial population of each state upon ionisation was calculated from the Franck-Condon factors from the neutral molecule $D^{37}Cl$. Calculations then showed how each level was depleted by tunnelling and radiative decay into the ground state during the time taken to reach the drift tube to arrive at the final fractions of the total beam current on entry to the drift tube. For v = 1 the fraction of the total beam entering the drift tube was calculated to be 43.5% with the remaining population in v = 0. Allowing for the Boltzmann distribution of the v = 1 population over rotational levels (at the ion source temperature) gave a final fractional population in the relevant lower state calculated to be 1.34x10^{-3} of the parent ion beam yielding N_l/g_l = 1.8x10^5 ions per second.

The intrinsic strength of a transition depends on its transition dipole moment, $d(R)$ and the wavefunctions of both states. The dipole moment is a function of internuclear separation, and calculated moments for DCl^{2+} were used in LEVEL [121] to calculate the intrinsic strength of each allowed transition within the $X^3\Sigma^-$ state of DCl^{2+}, the transition of interest was found to have an intrinsic strength of 3.2x10^{-60} C^2m^2 (0.323 $Debye^2$).

Each measurement interval represents a frequency range of 2 MHz, and all the laser power was concentrated in this frequency range. Assuming a cylindrical unfocussed laser beam of 6 mm diameter gave a calculated spectral energy

density of 1.35×10^{-12} $Jm^{-3}Hz^{-1}$, corresponding to a transition rate of about 1.5×10^{6} s^{-1}.

Finally, the signal / noise ratio from the ratio of upper state population to measured noise level is calculated and was found to have a value of

$$\frac{Signal}{Noise} = \frac{\left(1.8 \times 10^{5}\,\mathrm{s}^{-1}\right) \times 18.4}{166\,\mathrm{s}^{-1}}$$

the factor of 18.4 exceeds the maximum possible value of unity, and therefore the calculated signal / noise ratio is 1084, compared with the measured value of 589. Considering that this calculation relied on *ab-initio* calculations of populations (made with the assumption of rotational thermal equilibrium at the ion source temperature), lifetimes and transition strengths this must be considered excellent agreement. The fact that the final calculation of signal to noise ratio was governed solely by the number of ions in the lower state, and the number of fragment ions against which they were detected shows that the apparatus had achieved a sensitivity for a given initial ion current which was the maximum possible in this type of experiment. Greater signals could only have been achieved by using either a larger parent ion beam current, or for weaker transitions, larger laser beam powers.

2.6.4 *Dynamic Range*

For practical purposes when comparing transitions within a particular spectrum the above expression was not used; instead it is possible to define the integrated relative intensity, I_{rel} as a measure of transition strength

$$I_{\mathrm{rel}} = \text{peak area / laser power.}$$

For this to be a valid measure the laser power must be low enough to ensure that transitions are not saturated, that is that I_{rel} is independent of laser power. The same frequency unit of spectral width and same unit of laser power is used for all transitions. The measurement of I_{rel} in this manner is only reproducible to within a factor of 5 or so between different scans. Nevertheless, the strongest

transition for DCl^{2+} that were observed had I_{rel} = 549,780 whereas the weakest transition had I_{rel} = 39 and this measurement was therefore a useful guide to the intrinsic transition strength, and showed that the apparatus was capable of recording transitions over a dynamic range of 10^4.

2.7 Microwave Spectroscopy and Electric Field Dissociation

This section describes work mainly due to Alan N. Hughes and Andrew D. J. Critchley. The Newcastle Fast ion-beam/laser beam spectrometer [100] was modified to enable microwave spectroscopy and electric field dissociation (hereafter EFD) of H_2^+ (see chapter 1 for the theory of EFD). A schematic representation of the spectrometer as it was reconstructed can be seen in figure 2.6. The principle of the experiments is explained in the figure caption.

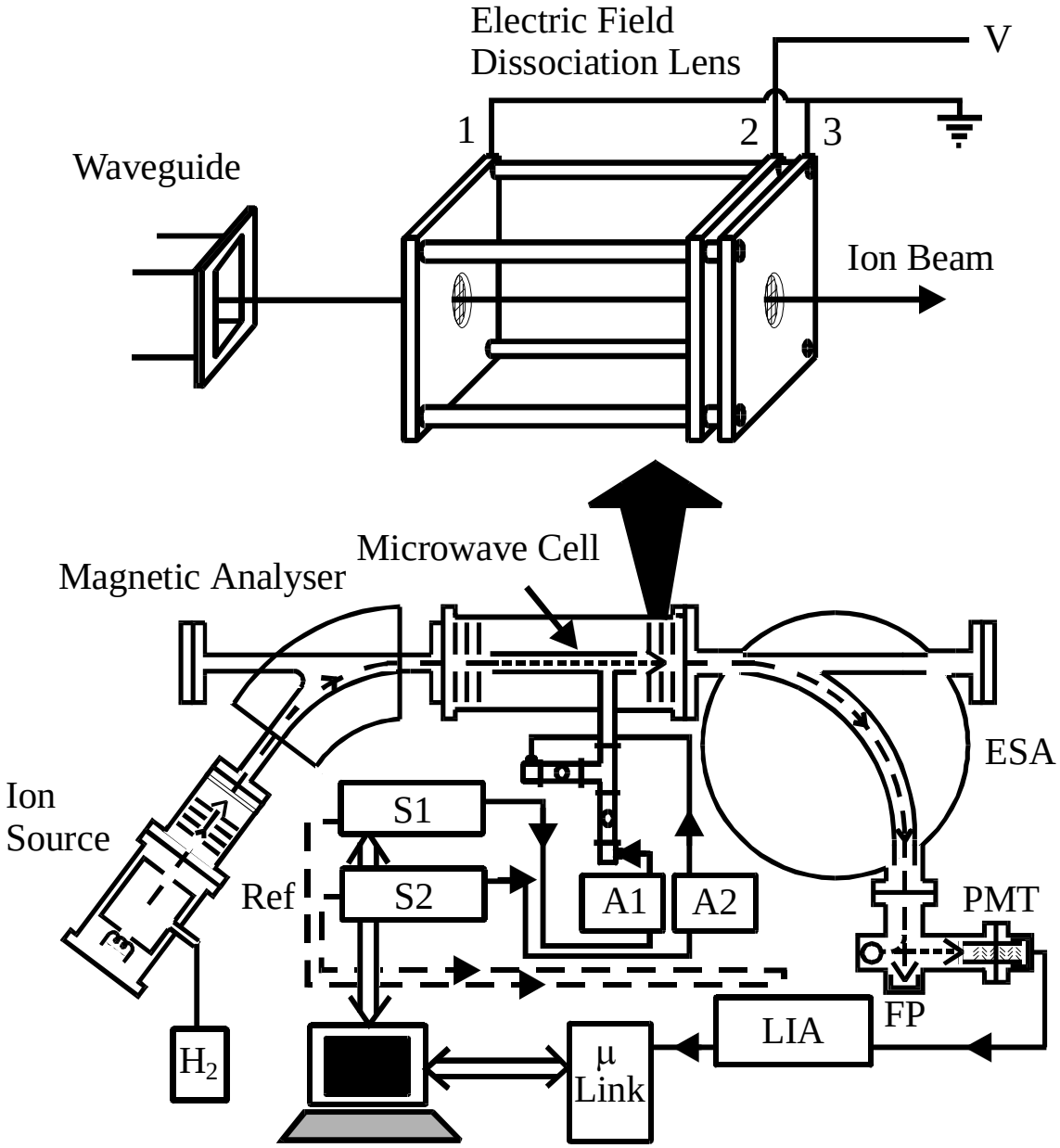

Figure 2.6

Microwave/fast-ion beam apparatus with a detailed view of the end of the microwave waveguide and the electric field dissociation lens. A beam of H_2^+ was selected using the magnet and focused into the microwave cell. Computer controlled synthesisers (S1,S2) provided microwaves that were amplified (A1,A2) and then attenuated to the desired power before being transmitted into the microwave cell. At resonance, population was transferred between levels and the population of one level was monitored by fragmentation induced by an electric field dissociation lens (see detail). Fragment ions were selected with an electrostatic analyser (ESA) and detected with an off-axis electron multiplier (PMT). The microwaves were amplitude modulated and the resultant signal was processed by a lock-in amplifier and passed to the computer controller via a microlink interface (μlink). (*Reprinted from Molecular Physics, Vol. 101, Nos. 4-5, Andrew D. J. Critchley, Alan N. Hughes, Iain R. McNab, and Richard E. Moss, "Energy*

shifts and forbidden transitions in H_2^+ due to electronic g/u symmetry breaking", Pages 651-661, Copyright (2003), with permission from Taylor and Francis Group)

2.7.1 *Overview*

Vibrationally hot H_2^+ ions were formed by electron impact on H_2 gas in a Vacuum Generators "in-line" ion source. The H_2^+ ions were accelerated to 2 or 4 keV (typical H_2^+ beam current $\approx 10^{-7}$ A). H_2^+ was selected with a magnetic sector and focused into a length of rectangular waveguide (WR-62, internal cross section 7.9×15.8 mm).

Microwaves were produced with two synthesisers (Wiltron models 6753B-10 and 6769B) that could be used either in isolation, or together. The power output of the synthesizers was set at 0 dBm* (1 mW) at all times and was directed via coaxial cable (capable of carrying frequencies <40 GHz) to an amplifier (HP 8346A) with a maximum output power of 20 dBm (100 mW). The amplified microwave output was kept at 20 dBm throughout our experiments. The amplified radiation was coupled into waveguide and passed through a mechanical attenuator (for power control) and into the vacuum chamber through a PTFE window (see below for details of construction).

Within the vacuum chamber the microwaves passed via an E-plane T to a 40 cm length of WR-62 waveguide, open at each end, in which interaction with the ion beam occurred. I chose to use WR-62 waveguide because the predicted (19,1) –(19,0) transition frequency was within the range of frequencies where propagation was limited to the fundamental mode, $TE_{0,1}$. After interacting with the microwaves the H_2^+ beam passed into an electric field dissociation lens.

* Power(dBm) = 10 $\log_{10}$ Power(mW)

2.7.2 *Electric Field Dissociation Lens (EFDL)*

Since the vibration-rotation levels concerned are naturally bound, an electric field dissociation lens (EFDL), situated between the microwave cell and the electrostatic analyser, was used to fragment the ions via a Stark perturbation of the potential energy curve, this is discussed in further detail in chapter 4. The EFDL is shown in greater detail in figure 2.7, below.

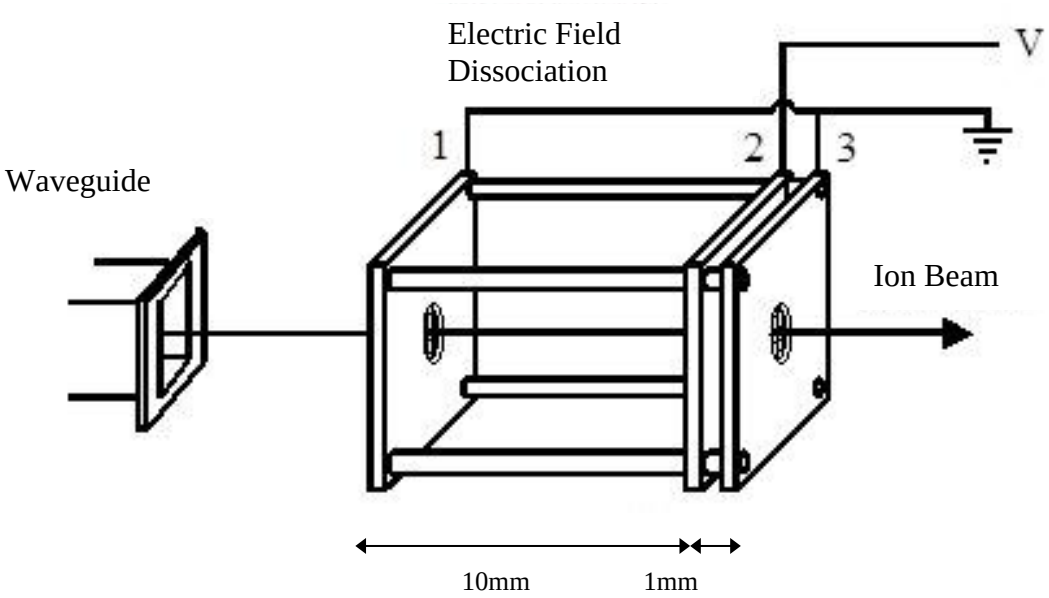

Figure 2.7

The Electric Field Dissociation Lens (EFDL) (not to scale) showing earth plates 1 and 3 either side of plate 2 which is connected to a 0 – 10 kV supply, and is capable of producing an electric field along the direction of the ion beam of up to 10^4 Vcm^{-1}. *(Reprinted with permission from "The Structure of Free Radicals", Andrew D. J. Critchley, PhD thesis, Department of Physics, Newcastle upon Tyne, 2000)*

The EFDL consisted of three plates each with a 7mm circular aperture to permit the transmission of the ion beam. The first and third plates were kept at Earth potential and a large positive potential (up to 10 kV) was applied to the second plate. To achieve a more uniform electric field between the plates, a fine steel gauze (transparency=66%) was spot welded over the plate apertures. With the lens an electric field of up to 10^4 V cm^{-1} could be applied along the direction of propagation of the ion beam. The electric field caused selective dissociation of weakly bound ions (see for example [3] and references therein).

2.7.3 *Modifications to the Mass Spectrometer*

It was necessary to make some engineering modifications to the mass spectrometer in order to support the microwave waveguide both inside the interaction region and outside the instrument, and also to allow the microwaves to pass along the waveguide into the instrument whilst maintaining vacuum.

Within the interaction region, the waveguide was held in place with two identical custom made supports, designed to electrically insulate the waveguide so that a potential could be applied to the waveguide in order to use it as a drift tube when desired, to allow for Doppler tuning of resonant transitions. Each support consisted of two short (approximately 1 cm thickness) concentric cylinders held apart with metal rods so that the two cylinders were electrically isolated; the outer cylinder being approximately 1.5 cm diameter smaller than the diameter of the inside of the interaction region so that it could be clamped in place using bolts. The centre cylinder of each support also used nylon bolts to fix the length of waveguide in place axially so that it was coaxial to the ion beam but electrically isolated from the vacuum chamber. This arrangement is shown schematically in figures 2.8 and 2.9.

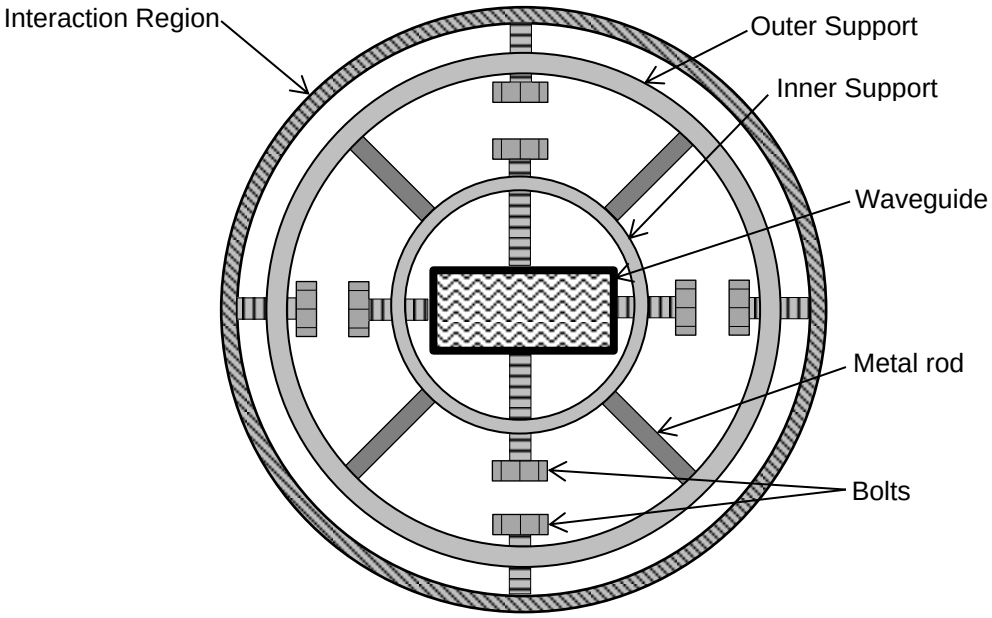

Figure 2.8

A schematic diagram along ion beam direction (not to scale) of one of the two concentric cylinders used to support the waveguide within the interaction region of the instrument. The waveguide is held in place using nylon bolts so that it is electrically isolated from the outer cylinder. The outer cylinder is kept in place by friction as the four outer bolts are tightened; the waveguide is also held in place by friction as the inner bolts are tightened.

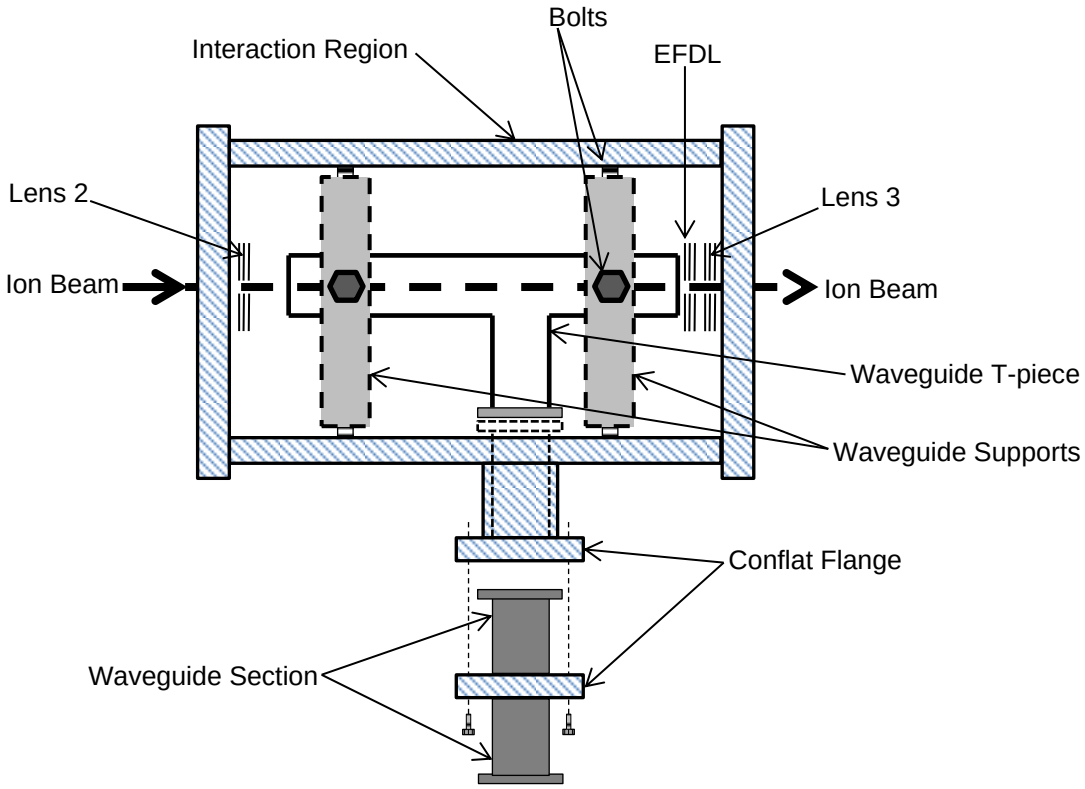

Figure 2.9

Diagram (in plan view - not to scale) of arrangement of waveguide T-piece supports within interaction region. The positions of the supports can be seen in relation to the position of the waveguide; also shown is the conflat flange where microwave radiation entered the waveguide within the interaction region.

With the waveguide T-piece supported inside the instrument, it was necessary to adapt a conflat flange in order to allow the microwave radiation to enter the instrument from the external waveguide. A blank conflat flange was used with a rectangular slot of the waveguide dimensions cut into it, and two short sections of waveguide with standard waveguide junction connections were silver soldered (because the metals were brass/silver and stainless steel) to the inside and outside of the flange. The flange was then bolted onto the external flange at the side of the interaction region (shown in figure 2.9) using a copper gasket to maintain the vacuum seal. Externally, another section of waveguide (from the synthesiser) was joined to the short welded section at the standard

waveguide junction but with a PTFE disc sandwiched between the two sides of the waveguide junction, each of which had a machined slot into which a Viton "O"-ring was placed, therefore forming a satisfactory vacuum seal while allowing microwaves through to the waveguide T-piece situated in the interaction region, as shown in figure 2.10.

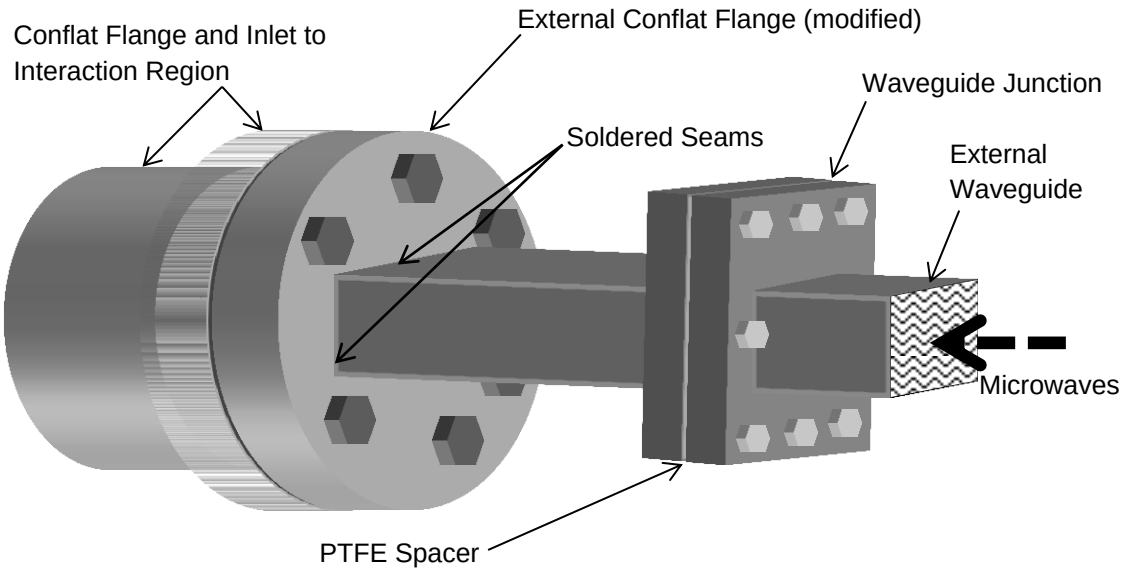

Figure 2.10

Modified conflat flange showing short section (external) of waveguide silver-soldered in place and waveguide junction with PTFE spacer.

Within the interaction region, the short section of waveguide welded to the inner side of the conflat flange was joined to the waveguide T-piece either directly (if electrical isolation was not required) or using another wafer of PTFE and nylon bolts if electrical isolation was required. Because of the large internal diameter of the waveguide, precision engineering of the parts was not necessary, it was sufficient that once the external conflat flange was fitted and the internal short section of waveguide attached to the T-piece that the ion beam passed within about 1 mm of the centre of the T-piece waveguide.

2.8 Summary

I have given a full description of the Newcastle fast ion-beam spectrometer in the configurations required for both laser beam and microwave spectroscopy. I have described in detail the how the instrument was designed in order to achieve the sensitivity required for the spectroscopic measurements made and those instrumental factors which affect precision and sensitivity and how they were overcome.

In the next chapter I give a detailed account of the theory of g/u symmetry breaking with particular relevance to the observations reported in chapter 4, and I describe the calculations performed.

Chapter 3: Theoretical Basis for the Measurability of a g/u Symmetry Breaking Transition in H_2^+

In this chapter I review theoretical work on g/u symmetry breaking in the hydrogen molecular cation. Much of this chapter was previously published in [98] Andrew D.J. Critchley, Alan N. Hughes, Iain R. McNab and Richard E. Moss, "Energy shifts and forbidden transitions in H_2^+ due to electronic g/u symmetry breaking", Molecular Physics vol. 101, 651-661, 2003. The work reviewed on H_2^+ is mostly by P. Bunker, R.E. Moss, and their co-workers [97] [92] [122]. R.E. Moss [79] and I. Gerdova [123] made similar calculations for D_2^+. The calculations of g/u symmetry breaking (also known as "g/u mixing" or "ortho-para mixing") included estimates of energy level shifts, transition wavenumbers and electric dipole transition moments of "forbidden" transitions in H_2^+ and D_2^+.

Since the original works were published Hilico and co-workers showed that the additional vibrational level $2p\sigma_u$ (v = 1, N = 0) exists [74] with a binding energy of just 0.00024 cm^{-1}; possibly the weakest chemical bond predicted to exist. Moss had suspected the existence of this level [78], but despite careful investigation was not able to detect it with the theoretical tools at his disposal. The effect of the $2p\sigma_u$ (v = 1, N = 0) level was not included in the original g/u symmetry breaking calculations described here, and although "*a posteriori*" the existence of this level does not change the principal conclusions, I show where the theory should be modified to take this additional level into account.

3.1 Introduction

Spectroscopic transitions occur when electromagnetic (EM) radiation interacts with an atom or molecule. EM radiation can be expanded as a sum of electric dipole, magnetic dipole, electric quadrupole etc. and absorption of EM radiation can result in any change of parity or angular momentum provided a sufficiently

high order interaction is considered (see Huestis for example [124]). Nevertheless, it is useful (particularly for consideration of astronomical spectra) to use selection rules and to classify transitions as allowed or forbidden according to their relative intensity under the interaction of interest, thus we consider transitions as electric dipole allowed or electric dipole forbidden. Selection rules are based on classifying individual energy levels according to symmetry. Some symmetry distinctions are exact, such as total angular momentum, $\boldsymbol{F}$, and parity, and lead to strict selection rules; others are approximate such as those involving angular momentum excluding electron and nuclear spin, $\boldsymbol{N}$, or very approximate, such as those involving vibration.

Amongst the most strongly forbidden transitions in molecular spectroscopy are those between adjacent rotational levels ($\Delta\boldsymbol{N}$=1) of a homonuclear diatomic molecule. Due to nuclear spin statistics adjacent rotational levels of a homonuclear diatomic molecule are always ortho (even total nuclear spin) and para (odd total nuclear spin) and the ortho and para forms of a molecule are sometimes called nuclear spin isomers. A pure rotational transition in a homonuclear diatomic molecule is therefore between an ortho and a para state and requires a change of the nuclear spin. Such transitions by radiative or non-reactive collisional processes are forbidden. So familiar is this (usually excellent) selection rule that it is often incorrectly believed that conversion of ortho to para species by means of radiative or non-reactive collisional processes is strictly forbidden (see for example [125]). However, as was noted in chapter 1, Herzberg [51] states:

> "*in the presence of nuclear spin the selection rule symmetric ↮ antisymmetric no longer holds absolutely*, although it is still very strict."

He later [126] cites Farkas (1933) [127]:

> "Owing to the smallness of the magnetic moment associated with the nuclear spin, the interaction with the rest of the molecule is very small indeed, and, as a result, the *transition probability between symmetric and antisymmetric states is extremely small*. It is so small that its reciprocal, the mean life, is of the order of years.."

We may restate this as hyperfine interactions couple nuclear spins to the rest of the molecule and mix together ortho and para states enabling transitions between them to gain intensity. This is referred to as g/u mixing of electronic states or, as g and u are used as symmetry labels, is also called electronic g/u symmetry breaking.

Transitions between adjacent rotational levels of a homonuclear diatomic molecule can gain intensity because of the g/u mixing induced by the hyperfine Hamiltonian close to a dissociation limit. The mechanisms for the increase in intensity were first discussed in detail by Broyer et al. [128] who were considering transitions in I_2. Hyperfine matrix elements are usually small (of the order of 100 MHz in open shell systems) compared to ortho-para energy level separations (if the separation is assumed to be due to adjacent rotational levels then the separation is usually more than 30 GHz for light molecules) and therefore ortho–para transition probabilities are usually small, but the transition probability scales with the magnitude of the hyperfine couplings and with the proximity of ortho and para states to one another, which can be small at a degenerate dissociation limit. For systems where ortho and para states are widely separated the transition probabilities are very small indeed; e.g., the rate of the $N = 0 \leftarrow N = 1$ ortho–para electric dipole transition in the ground vibrational and electronic state of molecular hydrogen is calculated to be about 2×10^{-13} per year [129]. Conversely for systems where the ortho and para states lie close in energy compared to hyperfine matrix elements, ortho–para electric dipole transitions can have measurable intensity.

Only a few observations of ortho–para transitions have been reported. Ozier et al. [130] measured ortho–para transitions in methane by tuning ortho and para levels through degeneracy using an applied magnetic field (see [131], figure 1). Bordé et al. [132] measured crossover resonances in infrared saturation spectra due to the mixing of vibration-rotation states of $^{32}SF_6$ by nuclear hyperfine interactions (see also figure 2 of [131]). Electronic g/u symmetry breaking was observed in $^{127}I_2$ at the $^2P_{3/2}$–$^2P_{1/2}$ dissociation limit [133] and in Cs_2 at the first

dissociation limit [134]. Ortho–para conversion in polyatomic molecules (particularly $^{12,13}CH_3F$) by collisions has been investigated using light-induced drift ([135] and references therein).

The first observation of an electronic transition in H_2^+ [87] was made by Carrington and his co-workers – they measured a microwave transition between near-dissociation levels of the ground electronic state ($1s\sigma_g \equiv X^2\Sigma_g^+$) and the first excited electronic state ($2p\sigma_u \equiv A^2\Sigma_u^+$). The specific transition observed was $1s\sigma_g\,(v = 19, \boldsymbol{N} = 1) \rightarrow 2p\sigma_u\,(v = 0, \boldsymbol{N} = 2)$, hereafter denoted (19,1)–(0,2), and in this initial measurement of the transition no splittings were observed. Further work on the $1s\sigma_g$–$2p\sigma_u$ spectrum by Carrington et al. [50] found unexpected hyperfine splittings in some transitions that were interpreted in terms of electronic g/u symmetry breaking. A subsequent re-measurement of the (19,1)–(0,2) transition, by Carrington et al. [91] also displayed hyperfine splittings and that transition was re-recorded by us and is shown in figure 4.2(a), chapter 4 (section 4.4). As can be seen, the transition actually consists of two hyperfine components (labelled by G=1/2 and G=3/2) separated by a 6.0 MHz hyperfine splitting. The observation of hyperfine structure in the $1s\sigma_g - 2p\sigma_u$ transitions was a surprise, as it had been thought that the hyperfine splittings in both states would be identical, so that all hyperfine components of the transition would occur at the same frequency. The observed hyperfine splittings were explained quantitatively by Moss [97] as arising from an electronic g/u symmetry breaking interaction that led to ortho–para mixing; one consequence of the mixing is to slightly lower the energies of the G=1/2 energy levels.

Bunker and Moss considered further the consequences of the electronic g/u symmetry breaking. They predicted [92] that “forbidden” pure rotation (and vibration-rotation) transitions between levels within the $1s\sigma_g$ and $2p\sigma_u$ electronic states of H_2^+ should have measurable intensity and their results are reproduced below in table 3.1. Subsequently, Moss [79] and Gerdova [123] made similar calculations for D_2^+using the same methodology.

v', N'	v'', N''	μ (bound) [c]	μ (continuum) [d]	μ/ea_0	ω/cm^{-1}
19,0	18,1	0.01648	0.01047	0.02695	19.8678
19,0	17,1	0.00308	0.00197	0.00505	146.9667
19,0	16,1	0.00050	0.00032	0.00082	419.1872
19,0	15,1	0.00009	0.00005	0.00014	832.4182
19,0	14,1	0.00002	0.00001	0.00003	1379.2334
19,1	19,0	0.07425	-0.24035	-0.16610	0.5230
19,1	18,0	0.01694	0.01550	0.03244	23.8228
19,1	17,0	0.00287	0.00266	0.00553	155.4026
19,1	16,0	0.00046	0.00043	0.00089	431.6450
19,1	15,0	0.00008	0.00007	0.00015	848.4812
19,1	14,0	0.00001	0.00001	0.00002	1398.6040
19,1	18,2	0.01730	0.01809	0.03539	14.0277
19,1	17,2	0.00336	0.00314	0.00650	132.0582
19,1	16,2	0.00053	0.00052	0.00105	396.1839
19,1	15,2	0.00009	0.00008	0.00017	802.1812
19,1	14,2	0.00002	0.00001	0.00003	1342.3710

[a] 1 $ea_0 \approx 2.54175$ D. 0
[b] From Ref. [78]; hyperfine shifts were not at the time published and were not included.
[c] The contribution to μ from bound levels of the excited electronic state.
[d] The contribution to μ from the continuum of the excited electronic state.

Table 3.1

Electric dipole transition moments μ [a] and transition wavenumbers ω [b] for forbidden $\Delta G = 0$ rotation and rotation–vibration transitions of H_2^+ involving the $v'=19$, $G=1/2$ levels *(Reprinted from Chemical Physics Letters, Vol.316, P. R. Bunker, R. E. Moss, "Forbidden electric dipole rotation and rotation–vibration transitions in H_2^+", Pages No.266-270, Copyright (2000), with permission from Elsevier B.V.)*

As may be seen from the table reproduced above, the pure rotation transition of H_2^+ that was predicted to be the most intense was $\boldsymbol{N} = 1 \leftarrow \boldsymbol{N} = 0$ in the last bound vibrational level ($v = 19$) of the electronic ground state. The transition was calculated to have a transition dipole of -0.16610 ea_0 (-0.42 Debye) [92] and to occur at a frequency of 14,960±3 MHz [136]. I now describe in some detail the theoretical work of Bunker and Moss [92] that led to this prediction. The

experiments made to confirm the prediction are described in the following chapter.

3.2 Theory

The electronic states of H_2^+ are classified by the labels gerade, g, and ungerade, u; for example the ground electronic state is usually given as $1s\sigma_g \equiv X^2\Sigma_g^+$ while the first excited electronic state is usually given as $2p\sigma_u \equiv A^2\Sigma_u^+$. The labels g and u refer to positive and negative symmetry with respect to the inversion operator, *i*, which inverts the electron coordinates in the centre of symmetry, but does not affect the proton coordinates or the nuclear spins. Therefore *i* is not a *true* symmetry operation of the H_2^+ ion as a whole, only a near symmetry operation [137] [138] – since it does not commute with the Fermi contact interaction operator (or the electron-spin nuclear-spin dipole-dipole operator), although it does with the rest of the molecular Hamiltonian. The operation p_{12} of permuting the spins of the protons is also not a symmetry operation of the H_2^+ ion as a whole, but a combination of the two is a true symmetry operation; in the notation of the molecular symmetry group [139] this combined operation is denoted (12)*, where (12) permutes the space and spin coordinates of the protons and the * indicates the inversion of the space coordinates of both the protons the electron in the molecular centre of mass [139]. The relationship between the operations i and p_{12}, and those of the molecular symmetry group are given in figure 2 of [97] reproduced below as figure 3.1.

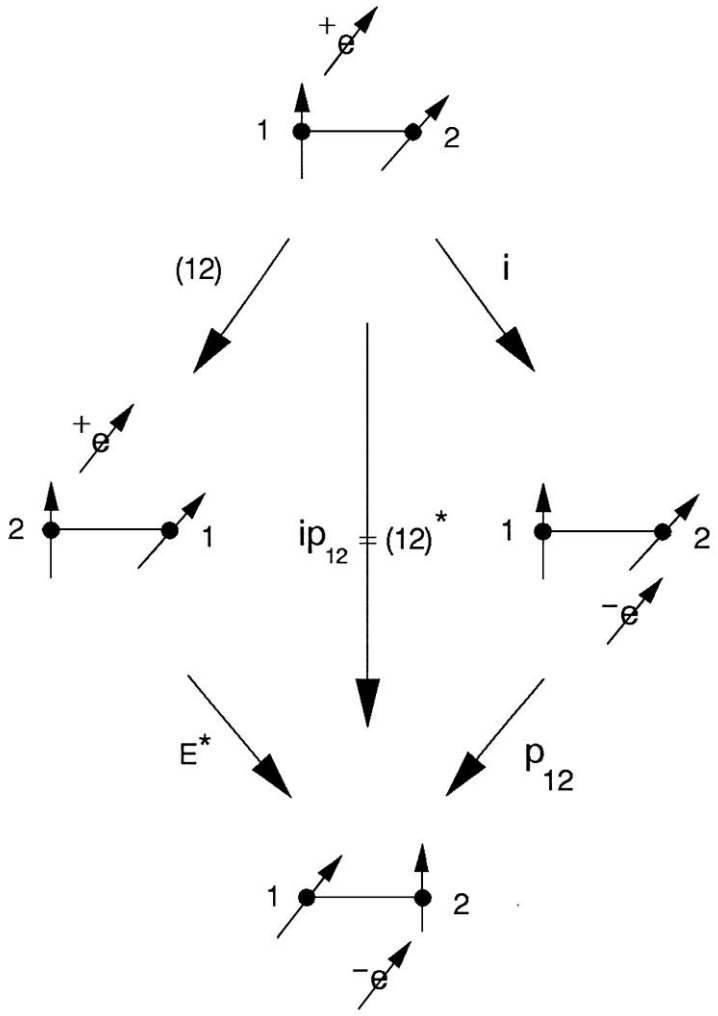

Figure 3.1

The relationship of the operations *i*, p_{12}, *E** and (12) for H_2^+. The + and – indicate whether the electron is above or below the plane of the figure. *(Reprinted from Chemical Physics Letters, Vol. 206 /number 1,2,3,4, Richard E. Moss, "Electronic g/u symmetry breaking in H_2^+", Pages No. 83-90, Copyright (1993), with permission from Elsevier B. V.)*

and the corresponding $D_{\infty h}$(M) character table [140] is presented as table 3.2. As stated above, those parts of the molecular Hamiltonian involving nuclear spin may in principle couple g and u electronic states. The hyperfine Hamiltonian for the hydrogen molecule ion with one electron and two I = 1/2 nuclear spins may be written for a single electronic state as [141],

$$\mathcal{H}_{hyp} = aI_z\Lambda + b\boldsymbol{I}.\boldsymbol{S} + cI_zS_z + d\boldsymbol{S}.\boldsymbol{N} + e(\boldsymbol{S}.\boldsymbol{S} - S_z^2) + f(\boldsymbol{I}.\boldsymbol{I} - I_z^2)$$

The term in *a* vanishes for a sigma state; the term in *e* represents an electron-spin/electron-spin term and for H_2^+ is necessarily 2nd order, and a weak perturbation; the term in *f* represents a nuclear-spin magnetic dipole / nuclear-spin magnetic dipole interaction, but the nuclei are far apart and the nuclear magnetic moments weak, so this too is a small term that is dominated by second order effects.

The terms in *b* and *c* are usually re-partitioned into a more physically meaningful form as follows:

$$b\boldsymbol{I}.\boldsymbol{S} + cI_zS_z = b_F\boldsymbol{I}.\boldsymbol{S} + \frac{c}{3}(3I_zS_z - \boldsymbol{I}.\boldsymbol{S})$$

The term in c now corresponds in form to the axial component of the interaction between the electron-spin magnetic dipole and the total nuclear-spin magnetic dipole (usually abbreviated to the words “dipole/dipole” interaction or “dipolar” interaction). The term in b_F = b+c/3 is a “Fermi contact” interaction corresponding to a non-dipolar interaction that occurs when the electron is within the radius of the nuclei – hence the word “contact”. The term in *d* corresponds to an interaction of the electron spin with the rotating nuclear framework (and disappears for a non-rotating molecule). Finally then, we can write an effective Hamiltonian for the hyperfine interaction in an individual vibration-rotation state by averaging the operators over the vibration-rotation wavefunctions to yield spectroscopic constants for the states concerned:

$$\mathcal{H}_{hyp}(v,N) = \langle b_F\rangle_{\boldsymbol{v,N}}\boldsymbol{I}.\boldsymbol{S} + \frac{1}{3}\langle c\rangle_{\boldsymbol{v,N}}(\boldsymbol{3}I_zS_z - \boldsymbol{I}.\boldsymbol{S}) + \langle \mathrm{d}\rangle_{\boldsymbol{v,N}}\boldsymbol{S}.\boldsymbol{N}$$

the spectroscopic constant for the spin-rotation interaction is usually given the symbol Greek lower case gamma, γ, by spectroscopists, where $\gamma_{v,N} = \langle \mathrm{d}\rangle_{\boldsymbol{v,N}}$

For the (19,1) level, b_F = 711.38 MHz and the terms in *c* and γ have approximate magnitudes less than 0.1 MHz [50]. Therefore, to account for g/u mixing in H_2^+ it was only necessary to use the largest of these terms, the Fermi contact interaction, to explain (and predict) experimental manifestations of g/u symmetry breaking. The much smaller [142] electron spin–nuclear spin dipolar

interaction can also, in principle, cause symmetry breaking, but it was not necessary to include it in an explanation of the observed effects.

$D_{\infty h}(M)$	E	(12)	E*	(12)*
Σ_g^+, +s	1	1	1	1
Σ_u^-, –s	1	1	–1	–1
Σ_g^-, –a	1	–1	–1	1
Σ_u^+, +a	1	–1	1	–1

Table 3.2

The $D_{\infty h}(M)$ character table [137]; the + and – labels indicate the parity, while s and a refer to the behaviour under (12). (*Reprinted from Molecular Physics, Vol. 101, Nos. 4-5, Andrew D. J. Critchley, Alan N. Hughes, Iain R. McNab, and Richard E. Moss, "Energy shifts and forbidden transitions in H_2^+ due to electronic g/u symmetry breaking", Pages 651-661, Copyright (2003), with permission from Taylor and Francis Group)*

Consideration of the total nuclear spin in H_2^+ shows which levels are *ortho*, which levels are *para* and which levels are split in energy by the nuclear spin. In H_2^+ the two proton spins couple to give a total nuclear spin $I = I_1 + I_2$. In the $1s\sigma_g$ ground state, rotational levels with rotational quantum number N even have I = 0 only (*para* H_2^+), while levels with odd N have I = 1 (*ortho* H_2^+). In the $2p\sigma_u$ excited state the position is reversed, odd N having I = 0 and even N have I = 1. The total nuclear spin couples with the electron spin to give a total spin $\boldsymbol{G} = \boldsymbol{I} + \boldsymbol{S}$. For I = 0 levels G = 1/2, while for I = 1 levels G = 1/2 or 3/2. Thus all ground state levels with odd N and excited state levels with even N are split by nuclear hyperfine interaction, but ground state even N and excited state odd N are not. The total spin angular momentum $\boldsymbol{G}$ couples to the rotational angular momentum $\boldsymbol{N}$ to give the total angular momentum $\boldsymbol{F}$ and further splittings will

occur. However spin–rotation coupling may be ignored in this work as may the electron spin–nuclear spin dipolar interaction.

By considering the symmetry of the total wavefunction we can deduce which states of H_2^+ can be mixed by the Fermi contact interaction. In the notation of the molecular symmetry group the ground and excited vibronic wavefunctions are +s and +a, respectively, the rotational wavefunctions are +s for N even and –a for N odd, and the nuclear spin functions are +a for I = 0 (*para*) and +s for I = 1 (*ortho*). The total wavefunction must be a, so that we can represent overall symmetry as follows:

ground electronic state ($1s\sigma_g$)

N = even (e.g. (19,0)), +s	I = 0	G = 1/2	+a
N = odd (e.g. (19,1)), -a	I = 1	G = 3/2, 1/2	–a

excited electronic state ($2p\sigma_u$)

N = even (e.g. (0,0)), +s	I = 1	G = 3/2, 1/2	+a
N = odd (e.g. (0,1)), -a	I = 0	G = 1/2	–a.

The Fermi contact interaction operator H_{FCl} commutes with both $\boldsymbol{G}$ and $\boldsymbol{N}$, so that G and N are good quantum numbers. For the $1s\sigma_g$ ground electronic state the (19,0) level, for which G = 1/2 only, is coupled just to N = 0, G = 1/2 levels of the excited $2p\sigma_u$ electronic state; these will include not only the two N = 0 bound levels (0,0), (1,0) but also all the continuum levels. Similarly, the G = 1/2 hyperfine level of (19,1) is mixed with N = 1, G = 1/2 levels of the excited electronic state, but the G = 3/2 level is unaffected, since there are no G = 3/2 levels of the $2p\sigma_u$ electronic state with N = 1.

In the work described here the g/u symmetry breaking has two important consequences. The first is that the (19,0) and (19,1) levels of the ground electronic state of H_2^+ are not pure g and both have a small admixture of the

$2p\sigma_u$ electronic state. The g/u selection rule is consequently broken and electric dipole transitions satisfying $\Delta N = \pm 1$ and $\Delta G = 0$ selection rules become allowed. Accordingly the forbidden (19,1)–(19,0) transition gains intensity. The second consequence is that account will have to be taken of small shifts in the relevant G = 1/2 hyperfine levels in estimating the (19,1)–(19,0) transition frequency. The G = 3/2 levels are involved in transitions, but only those allowed between the ground and excited electronic states.

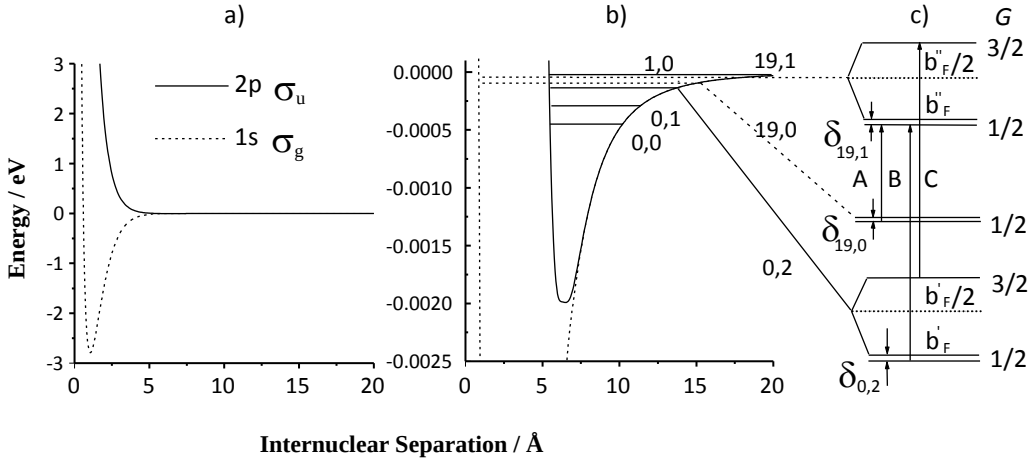

Figure 3.2

(a) Potential energy curves of H_2^+ (dashed line = $1s\sigma_g$, full line = $2p\sigma_u$) (b) Potential energy curves of H_2^+ near the first dissociation limit showing the shallow well in the $2p\sigma_u$ state and the relevant vibration-rotation energy levels (to scale). (c) Calculated hyperfine levels and observed microwave transitions between them (not to scale). The (0,0)/(1,0) and (0,1) hyperfine levels are similar to those for (19,1) and (19,0) respectively. The $2p\sigma_u$ (1,0) level (now added to original figure) has a dissociation energy of approximately 30 neV. Electronic g/u symmetry breaking energy shifts are shown as $\delta_{\upsilon,N}$ (transitions B and C were previously measured [91]). (*Adapted from Molecular Physics, Vol. 101, Nos. 4-5, Andrew D. J. Critchley, Alan N. Hughes, Iain R. McNab, and Richard E. Moss, "Energy shifts and forbidden transitions in H_2^+ due to electronic g/u symmetry breaking", Pages 651-661, Copyright (2003), with permission from Taylor and Francis Group)*

Most formulations of bound state perturbation theory ignore continuum states, but they must be considered here. Indeed, the effect of the continuum

dominates the calculated numbers. We therefore write down perturbation theory expressions that include both discrete and continuum states to allow calculation of perturbed wavefunctions and the transition dipoles between them. Although the ground electronic state supports 20 vibrational levels (having v = 0 through 19), the first excited electronic state only supports two. The two rotational levels $1s\sigma_g$ v = 19,(N = 0 and 1) of the ground state are above the $2p\sigma_u$ v = 0,(N = 0, 1 and 2) levels of the excited electronic state (see figure 3.2), but below the $2p\sigma_u$ v = 1, N = 0 level. Bound and continuum levels of any higher electronic states are sufficiently removed in energy to have an insignificant effect on any ground electronic state properties. The Fermi contact operator H_{FCI} mixes levels with the same rotational quantum number N, so that the first-order perturbed wavefunction for the (19,0) level of the ground electronic state is [92].

$$|19,0\rangle' = |19,0\rangle + \frac{\langle 0,0|H_{\mathrm{FCI}}|19,0\rangle}{E(19,0)-E(0,0)}|0,0\rangle + \frac{\langle 1,0|H_{\mathrm{FCI}}|19,0\rangle}{E(19,0)-E(1,0)}|1,0\rangle + \int_0^\infty \frac{\langle E,0|H_{\mathrm{FCI}}|19,0\rangle}{E(19,0)-E}|E,N\rangle\rho(E)\mathrm{d}E$$

where $|0,0\rangle$ and $|1,0\rangle$ are the bound (v = 0,1; N = 0) levels of the excited electronic state, $|E,N\rangle$ is a continuum state with energy E and $\rho(E)$ is the density of states. The $|1,0\rangle$ term has been added to account for the newly discovered (1,0) level of the excited state. Similarly, for (19,1)

$$|19,1\rangle' = |19,1\rangle + \frac{\langle 0,1|H_{\mathrm{FCI}}|19,1\rangle}{E(19,1)-E(0,1)}|0,1\rangle + \int_0^\infty \frac{\langle E,1|H_{\mathrm{FCI}}|19,1\rangle}{E(19,1)-E}|E,1\rangle\rho(E)\mathrm{d}E$$

The transition dipole between the levels (19,0) and (19,1) of the ground electronic state then includes three contributions, two from bound states and one from continuum levels of the excited electronic state:

$$\langle 19,1|\mu(R)|0,0\rangle\frac{\langle 0,0|H_{\mathrm{FCI}}|19,0\rangle}{E(19,0)-E(0,0)} + \langle 19,1|\mu(R)|1,0\rangle\frac{\langle 1,0|H_{\mathrm{FCI}}|19,0\rangle}{E(19,0)-E(1,0)} + \int_0^\infty \langle 19,1|\mu(R)|E,0\rangle\frac{\langle E,0|H_{\mathrm{FCI}}|19,0\rangle}{E(19,0)-E}\rho(E)\mathrm{dE}$$

borrowed from the allowed (19,1)–(0,0) and (19,1)-(1,0) transitions; and

$$\langle 19,0 \,|\, \mu(R) \,|\, 0,1\rangle \frac{\langle 0,1 \,|\, H_{\mathrm{FCI}} \,|\, 19,1\rangle}{E(19,1) - E(0,1)} + \int_0^\infty \langle 19,0 \,|\, \mu(R) \,|\, E,1\rangle \frac{\langle E,1 \,|\, H_{\mathrm{FCI}} \,|\, 19,1\rangle}{E(19,1) - E} \rho(E) \mathrm{dE}$$

borrowed from the allowed (19,0)–(0,1) transition, where $\mu(R)$ is the electronic transition dipole moment between the $1s\sigma_g$ and $2p\sigma_u$ electronic states, and R is the internuclear distance.

In addition to the usual hyperfine splittings the G = 1/2 levels of (19,0) and (19,1) are shifted by the g/u symmetry breaking and these energy shifts may be estimated using second order perturbation theory [97] as:

$$\Delta_{19,0} = \frac{|\langle 0,0 \,|\, H_{\mathrm{FCI}} \,|\, 19,0\rangle|^2}{E(19,0) - E(0,0)} + \frac{|\langle 1,0 \,|\, H_{\mathrm{FCI}} \,|\, 19,0\rangle|^2}{E(19,0) - E(1,0)} + \int_0^\infty \frac{|\langle E,0 \,|\, H_{\mathrm{FCI}} \,|\, 19,0\rangle|^2}{E(19,0) - E} \rho(E) \mathrm{d}E$$

$$\Delta_{19,1} = \frac{|\langle 0,1 \,|\, H_{\mathrm{FCI}} \,|\, 19,1\rangle|^2}{E(19,1) - E(0,1)} + \int_0^\infty \frac{|\langle E,1 \,|\, H_{\mathrm{FCI}} \,|\, 19,1\rangle|^2}{E(19,1) - E} \rho(E) \mathrm{d}E$$

To calculate these expressions we need to know the form of the operator and the wavefunctions. The usual form of the Fermi contact interaction operator is

$$H_{\mathrm{FCI}} = K[(\boldsymbol{S}.\boldsymbol{I}_1)\, \delta(\boldsymbol{R}_\mathrm{e} - \boldsymbol{R}_1) + (\boldsymbol{S}.\boldsymbol{I}_2)\, \delta(\boldsymbol{R}_\mathrm{e} - \boldsymbol{R}_2)]$$

where $\boldsymbol{R}_\mathrm{e}$ is the position of the electron, $\boldsymbol{R}_1$ and $\boldsymbol{R}_2$ are the positions of the two protons, and $K = (8\pi/3)\,(g g_\mathrm{N} \mu_\mathrm{B} \mu_\mathrm{B} / 4\pi\varepsilon_0 c^2)$. It is convenient for our purposes to rewrite this as

$$H_{\mathrm{FCI}} = (1/2) K \boldsymbol{S}.[\boldsymbol{I}_+ \delta_+ + \boldsymbol{I}_- \delta_-]$$

where $\boldsymbol{I}_\pm = \boldsymbol{I}_1 \pm \boldsymbol{I}_2$ and $\delta_\pm = \delta(\boldsymbol{R}_\mathrm{e} - \boldsymbol{R}_1) \pm \delta(\boldsymbol{R}_\mathrm{e} - \boldsymbol{R}_2)$

Both the operators $(\boldsymbol{S}.\boldsymbol{I}_+)\delta_+$ and $(\boldsymbol{S}.\boldsymbol{I}_-)\delta_-$ are invariant to the molecular symmetry group operation (12)*, but $(\boldsymbol{S}.\boldsymbol{I}_+)\delta_+$ is symmetric with respect to i, while $(\boldsymbol{S}.\boldsymbol{I}_-)\delta_-$ is antisymmetric with respect to i. Therefore, $(\boldsymbol{S}.\boldsymbol{I}_+)\delta_+$ is diagonal in the electronic states considered and is responsible for the usual Fermi contact interaction splittings, while $(\boldsymbol{S}.\boldsymbol{I}_-)\delta_-$ is responsible for electronic g/u symmetry breaking and couples the ground and excited electronic states.

The perturbation used is that part of the Fermi contact interaction that breaks symmetry, namely (1/2)K($\boldsymbol{S}.\boldsymbol{I}_-$)$\delta_-$.The matrix elements of the spin operators may be obtained in the $|I_1, I_2, I, S, G\rangle$ basis using standard techniques. In particular, use may be made of

$$\boldsymbol{S}.\boldsymbol{I}_+ = (1/2)(\boldsymbol{G}^2 - \boldsymbol{I}^2 - \boldsymbol{S}^2)$$

and [143], for S = ½,

$$[\boldsymbol{S}.\boldsymbol{I}_-]^2 = (1/4)(2\boldsymbol{I}_1{}^2 + 2\boldsymbol{I}_2{}^2 + \boldsymbol{S}^2 - \boldsymbol{G}^2)$$

To calculate the various perturbation expressions we need to use appropriate wavefunctions. Unfortunately, high quality nonadiabatic wavefunctions were not available. We therefore calculated adiabatic wavefunctions using LEVEL [121] with the adiabatic potentials of Kennedy [142], and these adiabatic wavefunctions have been adequate in other work for calculating many properties of H_2^+, including electron densities [68, 97]. For a given bond length, R, the matrix elements of the delta function operators between the zeroth order electronic wavefunctions may be expressed in terms of the electron densities at the protons in the ground and excited electronic states, $\rho_{GS}(R)$ and $\rho_{ES}(R)$. In particular, the matrix element of δ_- between the $1s\sigma_g$ and $2p\sigma_u$ electronic wavefunctions is approximately $\pm 2[\rho_{GS}(R)\ \rho_{ES}(R)]^{1/2}$ where the sign depends on the choice of phase for the wavefunctions. The matrix element of this function of internuclear distance, between the vibration-rotation wavefunctions of the coupled levels, is then needed. However, the vibration-rotation levels of interest here are so close to dissociation and sample such long bond lengths that the electron densities over the important range of R are essentially half the free atom value. This means that the rovibronic matrix elements of $K\delta_-$ between the ground and excited electronic state wavefunctions may be approximated in terms of a, the hydrogen atom hyperfine parameter, and S_{gu}, the overlap integral (Franck–Condon factor) between the relevant vibration-rotation wavefunctions for the ground and excited electronic states, by

$$\pm aS_{\mathrm{gu}} = \pm a\int_0^\infty \psi_{\mathrm{g}}(R)\psi_{\mathrm{u}}(R)\mathrm{d}R$$

In addition, the electronic transition dipole moment $\mu(R)$ (in atomic units of ea_0) may be approximated to $R/2$ [144]; this approximation becomes increasingly good at the long bond lengths that are of relevance in this work. Accordingly, the matrix elements required are

$$\pm\frac{1}{2}R_{\mathrm{gu}} = \pm\int_0^\infty \psi_{\mathrm{g}}(R)\frac{R}{2}\psi_{\mathrm{u}}(R)\mathrm{d}R = \pm\int_0^\infty \psi_{\mathrm{g}}(R)\mu(\mathrm{R})\psi_{\mathrm{u}}(R)\mathrm{d}R\,.$$

To evaluate the energy shifts and transition dipoles therefore required overlap integrals and matrix elements of R to be calculated for both bound and continuum states.

The overlap integrals and the matrix elements of R for the bound levels were calculated using the LEVEL program of Le Roy [121] with the adiabatic potentials of Kennedy [142]. It is important to note that within this approximation, the $|1,0\rangle$ level of the excited state could not be located, and therefore these terms in the expressions given above were not evaluated. As will be seen in Chapter 4, even without including the $|1,0\rangle$ level, excellent agreement was found between theory and experiment. The size of the integrals with the $|1,0\rangle$ level must therefore be small compared with those that were evaluated. We can rationalize this by considering the form of the vibrational wavefunction for a potential with a steep inner wall and gently sloping outer wall – the greatest amplitude for the wavefunction is towards the outer turning point (see for example, figure 9a of [50]), where overlap with the bound state wavefunctions (restricted to *R* less than 10 Å or so) will be minimal. For the level concerned, the long range potential is well approximated as a proton polarizing a hydrogen atom: $V(R) = -(1/2)\alpha E^2$, where α is the polarizability of atomic Hydrogen ($0.667*4\pi\varepsilon_0.\text{Å}^3 = 7.4213755\text{x}10^{-41}\ \text{C}^2\text{m}^2\text{J}^{-1}$ [145]) and E is the electric field due to the proton a distance R away. We may therefore estimate the outer turning point for levels close to dissociation by the expression

$$V(R) = -\ (2.523\ \text{eV})\ /\ (R\ \text{Å})^4$$

It is readily seen from the potentials in figure 3.2b that this is an excellent approximation for both electronic states beyond R =10 Å. The outer turning point for a binding energy of 30 neV is thereby calculated to occur at a distance of 112 Å and it is not surprising that the matrix elements involving this level would be vanishingly small.

The inclusion of the continuum state contributions was found to be essential to make accurate calculations. Earlier calculations [50] did not include such contributions and gave energy shifts of the opposite sign to those measured experimentally. Because the (19,0) and (19,1) levels of the ground state lie above the important (v = 0) bound levels of the excited state there is a competition between the bound and continuum parts of the excited state and their contributions are opposite in sign. In performing the integration over continuum states we used the density of states normalization of Le Roy [146] [147, 148] for the continuum wavefunction $\psi_{EN}(R)$

$$\int_0^\infty \psi_{EN}(R) R \psi_{E'N}(R) \mathrm{d}R = \frac{\delta(E - E')}{\rho(E)}$$

where E is the energy above the dissociation limit. The density of states $\rho(E)$ = $(8\mu c/hE)^{1/2}$, where μ is the reduced mass, is appropriate for continuum wavefunctions that oscillate asymptotically with unit amplitude.

For the continuum contributions the integrals, $\mathrm{S_{gu}}(E)$ and $\mathrm{R_{gu}}(E)$, between the vibration-rotation wavefunctions and the continuum wavefunctions were determined, as a function of E, using the BCONT program of Le Roy [147, 148] from very small values of E (c. 0.001 cm^{-1}) to very high values (>105 cm^{-1}). The continuum contributions to the transition dipole and the second order correction to the energy were proportional to integrals that could be evaluated numerically,

$$\frac{a\mu^{1/2}}{2} \int_0^\infty \frac{S_{\mathrm{gu}}(E) R_{\mathrm{gu}}(\mathrm{E}) \mathrm{d}E}{(E_0 + E) E^{1/2}}$$

and

$$a^2 \mu^{1/2} \int_0^\infty \frac{S_{\mathrm{gu}}(E)^2 \, \mathrm{d}E}{(E_0 + E) E^{1/2}}$$

respectively, where E_0 is the dissociation energy of the bound level of interest. The proportionality constant depends on the details of the BCONT program [147, 148] and the units used. For μ in atomic mass units, and a, E and E_0 in cm^{-1} the proportionality constant is 0.0775268 MHz $(\mathrm{cm}^{-1}\mathrm{amu})^{-1/2}$ and gives the energy shift in MHz. The integrand does not diverge at the lower limit, since in all cases $S_{\mathrm{gu}}(E)$ and $R_{\mathrm{gu}}(E)$ tend to 0, as E tends to 0, faster than $E^{1/2}$, even in the case of $N = 0$. If $S_{\mathrm{gu}}(E)$ and $R_{\mathrm{gu}}(E)$ were independent of E and could be factored out of the integral, the integral would be evaluable analytically and this provided a method of checking that truncation of the integral at large or small E did not introduce any error. The integral was then evaluated numerically using a simple trapezoidal rule. Care was taken that the phases of the wavefunctions were consistent throughout.

Bound State Contributions

Borrowed from (19,1)–(0,0)	Borrowed from (19,0)–(0,1)
$c_0 = \dfrac{\langle 19,0 \mid H_{\mathrm{FCI}} \mid 0,0 \rangle}{E(19,0) - E(0,0)} = 5.10 \times 10^{-3}$	$c_0 = \dfrac{\langle 19,1 \mid H_{\mathrm{FCI}} \mid 0,1 \rangle}{E(19,1) - E(0,1)} = 5.45 \times 10^{-3}$
$\langle 0,0 \mid \mu(R) \mid 19,1 \rangle = 6.22 \ ea_0$	$\langle 0,0 \mid \mu(R) \mid 19,1 \rangle = 7.84 \ ea_0$
Contribution = $3.17 \times 10^{-2} \ ea_0$	Contribution = $4.27 \times 10^{-2} \ ea_0$

Continuum Contributions
Borrowed from (E,0)–(19,1) = $-9.63\times10^{-2}\ ea_0$
Borrowed from (E,1)–(19,0) = $-14.41\times10^{-2}\ ea_0$
Total Transition Dipole = $-0.166\ ea_0$ = –0.422 D

Table 3.3

Details of the calculation of the transition dipole for the (19,1)–(19,0) transition in H_2^+. 1 $ea_0 \approx 2.54175$ D. (*Reprinted from Molecular Physics, Vol. 101, Nos. 4-5, Andrew D. J. Critchley, Alan N. Hughes, Iain R. McNab, and Richard E. Moss, "Energy shifts and forbidden transitions in H_2^+ due to electronic g/u symmetry breaking", Pages 651-661, Copyright (2003), with permission from Taylor and Francis Group)*

The details of the results of the calculation of the (19,1)–(19,0) transition dipole are given in table 3.3. Since the levels involved are close to the dissociation limit and to each other, the rovibronic zero order energies used in the perturbation equations are the most accurate available and include all nonadiabatic effects, and relativistic and radiative corrections [78]. Due to the proximity of the dissociation limit the Fermi contact parameter is very close to half the free atomic value of a = 1422 MHz (Kennedy [142] has calculated the parameter to be 711.4 MHz for the (19,1) level of the H_2^+ $1s\sigma_g$ state). Allowance for the diagonal hyperfine shifts should also be made, since *ortho–para* mixing is involved and only one of a pair of interacting levels will involve a hyperfine shift, although the shifts are less than 1% of the energy differences involved and are not critical for the estimation of the transition dipole or for the electronic g/u symmetry breaking shifts in table 3.4. The (19,1)–(19,0) transition dipole is estimated to be 0.42 D.

Dissociation Energy Contributions	(19,0)	(19,1)	(19,1)–(19,0) Transition Frequency/MHz
Nonadiabatic/cm^{-1} [78]	0.744 22	0.221 06	
Relativistic Correction/ cm^{-1} [142] [78]	–0.000 6	–0.000 4	
Radiative Correction/ cm^{-1} [78]	+0.000 0	+0.000 0	
Total (ignoring hyperfine)/cm^{-1} [78]	0.743 62	0.220 66	
Total (ignoring hyperfine)/MHz	**22 293**	**6 615**	**15 678 ±3**
Diagonal Fermi Contact Contribution/MHz [142]	+711.4	0.0	
Off-diagonal Fermi Contact Bound State Contribution/MHz [97]	+2.0	+2.1	
Off-diagonal Fermi Contact Continuum Contribution/MHz [97]	–11.9	–4.9	
Final Dissociation Energy/MHz	**21 571.9**	**6 612.4**	**14 960 ±3**

Table 3.4

Details of the calculation of the (19,1)–(19,0) transition frequency. The relativistic and radiative corrections are relative to the atomic limits of –1.46092 and 0.27066 cm^{-1}, respectively. (*Reprinted from Molecular Physics, Vol. 101, Nos. 4-5, Andrew D. J. Critchley, Alan N. Hughes, Iain R. McNab, and Richard E. Moss, "Energy shifts and forbidden transitions in H_2^+ due to electronic g/u symmetry breaking", Pages 651-661, Copyright (2003), with permission from Taylor and Francis Group)*

However, inclusion of the diagonal Fermi contact interaction is essential in estimating the (19,1)–(19,0) transition frequency to a few MHz, the details of which are given in table 3.4. The transition frequency, ignoring hyperfine interactions is thought to be good to ±3 MHz. This optimism is based on the success of the calculations [97], [78] in matching the experimental frequencies of the allowed transitions involving levels close to dissociation observed by Carrington et al. [91] (see table 4.1, chapter 4); the allowed transitions are either *ortho–ortho* or *para–para*, so that either neither level involved in an allowed transition has a hyperfine interaction or both levels have very similar diagonal hyperfine shifts of close to half the atomic limit.

In the second half of table 3.4 it can be seen that there is a highly significant diagonal Fermi contact contribution to the transition frequency from (19,0) and that the g/u symmetry breaking shifts are also significant, particularly the continuum contributions. The final estimate for the (19,1)–(19,0) transition frequency was 14 960 ± 3 MHz.

In the following chapter I detail the experiments that we performed to test the theoretical prediction that the “forbidden” (19,1)-(19,0) did indeed have measureable intensity. Although the “forbidden” transition was calculated to have an intensity some 3000 weaker than the “allowed” (19,1)-0,2) transition, the transition was successfully measured in both single and double resonance, under a variety of conditions.

3.3 Summary

In this chapter I have given a full account of the theory of g/u symmetry-breaking and an analysis of the calculations involved. I have described those factors which are relevant and shown why g/u symmetry-breaking is of greater significance for vibration-rotation levels near to dissociation. In the next chapter I describe in detail the experimental methods used to observe the forbidden (19,1)-(19,0) pure rotation transition in the $1s\sigma_g$ ground state of H_2^+ giving a summary of the results. I also describe my efforts to observe the (0,1)-(0,0) transition in the $2p\sigma_u$ level of H_2^+ with a detailed account of the experimental methods employed.

Chapter 4: Direct Measurement of a Pure Rotation Transition in H_2^+

The first part of this chapter describes the observation of the (19,1)-(19,0) pure rotation transition in the ground ($1s\sigma_g$) electronic state of H_2^+. Preliminary results were made in conjunction with Andrew Critchley and were submitted by him in partial fulfilment of requirements for the degree of Doctor of Philosophy [(Newcastle University, 2001)] and also published as a letter [93]. A full description of these measurements were subsequently published as a paper [98].

The second part of this chapter describes an unsuccessful search for the (0,0)-(0,1) pure rotation transition in the first excited ($2p\sigma_u$) electronic state of H_2^+.

For the sake of clarity, I have repeated (and elaborated) on the description of important aspects of the apparatus that were first described in Chapter 2.

4.1 Apparatus Overview

To measure the (19,1)–(19,0) transition the Newcastle Fast ion-beam/laser beam spectrometer [100] was modified to enable microwave spectroscopy and electric field dissociation. A schematic representation of the spectrometer as it was reconstructed can be seen in figure 4.1. The principle of the experiments is explained in the figure caption.

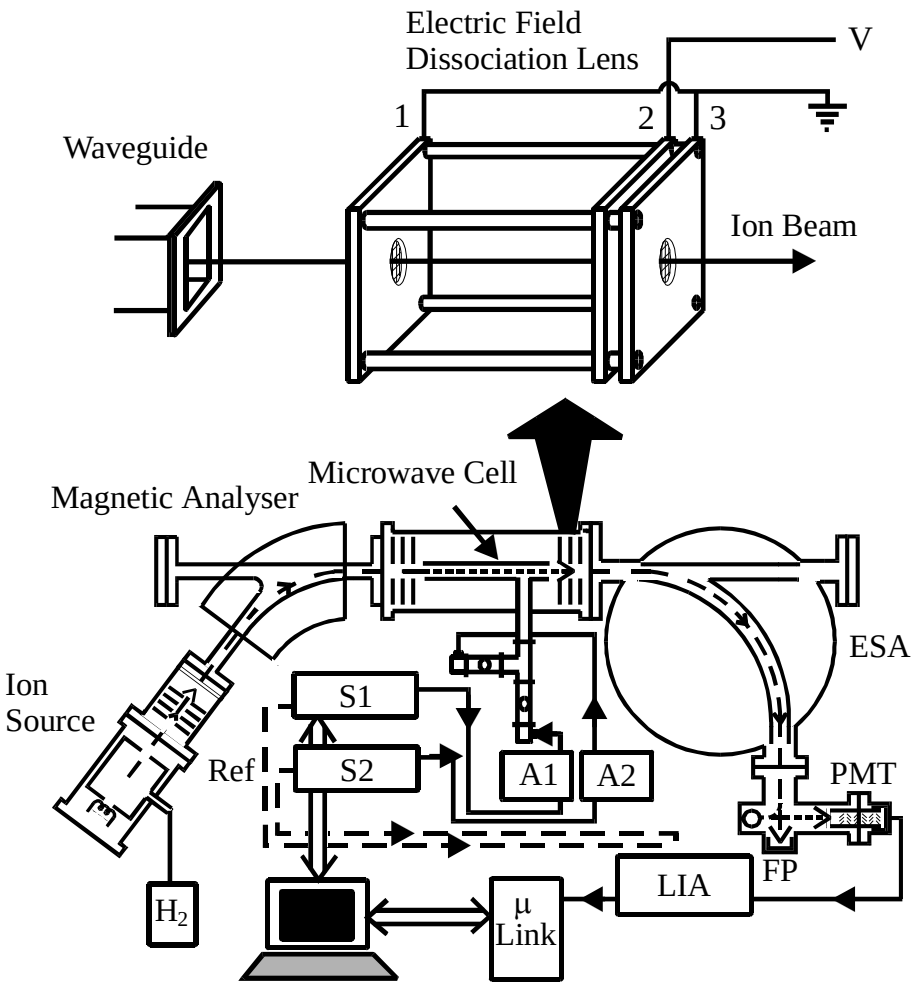

Figure 4.1

Microwave/Fast-ion beam apparatus with a detailed view of the end of the microwave waveguide and the electric field dissociation lens. A beam of H_2^+ was selected using the magnet and focused into the microwave cell. Computer controlled synthesizers (S1, S2) provided microwaves that were amplified (A1, A2) and then attenuated to the desired power before being transmitted into the microwave cell. At resonance, population was transferred between levels and the population of one level was monitored by fragmentation induced by an electric field dissociation lens (see figure 4.3 for detail). Fragment ions were selected with an electrostatic analyser (ESA) and detected with an off-axis electron multiplier (PMT). The microwaves were amplitude modulated and the resultant signal was processed by a lock-in amplifier and passed to the computer controller via a Microlink interface (μlink). (*Reprinted from Molecular Physics, Vol. 101, Nos. 4-5, Andrew D. J. Critchley, Alan N. Hughes, Iain R. McNab, and Richard E. Moss, "Energy shifts and forbidden transitions in H_2^+ due to electronic g/u symmetry breaking", Pages 651-661, Copyright (2003), with permission from Taylor and Francis Group)*

Vibrationally hot H_2^+ ions were formed by electron impact on H_2 gas in a Vacuum Generators "in-line" ion source. H_2^+ ions were accelerated to 2 or 4 keV (typical H_2^+ beam current $\approx 10^{-7}$ A). H_2^+ was selected by means of a magnetic sector and focused into a length of rectangular waveguide (WR-62, internal cross section 7.9 $\times$ 15.8 mm). Microwaves were produced with two synthesisers (Wiltron models 6753B-10 and 6769B) that could be used either in isolation for single resonance experiments, or together for double resonance experiments. The power output of the synthesizers was set at 0 dBm* (1 mW) at all times and was directed via coaxial cable (capable of carrying frequencies <40 GHz) to an amplifier (HP 8346A) with a maximum output power of 20 dBm (100 mW). The amplified microwave output was kept at 20 dBm throughout our experiments. The amplified radiation was coupled into waveguide and passed through a mechanical attenuator (for power control) and into the vacuum chamber through a PTFE window. Within the vacuum chamber the microwaves passed via an E-plane T to a 40 cm length of WR-62 waveguide, open at each end, in which interaction with the ion beam occurred. After interacting with the microwaves the H_2^+ beam passed into an electric field dissociation lens.

4.2 Electric Field Dissociation Lens (EFDL)

Since the vibration-rotation levels concerned are naturally bound, an electric field dissociation lens (EFDL), situated between the microwave cell and the electrostatic analyser, was used to fragment the ions via a Stark perturbation of the potential energy curve. An example of this effect is shown in figure 4.2, which is taken from Carrington et al. (1993) [50] where the $1s\sigma_g$ ground state potential energy curve of H_2^+ is shown with and without the presence of a strong external electric field (see figure caption). As the field strength is increased, the potential energy curve is depressed further below the dissociation limit thus causing vibration-rotation levels near the dissociation limit to become increasingly less bound which allowed selective dissociation of weakly bound vibration-rotation levels.

* Power(dBm) = 10 $\log_{10}$ Power(mW)

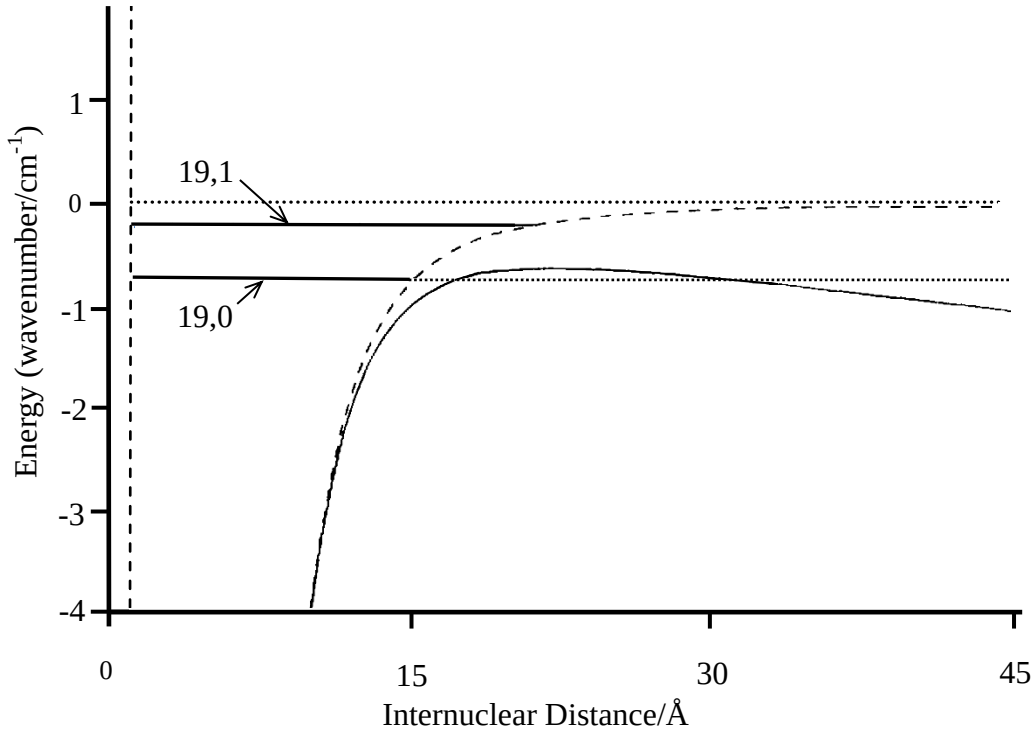

Figure 4.2

The $1s\sigma_g$ ground state potential energy curve of H_2^+ near the dissociation limit, showing the v=19, N=0 and v=19, N=1 vibration rotation levels; the dashed line indicates the field-free potential, the solid line shows the effect of an applied electric field of several kV. (*Reprinted from Journal of the Chemical Society, Faraday Transactions, Vol. 89, No. 4, Alan Carrington et al. "Microwave electronic spectroscopy, electric field dissociation and photofragmentation of the H_2^+ ion,", Pages 603-614, Copyright (1993), with permission from R. S. C. Publishing)*

The position of the EFDL is shown in figure 4.1 and its construction is shown in greater detail in figure 4.3.

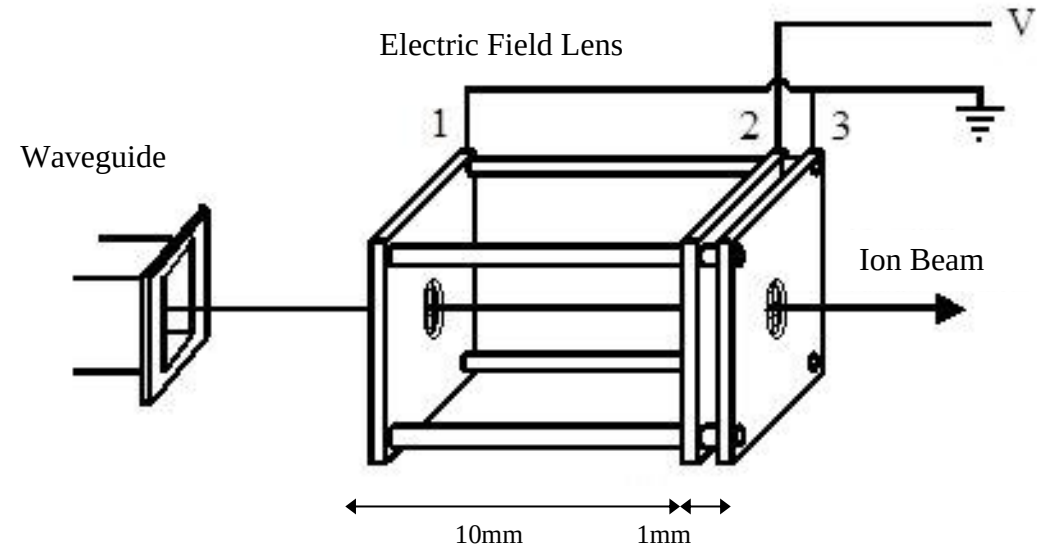

Figure 4.3

The Electric Field Dissociation Lens (EFDL) (not to scale) showing earth plates 1 and 3 either side of plate 2 which is connected to a 0 – 10 kV supply, and is capable of producing an electric field along the direction of the ion beam of up to 10^4 Vcm^{-1}. *(Reprinted with permission from "The Structure of Free Radicals", Andrew D. J. Critchley, PhD thesis, Department of Physics, Newcastle upon Tyne, 2000)*

The EFDL consisted of three plates each with a 7mm circular aperture to permit the transmission of the ion beam; the plates being supported and held apart by ceramic insulators. The first and third plates were kept at Earth potential and a large positive potential (up to 10 kV) was applied to the second plate. To achieve a more uniform electric field between the plates, a fine steel gauze (transparency=66%) was spot welded over the plate apertures. With the lens in this configuration an electric field of up to 10^4 Vmm^{-1} could be applied along the direction of propagation of the ion beam subject to a maximum voltage set by electrostatic discharge across the ceramic spacers between the plates; in practice far lower fields were used. The electric field caused selective dissociation of weakly bound ions (see [3] and references therein).

When a transition was in resonance, population transfer occurred and depending upon the measurement in progress, we detected electric-field induced fragmentation arising from one of the (19,1), (19,0) or (0,2) levels . Each change in population of a vibration-rotation level that fragments within the electric field lens does so with a characteristic dissociation energy and the

electrostatic analyser was used to select the fragments of interest. This gives high selectivity for which state is monitored, but has the disadvantage that locating a transition becomes a two dimensional search in frequency and fragment kinetic energy. For the case of H_2^+, where the potential curves are known to high accuracy, it is possible to calculate the electric field that will cause fragmentation of a particular level and hence the position in a lens at which fragmentation will occur, and the resultant fragment kinetic energy [50] [59]. We did not undertake such a calculation, instead we used a compromise lens design (for a detailed study see [50]) that enabled us to monitor some fragments from all levels at a single kinetic energy. Extensive modelling of lens designs was undertaken using the SIMION ion-optics software [106] however space was limited within the interaction region of the instrument between the microwave waveguide end and the electrostatic analyser. This prevented the use of more complicated lens designs which utilised several high voltage plates to achieve extremely linear fields but required more space. The final lens design, although simple, allowed us to confine the high-field region to within a narrow space (between plates 2 and 3 in figure 4.3) immediately before the ion beam entered the electrostatic analyser. Although the lens design was simple it was found using the SIMION software to produce a reasonably linear field.

Once a transition was observed, its detection was optimised by changing the ESA voltage to the optimum setting for the level of interest. A typical ESA scan of the H^+ fragments formed at different dissociation energies is given in figure 4.4. Also shown is the earth proton fragment peak, which arises from spontaneous and collision induced dissociation processes occurring at earth potential, both outside the EFDL, and at the gauzes at the entrance and exit of the EFDL.

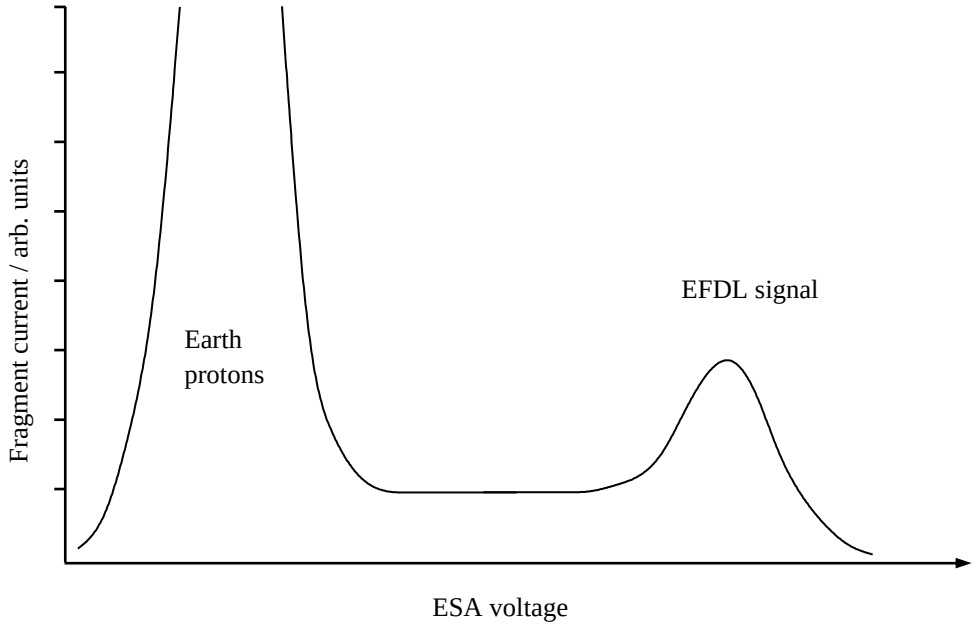

Figure 4.4

A schematic representation of a typical ESA scan of the fragments arriving at the photomultiplier, showing the fragments of the level(s) dissociated within the EFDL and also the earth proton fragment peak.

The EFDL voltage was set to a value just high enough to allow the required level to fragment (the greater the field applied to the ions, the greater the depression of the dissociation limit). This minimised background fragments from levels with greater dissociation energies. In practice it was found that an operating voltage of 300V – 800V was sufficient to dissociate the levels of interest.

4.3 Microwave Propagation

In this experiment we used WR-62 waveguide which has an optimum frequency transmission range of 12400 MHz to 18000 MHz [149] which encompasses both the (19,1)–(19,0) transition, predicted to be at a frequency of 14960 $\pm$ 3 MHz, and also the (19,1)-(0,2) microwave transition measured by Carrington et al. [50, 87] at frequencies of 17604.4 MHz (for G=1/2) and 17610.4 MHz

(G=3/2). Within this range of frequencies propagation of microwaves was limited to the fundamental mode, $TE_{1,0}$. At frequencies higher than this optimum range, microwaves are still propagated but will include higher modes $TE_{m,n}$ each of which appears at slightly different apparent frequencies; this is discussed in greater detail in section 4.6. For our final measurements we selected H^+ fragments at the kinetic energy appropriate to the (19,1), (19,0) or (0,2) level using the ESA and thereby detected the desired signal against a small background. The ion current was detected using an off-axis electron multiplier (Thorn EM119) / deflector system. The current from the electron multiplier passed through a transimpedance amplifier (Brookdeal 5002) to a lock-in amplifier (Stanford Research 850). The microwave frequency was scanned directly and the microwaves were 100% amplitude modulated at a frequency of 333 Hz, with a 50% duty cycle.

Reflection of microwaves from the open ends of the waveguide cell led to microwaves that co- and counter-propagated to the ion beam; hence each resonance was split into two components due to Doppler shifts:

$$\nu_{ion}^{CT} = \nu_{rest}\left[(1 \mp \mathrm{v}/c)/(1 \pm \mathrm{v}/c)\right]^{1/2} = \nu_{rest} K_{CT}^{CO},$$

where upper and lower signs refer to radiation co-(CO) and counter-(CT) propagating with respect to the ion beam travelling with velocity, v. As can be seen in the spectra, transitions measured from co- and counter-propagating microwaves do not have equal intensity. This lack of symmetry is due to instrumental factors (principally electrostatic focusing conditions) and by re-optimizing the instrument the relative intensities could be changed.

Where we observed both Doppler shifted frequencies the two observations were used to extract the rest frequency of the transition, ν_{rest}, and the Doppler shift factors K_{CT}^{CO}.

4.4 Microwave Spectra

In order to calibrate our apparatus, and verify operation, a spectrum of the previously observed (19,1)–(0,2) transition was re-recorded. Table 4.1 below shows a comparison [91] of calculated [97] and experimental [50, 87] frequencies of allowed vibration-rotation transitions within the H_2^+ electronic spectrum $2p\sigma_u–1s\sigma_g$. There is excellent agreement between theory and experiment with a difference no greater than 2 MHz.

		Transition Frequency/MHz	
Transition	*G* value	Calculated [97]	Experiment [50, 87]
(19,1)–(0,2)	1/2	17603	17 604.4
	3/2	17 609	17 610.4
(19,0)–(0,1)	1/2	52 893	52 894.6
(19,1)–(0,0)	1/2	96 423	96 424.2
	3/2	96 431	96 431.8

Table 4.1

Comparison of calculated and experimental transition frequencies for allowed $2p\sigma_u–1s\sigma_g$ electronic transitions in H_2^+. *(Reprinted from Chemical Physics Letters, Vol.206, Alan Carrington, Christine A. Leach and Mark R. Viant, "Nuclear hyperfine structure in the electronic millimetre wave spectrum of H_2^+", Pages No.77-82, Copyright (1993), with permission from Elsevier B.V.)*

The spectrum of the (19,1)–(0,2) transition was re-recorded at regular intervals throughout the measurements to ensure that the EFD and ESA settings were optimised. An example is shown in figure 4.5(a). The peaks in the spectrum

correspond to increased fragmentation of the (19,1) level indicating that population was transferred from the (0,2) level. The transition frequencies for *G*=1/2−1/2 and *G*=3/2−3/2 were derived from the geometric mean of the Doppler shifted frequencies observed for each hyperfine transition. Two Doppler shifted resonances observed in different scans but at the same ion beam source voltage (and hence beam velocity) are related by the equation

$$\nu_{1(CO/CT)}\nu_{2(rest)}=\nu_{2(CO/CT)}\nu_{1(rest)}$$

The rest frequency for a transition $\nu_{1(rest)}$ can therefore be determined from one Doppler shifted component $\nu_{1(CO/CT)}$ if the rest frequency of another transition $\nu_{2(rest)}$ has been previously determined from two Doppler shifted components, $\nu_{2(CO/CT)}$ and its counterpart $\nu_{2(CT/CO)}$.

Since the (19,1)−(19,0) transition was calculated to be 3000 times weaker than the (19,1)−(0,2) transition (recorded in about ten minutes), signal averaging was performed over a large number of scans in our attempted detection. Our first definite observation is shown in figure 4.5(b) and was made using the EFDL lens set at 500 V and resulted from signal averaging over 999 scans (a weekend) at 4 kV beam potential. The observation appeared to be a single transition at 14937±1 MHz which is now labelled as CT in the figure.

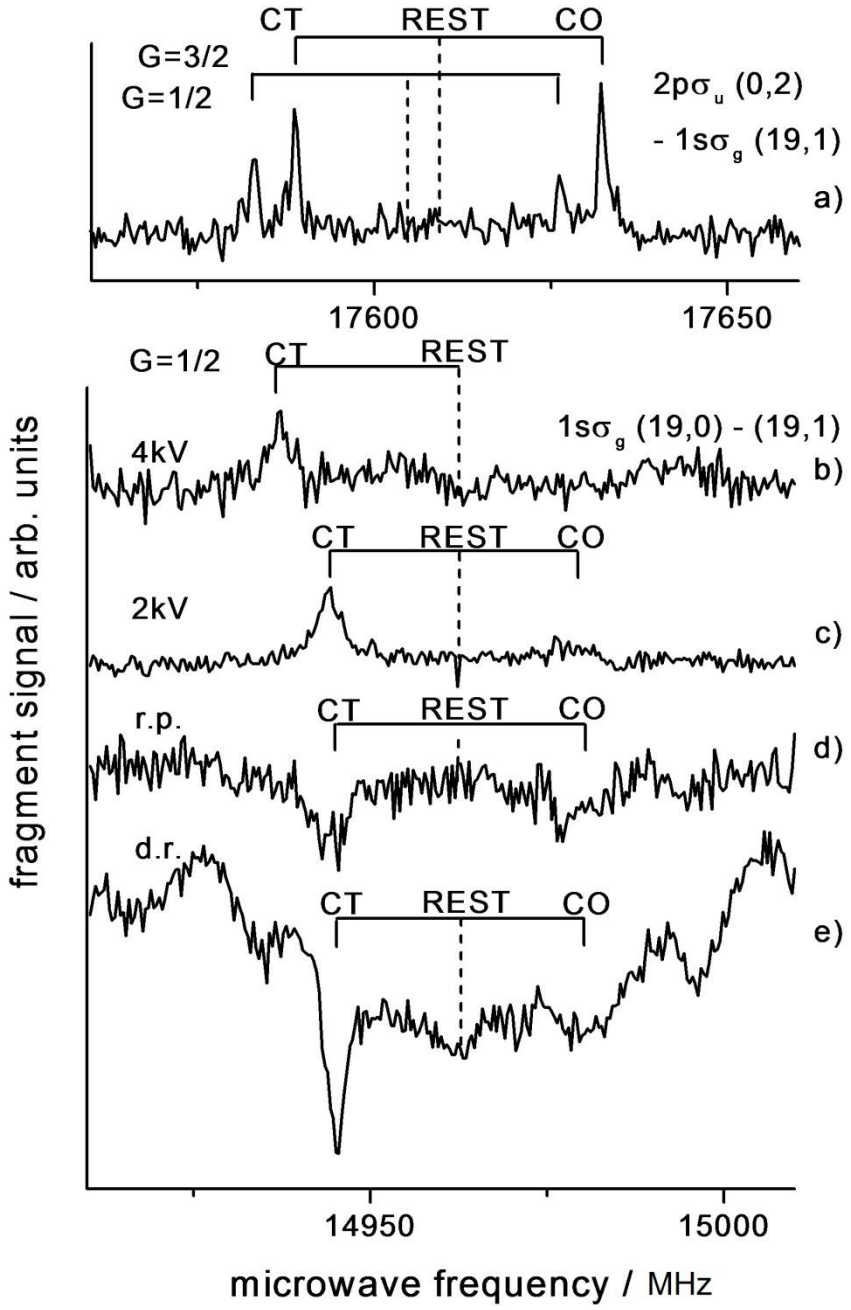

Figure 4.5

(a) (19,1)–(0,2) transition in H_2^+ observed at 2 kV. Each ΔG=0 transition appears at two different frequencies, corresponding to co- (CO) and counter- (CT) propagating microwave/ion beam geometry. (b) (19,1)–(19,0) transition observed at 4 kV via fragmentation of the (19,0) level. (c) (19,1)–(19,0) transition spectrum observed at 2 kV via fragmentation of the (19,0) level. (d) (19,1)–(19,0) transition spectrum observed in reverse phase (r.p.) via fragmentation of the (19,1) level. (e) (19,1)–(19,0) transition spectrum observed in double resonance (d.r.) with the (19,1) –(0,2) transition.

(*Reprinted from Molecular Physics, Vol. 101, Nos. 4-5, Andrew D. J. Critchley, Alan N. Hughes, Iain R. McNab, and Richard E. Moss, "Energy shifts and forbidden transitions in H_2^+ due to electronic g/u symmetry breaking", Pages 651-661, Copyright (2003), with permission from Taylor and Francis Group)*

In order to determine if the observed line was a co- or counter-propagating component we re-recorded the spectrum at a lower source potential to observe the sign of change of the Doppler shift. The source potential used was 2 kV and the resultant spectrum is shown in figure 4.5(c). The peak was shifted to a new frequency of 14962.4±1.3 MHz. The frequency shift showed the component to be counter-propagating, as the resonant frequency increased with decreasing source potential, and with this information a much weaker co-propagating component observed in the spectrum at 14977.5±1 MHz could also be definitely assigned. Analysing this information, together with the data from the calibration spectra gave a rest frequency of (14960.7±0.7) MHz. Since the signal to noise ratio was significantly improved at the lower beam potential, the source voltage was set at 2 kV in all further studies of the (19,1)–(19,0) transition. The increase in signal to noise was due to the increased interaction time in the waveguide at the lower beam velocity, which resulted in greater population transfer between levels, and hence in an increased number of observed fragments.

4.5 Verification of Spectra

In order to verify experimentally that we had indeed observed the (19,1)–(19,0) transition we made two further measurements. We checked that the transition could be observed with reversed phase by monitoring fragmentation of the (19,1) fragments (figure 4.5(d)), and we checked that the transition could be observed in double resonance with the (19,1)–(0,2) transition (figure 4.5(e)).

From a consideration of the above experiments we were convinced that we had observed the forbidden (19,1)–(19,0) transition at a rest frequency of 14961.7±1.1 MHz in excellent agreement with the theoretically predicted frequency of 14960±3 MHz. The other theoretical prediction was that the transition should have a dipole strength of about –0.42 D. We were not able to

verify this directly, but the following analysis shows that our measurements are consistent with this value.

In order to verify the theoretical prediction that the (19,1)–(19,0) transition should have a dipole strength of –0.42 D we made a comparison with the intensity of the (19,1)–(0,2) transition. The two spectra used are shown in figure 4.5 parts (a) and (c). In principle the relative transition probability could have been measured using the radiative broadening, but the more intense transition was saturated at higher microwave powers due to the minute number of ions available in the ion beam. Our observed intensity can be written [100] as $I \propto CFP(N_u - N_l)|\langle u|\mu|l\rangle|^2$, where C is the collection efficiency for fragment protons, F is the fragmentation rate from the level monitored, P is the microwave power, $(N_u - N_l)$ is the population difference and $\langle u|\mu|l\rangle$ is the transition dipole. As we monitored transitions from one level (19,1) in both measurements, using identical instrument settings, the only factors that differed between the two transitions were the microwave powers (known), the transition dipoles (to be compared) and the population differences between the states. Unfortunately we had no way of measuring or calculating the population differences; earlier work [3] (and references therein) showed that Franck-Condon factors for ionisation are not predictive of populations for upper levels of D_2^+ in an ion beam and therefore would probably not be predictive for H_2^+. In the absence of other data, we arbitrarily assumed that the population differences were the same for the two transitions. Accepting this approximation, we expected to observe the transitions in the ratio of the square of the theoretically predicted transition dipoles, that is in the ratio

$$\frac{I(19,1-0,2)}{I(19,1-19,0)} = \frac{(23\ \mathrm{D})^2}{(0.42\ \mathrm{D})^2} \approx 3000$$

In order to measure the relative intensities of the transitions we assumed that the noise level was constant, and defined the intensities by $I = (S\Gamma)/(NP\sqrt{\omega})$ where S = signal, Γ = linewidth, N = noise, P = microwave power and ω = measurement bandwidth. We ignored the power broadening of the transitions.

Within these approximations we found the ratio of intensities to be 8000 in reasonable agreement with the predicted value of ≈3000.

We can reverse the argument above to calculate the ratio of population differences between upper and lower states. Assuming the theoretical intensity ratio to be correct, we can calculate the ratio of the differences in populations to be

$$\frac{\left(N_{0,2} - N_{19,1}\right)}{\left(N_{19,0} - N_{19,1}\right)} = \frac{8}{3}$$

4.6 The Search for the (0,1)-(0,0) Transition in the 2pσ$_u$ Electronic State of H_2^+

Following our successful observation of the (19,1)–(19,0) transition we searched for the "forbidden" transition calculated to have the next greatest intensity, the (0,1)-(0,0) transition in the 2pσ$_u$ level of H_2^+, which is shown in the schematic energy level diagram below (figure 4.6).

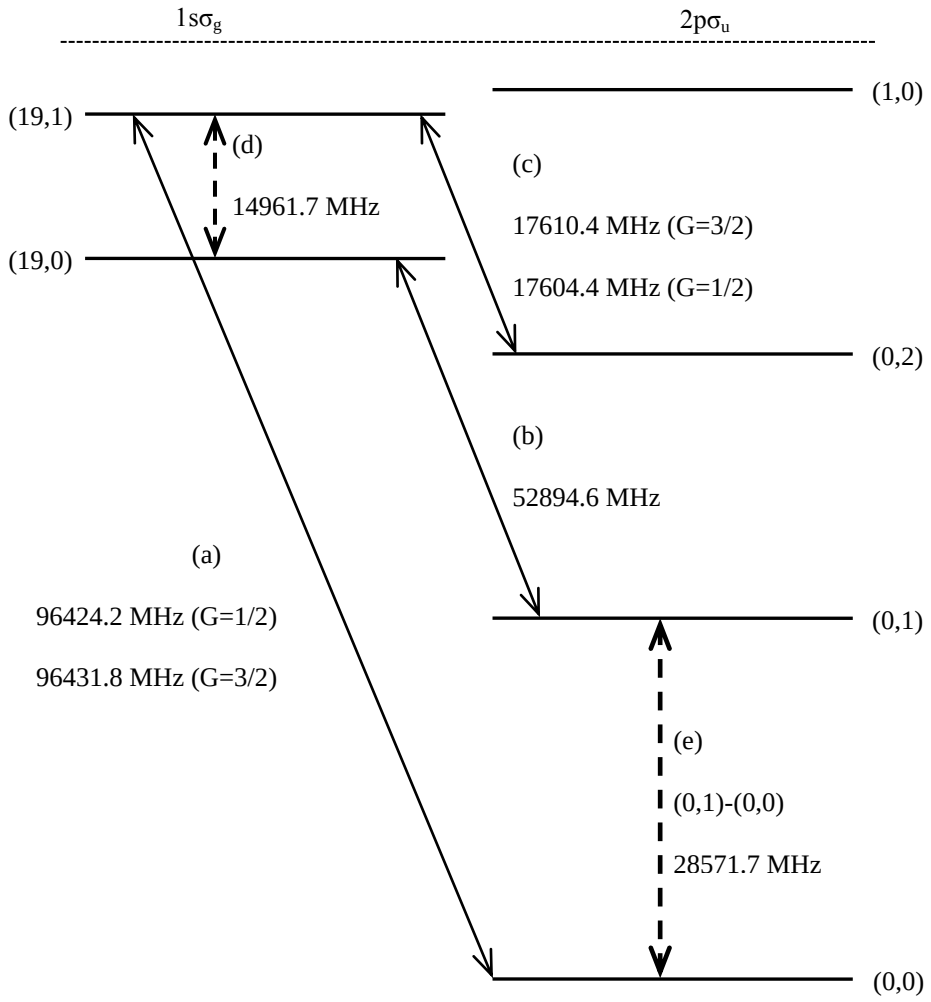

Figure 4.6

Energy level diagram for H_2^+ (not to scale) showing the (v=19, N=0) and (v=19, N=1) energy levels of the $1s\sigma_g$ ground state and the (v=0, N=0), (v=0, N=1), and (v=0, N=2); and the (v=1, N=0) first excited state $2p\sigma_u$. The transitions labelled (a), (b), and (c) were measured by Carrington *et al.* [50, 87] ; transition (d) was measured by Critchley *et al.* [93] and is described in detail in this work; transition (e) is the (0,1)-(0,0) transition, the search for which is described in the current work. (Hyperfine splittings are not shown).

From previous measurements and calculations of the transition frequencies labelled (a), (b) and (d) in figure 4.6, the $2p\sigma_u$ (0,1)-(0,0) transition rest frequency was calculated to be 28571.7 ± 1.3 MHz (from experiment - disregarding the hyperfine components), and 28574 ± 3.3 MHz (from theory)

The microwave equipment was on loan to our group for a limited time and we had access only to the WR-62 waveguide. At the $2p\sigma_u$ (0,1)-(0,0) transition

frequency of 28571.7 MHz the WR-62 waveguide transmits multiple $TE_{m,n}$ modes. It was therefore necessary to search for a pattern of absorption frequencies arising from the *mode structure* and Doppler shifts, rather than just a forward and backward shifted Doppler split transition (details follow below).Our search strategies were as follows

1. The search was first conducted in single resonance attempting to observe the (0,1)-(0,0) transition directly having first located and observed the (19,0)-(0,1) transition, and used this transition to optimise instrumental settings.

2. We then searched for the (0,1)-(0,0) transition in double resonance with the (19,0)-(0,1) transition, hoping that the population transfer to the (0,1) level would aid detection.

4.6.1 *Microwave Mode Structure*

In free space, microwaves propagate as a transverse electromagnetic wave, with both the electric and magnetic components perpendicular to each other and to the direction of propagation. Such a wave is called a TEM wave – but this type of wave cannot be supported by a hollow conductor (waveguide); instead the wave propagates with *either* the electric *or* the magnetic field component in the direction of propagation; these are labelled TM and TE respectively. A TE wave has an electric field perpendicular to the direction of propagation with magnetic components both parallel and perpendicular to the direction of propagation; a TM wave has a magnetic field perpendicular to the direction of propagation with electric components both parallel and perpendicular to the direction of propagation. Theoretically an infinite number of TE and TM waves (called ‘modes’) can be supported and each of these modes is labelled with the subscripts m and n giving the number of half-wave variations of the transverse field within the waveguide in the x- and y- directions respectively. For waveguide of a given size there are wavelength regions in which only the $TE_{1,0}$ mode can be propagated, and this is considered to be the normal operational range of the waveguide. For a waveguide operating outside this range other modes may be propagated – which modes are present

depends upon factors such as the geometry of the waveguide system, and the mechanism used to launch the wave (i.e. the output coupler). As will be shown below, the radiation for each of the $TE_{m,n}$ and $TM_{m,n}$ modes propagates at a different phase velocity (and power) so that numerous Doppler-shifted spectral features of different intensities for a given resonance are observed. However, for each pair of values of m and n, the $TE_{m,n}$ and $TM_{m,n}$ modes propagate at the same phase velocity, and so both contribute to the same Doppler-shifted peak. Thus for convenience this work refers only to the $TE_{m,n}$ modes.

Each mode $TE_{m,n}$ of a rectangular waveguide of width a and height b (and a>b) has a characteristic cut-off frequency, $f_{cut-off}^{m,n}$ given by the following expression (for further detail see [150]):

$$f_{cut-off}^{m,n} = \frac{c}{2}\sqrt{\left(\frac{m}{a}\right)^2 + \left(\frac{n}{b}\right)^2}$$

Where c = the speed of light in free space. WR-62 waveguide has the dimensions [149] a = 15.8 mm and b = 7.9 mm. For each mode $TE_{m,n}$ microwaves with a free-space frequency $f_{free\text{-}space}$ and wavelength λ will be propagated through the waveguide with a characteristic reduced wavelength λ_{guide} and corresponding increased velocity (since the frequency of waves entering the waveguide, and thus propagating through it, remains unchanged). This characteristic velocity, termed the phase velocity is related to the cut-off frequency as follows:

$$v_{phase}^{m,n} = \frac{c}{\sqrt{1 - \left(\frac{f_{cut-off}^{m,n}}{f_{free-space}}\right)^2}}$$

The other characteristic velocity for microwaves in a waveguide is the group velocity and $V_{group}*V_{phase}=c^2$.The group velocity is the velocity at which energy is transmitted through the guide, while the phase velocity is the velocity with which wave-fronts pass across a fixed point within the guide.

For a given waveguide (of dimension a and b), operating with a free-space frequency $f_{free\text{-}space}$ the values of $f_{cut-off}^{m,n}$ and therefore $v_{phase}^{m,n}$ can be calculated for each $TE_{m,n}$ mode.

In order to search for the $2p\sigma_u$ (0,1)-(0,0) transition at a frequency of 28571.7 MHz it was necessary to calculate and search for a pattern of lines arising from the mode-structure in the guide, and to the Doppler shifts due to Co and Counter propagating waves in the guide. Using a value of 28572 MHz for the value of $f_{free\text{-}space}$ in the expression for $v_{phase}^{m,n}$ a range of such values was calculated for the modes $TE_{m,n}$ possibly present (since not all modes may be propagated). This is a first approximation, since $v_{phase}^{m,n}$is a function of $f_{free\text{-}space}$ which will change as the microwave synthesiser is scanned across a range of frequencies to locate the mode structure; however the maximum scanning range used was of the order of 100 MHz and this change does not affect the calculated positions of the modes significantly.

$TE_{m,n}$	$f_{cut-off}^{m,n}$ (GHz)	$v_{phase}^{m,n}$ (x 10^6 ms^{-1})
$TE_{1,0}$	9.49	317.836
$TE_{0,1}$	18.97	400.905
$TE_{0,2}$	37.95	Not propagated
$TE_{2,0}$	18.97	400.905
$TE_{1,1}$	21.22	447.432
$TE_{1,2}$	39.14	Not propagated
$TE_{2,1}$	26.84	871.916
$TE_{3.0}$	28.47	3389.167

Table 4.2

Values of $f_{cut\text{-}off}$ and v_{phase} for the first 8 modes $TE_{m,n}$ of WR-62 waveguide with the dimensions a = 15.8 mm and b = 7.9 mm using an approximate transition value of 28572 MHz for $f_{free\text{-}space}$. The values of v_{phase} for $TE_{0,2}$ and $TE_{1,2}$ are not shown as the cut-off frequency for these modes is too high and so they will not propagate through the waveguide at the range of frequencies required to search for the $2p\sigma_u$ (0,1)-(0,0) transition.

The Doppler shifted components for each of the $TE_{m,n}$ modes can then be calculated with the standard Doppler shift equation using the phase velocity of the microwaves within the waveguide rather than the speed of light, *c* as follows:

$$f_{Dopp}^{m,n} = f_{transition}\sqrt{\frac{1\mp\left(\frac{v_{ion}}{v_{phase}^{m,n}}\right)}{1\pm\left(\frac{v_{ion}}{v_{phase}^{m,n}}\right)}}$$

In the above, the value of the velocity of the ion, labelled v_{ion}, will be (for a given ion) determined by the source potential, V_{source} by the relation

$$v_{ion} = \sqrt{\frac{2eV_{source}}{m_{ion}}}$$

where e is the charge of the ion, and m_{ion} is its mass.

4.6.2 *Mode Structure for the (0,1)-(0,0) Transition in the 2pσ$_u$ Electronic State of H_2^+*

The Doppler-shifted components for the (0,1)-(0,0) transition calculated to have a rest frequency of 28571.9 MHz were determined for a range of source potentials, V_{source} and these are shown in table 4.3.

Mode $TE_{m,n}$	Frequency (MHz)			
	V_{source} = 1.0 kV	V_{source} = 2.0 kV	V_{source} = 4.0 kV	V_{source} = 5.0 kV
Counter-propagating mode 1,0	28544.1	28532.6	28516.3	28509.8
Counter-propagating mode 0,1	28549.9	28540.7	28527.8	28522.6
Counter-propagating mode 2,0	28549.9	28540.7	28527.8	28522.6

Counter-propagating mode 1,1	28552.2	28544.0	28532.4	28527.8
Counter-propagating mode 2,1	28561.8	28557.6	28551.6	28549.3
Parallel mode 2,1	28582.0	28586.2	28592.2	28594.6
Parallel mode 1,1	28591.7	28599.9	28611.4	28616.1
Parallel mode 2,0	28594.0	28603.1	28616.0	28621.2
Parallel mode 0,1	28594.0	28603.1	28616.0	28621.2

Table 4.3

Values of Doppler-shifted frequencies for each mode $TE_{m,n}$ at various source potentials, V_{source} for the (0,1)-(0,0) transition in the $2p\sigma_u$ electronic state of H_2^+ which was determined using previous observations to have a rest frequency of 28571.9 MHz.

The values calculated and shown in table 4.3 were plotted to produce an overlay for comparison with frequency scans once the instrument was optimised. An example is shown in figure 4.7.

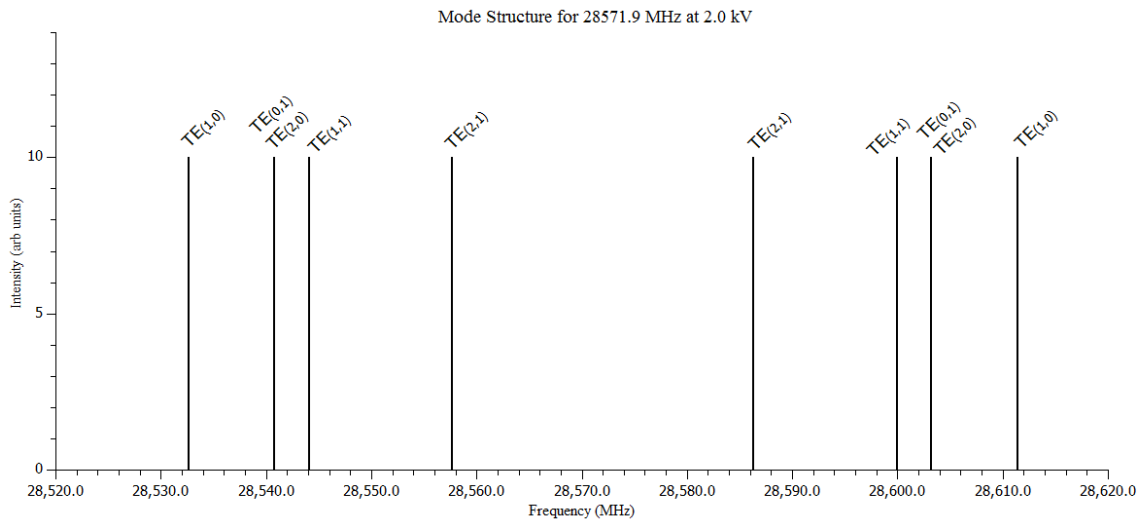

Figure 4.7

Mode structure for the (0,1)-(0,0) transition in the $2p\sigma_u$ electronic state of H_2^+ which was determined to have a rest frequency of 28571.9 MHz: the Doppler shifted components in this example are shown at a source potential of 2.0 kV.

4.6.3 *Experimental Approach to find the (0,1)-(0,0) Transition in the $2p\sigma_u$ Electronic State of H_2^+*

Our initial attempts to observe the (0,1)-(0,0) transition were made in single resonance by frequency scanning over the range 28460-28660 MHz using a source potential of 7 kV. A high source potential was chosen initially to maximise the possibility of observing fragments from the (0,1) level. The EFDL was set to 1.5 kV and the electrostatic analyser was set to observe the middle of the EFDL peak. This was repeated at source potentials of 1, 2, 4, and 5 kV but with nothing conclusive found, despite scanning for a total of 40 – 50 hours at each potential.

Our second attempt at observation was to search for the transition in in double resonance while pumping the previously measured (19,0)-(0,1) transition at 52894.6 MHz [50]. This allowed us to optimise the instrumental set-up to see EFDL fragmentation from the (1,0) level and we anticipated that the population transfer from 19,0 would enhance the population available for transfer in the desired transition, allowing for greater sensitivity.

The pump frequency for the (19,0)-(0,1) transition was provided from a Wiltron 6753B-10 microwave synthesizer with an output frequency range of 2-26.5 GHz, frequency doubled with a Millitech MUD-15 doubler. The scan frequency used to search for the (0,1)-(0,0) transition was supplied by a Wiltron 6769B synthesizer with output frequency range of 10 MHz – 40 GHz. We first observed the (19,0)-(0,1) transition at 52894.6 MHz to optimize the EFD fragmentation. At each source potential to be used, we calculated the Doppler shifts for each of the $TE_{m,n}$ modes which might propagate.

The (19,0)-(0,1) transition was first observed at a source potential of 2 kV, and with the electric field dissociation lens set at 500 V. Several $TE_{m,n}$ modes are apparent and these are indicated in red on the spectra in figure 4.8.

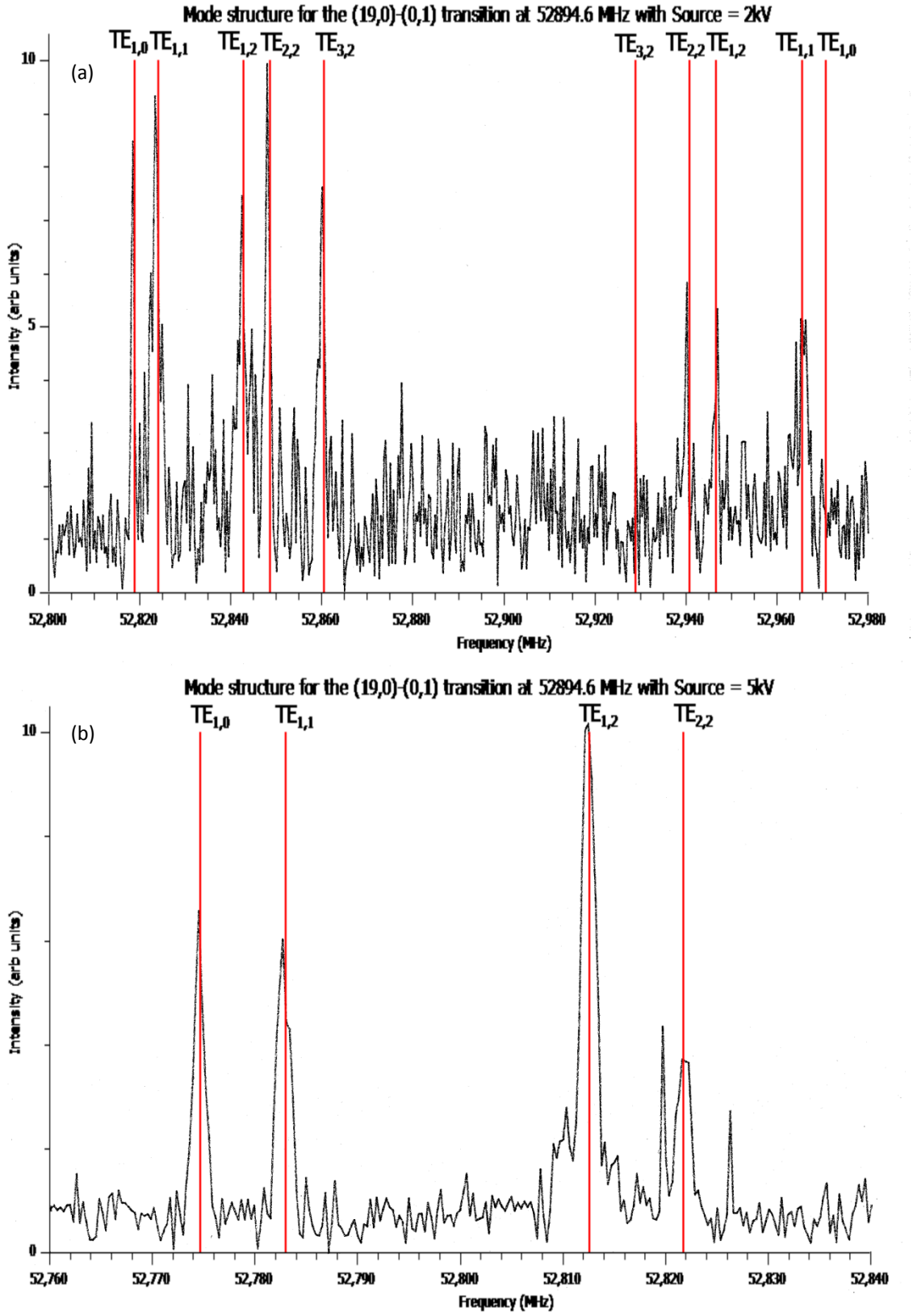

Figure 4.8

The (19,0)-(0,1) transition in H_2^+ observed with an ion beam potential of (a) 2 kV with the EFDL set to 500 V and (b) 5 kV with the EFDL set to 1500 V; both show good agreement with the predicted mode structure.

However, not all of the $TE_{m,n}$ modes were present; as can be seen in figure 4.8 (a) there were 5 counter-propagating modes consisting of $TE_{1,0}$, $TE_{1,1}$, $TE_{1,2}$, $TE_{2,2}$ and $TE_{3,2}$; three parallel modes were observed which were $TE_{1,1}$, $TE_{1,2}$, and $TE_{2,2}$. We verified that this was the (19,0)-(0,1) transition by observing the transition at a source potential of 5 kV. The spectrum is shown in figure 4.8 (b) and displays the dominant modes $TE_{1,0}$, $TE_{1,1}$, $TE_{1,2}$, and $TE_{2,2}$.

To maximise the possibility of observing the (0,1)-(0,0) transition, we used the $TE_{1,2}$ counter-propagating mode of the (19,0)-(0,1) transition (at 52812.5 MHz for V_{source} set to 5 kV) as the pump signal. Therefore, pumping at 52812.5 MHz with -7.0 dbm microwave power, with the EFDL and ESA optimized for transmission of fragments from 19,0 we scanned over the frequency range for the (0,1)-(0,0) transition over a period of 18 hours. Our initial search used a scan range of 28585-28645 MHz (hoping to detect the parallel components); and we later tried again using a scan range of 28500-28560 MHz (hoping to detect the counter-propagating components).

Sadly, the results of these scans were inconclusive.

To summarise, we were unable to observe the (0,1)-(0,0) transition in H_2^+ either in single resonance or in double resonance given the time at our disposal. The search had to be abandoned when we were requested to return the microwave equipment. The search was not conducted with the most appropriate waveguide size, thus unnecessarily introducing the added complexity of multi-mode microwave propagation, which necessarily splits the intensity of a transition across multiple peaks and it seems most probable that the signals were far too weak.

4.7 Discussion

We measured the 19,0-19,1 pure rotation transition in H_2^+ between levels close to dissociation in the $1s\sigma_g$ ground state where significant electric dipole intensity results from *ortho–para* mixing caused by the Fermi contact hyperfine

interaction; the frequency of the transition is in excellent agreement with the value predicted and the intensity is consistent with the theoretical value. We also made unsuccessful searches for the equivalent pure rotation transition (0,0)-(0,1) in the $2p\sigma_u$ first-excited state, but despite the precisely known transition frequency, these searches were unsuccessful. This was partly because of the limited time at our disposal, but most likely because an extremely weak transition signal was broadened over multiple microwave modes.

There are many other forbidden pure rotation and vibration-rotation transitions that could be detected with suitable frequency sources. The possibilities for such further work are the subject of chapter 5.

Chapter 5: Future Developments in the Spectroscopy of g/u Symmetry Breaking Transitions and the Spectroscopy of H_2^+ and D_2^+

In this chapter I consider the proposal for a new experiment made by Hilico [74], together with possible extensions of the measurements reported in chapter 4, on spectra involving g/u symmetry breaking.

5.1 Possibility of Experimental Detection $2p\sigma_u$ (v =1, N=0) in H_2^+

Hilico and his co-workers recently proved that the vibrational level $2p\sigma_u$ (v=1, N=0) exists [74]. Hilico suggests that using an experiment similar to that described in Chapter 4, detection of this level might be possible. We now give a brief discussion of this possibility, and indicate what calculations would be necessary in order to convince an experimentalist to undertake the search.

Hilico [74] states that the $2p\sigma_u$ (1,0) excited vibrational level has an electric dipole allowed transition to the $1s\sigma_g$ (19,1) level and that the transition between these levels should be observable in the 6 GHz range using methods similar to those described in chapter 4 to observe and measure the $1s\sigma_g$ (19,1)-(19,0) transition in H_2^+.

5.1.1 *Populations of the Levels Involved*

The two levels involved in the suggested measurement are $2p\sigma_u$ (1,0) (with essentially zero binding energy) and $1s\sigma_g$ (19,1) which is calculated to be bound by just 0.22 cm^{-1} [93] . The extremely weak binding energy of the $2p\sigma_u$ (1,0) state will result it in being dissociated by electric fields of (at most) a hundred volts per metre. As all ions are subjected to fairly high electric fields during focusing as the ion beam travels through the machine (and also to a magnetic field, which can also cause “EFD” dissociation [56, 57]) it is likely that any population of the $2p\sigma_u$ (1,0) level which is created in the ionization process will be destroyed before the ion beam reaches the region of interaction with the microwave cell. The detection scheme, therefore, would necessarily be

$1s\sigma_g$ (19,1) → $2p\sigma_u$ (1,0) → EFD creation of H^+ fragments → H^+ detection

5.1.2 *Microwave Waveguide to be Used*

The $1s\sigma_g$ (19,1) → $2p\sigma_u$ (1,0) transition occurs in the 6 GHz range, and for single resonance detection, this would require WR-137 (C-band) waveguide (with large internal dimension) to be used. However, it is likely that to enhance the available population in the $1s\sigma_g$ (19,1) level, that a double resonance detection scheme would be needed increasing the population of the (19,1) level by pumping via the (19,1)-(0,0) transition (96424.2 MHz for G=1/2) or the (19,1)-(0,2) transition (17604.4 MHz for G=1/2) both of which were measured by Carrington et al. [50, 87]. The large internal dimensions of the waveguide will pass many modes of the second frequency, and the better choice of pump transition would be (19,1)-(0,2) as this has the lower frequency and would therefore have a less complicated $TE_{m,n}$ mode structure in the WR-137 waveguide.

5.1.3 *Production and Detection of Fragment H^+ Ions*

The minimal binding energy of the $2p\sigma_u$ (1,0) state will be extremely sensitive to electric field dissociation. We estimate a field of just ~50 V/m would be sufficient to dissociate the level; these fields are weak enough to be produced by contact potentials between dissimilar metals in the vacuum system. The problem then is to use an EFDL design capable of separating fragments produced at low electric fields from the background fragments produced (largely) at earth potential. Carrington [50] describes some EFDLs that are more complicated than those used by us which might aid the detection. In addition to optimizing the design of the EFDL, it would be necessary to minimize “accidental” electric field dissociation following passage of the ion beam through the waveguide. It would therefore be necessary to remove the ion-beam focussing lens which is situated between the waveguide and the electrostatic analyser and reduce any “field-free” regions between the waveguide, EFDL and ESA to a minimum to reduce the effects of any electric fields not produced by the EFDL. Amongst other measures such as the introduction of a Faraday cage arrangement between the waveguide end and the ESA (enclosing the EFDL), the waveguide

itself must be held at earth potential and to avoid contact potential differences the EFD and the Faraday cage must be made of the same metals, and connected with a wire of the same metal.

5.1.4 *The Noise Background*

The fragment H^+ ions created in the EFDL will be detected against a background of H^+ ions arising from other processes in the apparatus (mostly at earth potential). A successful detection would require that these be minimized as far as possible. The principle source of background ions is from collision induced dissociation, which can occur both with residual background gas, and in collision with ion-optic elements such as the wire gauzes used in the EFD, or else on the edges of focusing optics. An updated version of the vacuum pumping system described in chapter 2 would be necessary to achieve and maintain ultra-high vacuum conditions within the instrument to reduce the effects of background collisional processes. Essentially this would require the use of much higher pumping speeds and better differential pumping between the ion source region and the first and second field free regions in the spectrometer.

5.1.5 *Stability of the Ion Beam System*

Even though the proposed measurement is of an allowed transition, the detection of a weak signal on a large background might require long scanning times (of the order of several days) during which the stability of the parent ion beam would be crucial (the frequency synthesizers are stable over many days and do not represent a limiting factor).

One of the main sources of instability is the large current required to produce the magnetic field used for steering the ion beam and mass/charge selection, which causes heating over long periods of scanning; this could be addressed with a suitable cooling system; and also an ion-beam stabilisation system. Such a stabilisation system was designed and built by the Newcastle group which detected changes in the ion beam steering and applied correction voltages to the magnet control system using feedback methods. This could be achieved more effectively using a similar system but with computer monitored and

controlled feedback and correction. Alternatively, an electrostatic mass analyser could be used (electric quadrupole analyser), which would not suffer from the hysteresis and heating problems associated with a magnetic analyser. A third possibility would be to do away with the mass analysis completely [see for example Coe, Saykally etc. [151]] relying upon Doppler shifts and fragment kinetic energy analysis to identify the species of interest.

5.1.6 Summary of Possibility of Detecting the $2p\sigma_u$ (1,0) - $1s\sigma_g$ (19,1) Transition

It would be a challenging experiment to measure the $2p\sigma_u$ (1,0) - $1s\sigma_g$ (19,1) transition with our methods. Although the transition is fully electric dipole allowed, the population of (19,1) is a small fraction of the total population of the ion beam and fragments from the (1,0) level would be detected against a large background arising from earth field fragmentation of the ion beam produced by other processes. Use of better pumping speeds (to minimize CID fragmentation) together with a carefully constructed EFDL may enable the transition to be measured. The number which gives us greatest confidence is the huge transition dipole to be expected for this transition – this is a “charge transfer” type transition, and so to an excellent approximation the transition dipole is given by $e\Delta R/2$, which from the calculated values will be of order 900 Debye, some 2100 times greater than the allowed transition (19,1)-(0,0) and possibly the largest transition dipole for any calculated transitions.

5.2 g/u Symmetry Breaking Measurements in Other Ions

Our measurement of a symmetry breaking transition in H_2^+ can be viewed as a prototype for a class of similar transitions in homonuclear diatomic molecules. The only requirement is that levels exist close to a degenerate dissociation limit with a suitable hyperfine interaction present to cause g/u mixing. I now discuss some candidates for similar measurements.

5.2.1 *Brief Review of g/u Mixing*

There have only been a few direct observations of g/u mixing. Apart from the work on the molecular ions H_2^+ and D_2^+ [123] previously described, all other observations of g/u mixing were of neutral molecules and made either spectroscopically [130, 132-134, 138, 152] or using light-induced drift [135]. In diatomic molecules the effect has been seen in I_2 [133, 153-155] and Cs_2 [134]. For the Cs_2 molecule splittings ranging from 60 MHz to 2.4 GHz were observed and an approximate theoretical description given [134]. For I_2 the dissociation was to $^2P_{1/2}$ and $^2P_{3/2}$ atomic states, involving ten electronic states with a common dissociation limit, but each with a different long-range interaction. Also the P states allowed additional couplings that are absent for S states. Hence the analysis employed for the I_2 investigations is not applicable to the systems of interest here.

We understand from the work described in chapter 3 that g/u mixing will occur automatically in diatomic molecular ions close to a degenerate dissociation limit, and that it is **not** necessary that both interacting states have bound levels, because the continuum contribution may be significant. The g/u mixing in these cases will contribute significantly to the hyperfine structure and therefore permits transitions in both scattering and spectroscopy that would normally be considered forbidden. Using ion beam spectroscopy of diatomic molecular ions, it would be possible to access information which is complementary to that from ultra-low energy scattering experiments [156] [14] [157] [158], in which the same interactions are important. The limiting difficulty in such studies is the production of ion beams of sufficient strength. For gaseous precursors, this is simple to achieve with conventional electron impact ion sources. Other systems of great potential interest would be diatomic ions of the alkali metals, Li_2^+, Na_2^+, K_2^+, Rb_2^+ and Cs_2^+. The limiting difficulty here would be to achieve ion beams of sufficient strength to be useful in spectroscopic measurements. Our experience shows that beam currents of nA are sufficient for microwave spectroscopy with electric field dissociation. Such beams of alkali metals may in principle be formed using liquid metal ion source technology (LMIS) [159], which is well

developed for non-corrosive metals, and is used in the semiconductor industry. The operation of liquid metal ion sources with corrosive metals has been demonstrated, but is far from trivial [160].

Consideration of the availability of isotopes with nuclear spin (table 5.1)

Isotope	Abundance	Spin	magnetic moment (μ_N)	quadrupole moment (Qfm^{-2})
^{1}H	99.9%,	1/2	+2.79	
^{2}D	0.01%	1	+0.85	+0.3
^{3}He	1 in 10^{6}	1/2	-2.127	
^{21}Ne	0.27%,	3/2	-0.66	+10.3
^{83}Kr	11.5%	9/2	-0.97	+27.0
^{129}Xe	26.4%,	1/2	-0.77	
^{131}Xe	21.2%,	3/2	+0.69	-12.0
^{6}Li	7.5%,	1	+0.82	-0.06
^{7}Li	92.5%,	3/2	+3.256	-3.66
^{23}Na	100%,	3/2	+2.217	+10.2
^{39}K	93%,	3/2	+0.39	+4.9
^{41}K	6.7%,	3/2	+0.21	+6
^{85}Rb	72%	5/2	+1.35	+27.4
^{87}Rb	28%	3/2	+2.75	+13.2
^{133}Cs	100%,	7/2	+2.58	-0.3

Table 5.1

Comparison of isotopes in which g/u symmetry breaking may be studied, showing their abundance in the naturally occurring element, nuclear spin, nuclear magnetic moment, and quadrupole moment [161].

Our measurements of g/u symmetry breaking in H_2^+ were spectroscopic, but it is possible that g/u symmetry breaking might also be observable in H^+/ H collisions. One possibility for such observations would be atom-ion (e.g. H/H^+) cold collisions where g/u interactions are significant could now be investigated

through the nuclear spin-exchange process (related to charge-exchange) [162]. Calculations of low energy H/H^+ collisions have assumed no coupling between the $1s\sigma_g$ and $2p\sigma_u$ states [162, 163], but at collision energies lower than ~meV the effect of coupling between g and u states may become important and this effect increases as the collision energy is lowered. Also relevant to such a project would be creation of an ultracold atom-ion collision. Collisions of atoms at ultracold temperatures are critical in cooling and trapping atoms and molecules and in photoassociation spectroscopy [164]. Ultracold neutral plasmas have been created [165, 166] and have stimulated theoretical interest in ultracold atom-ion (Na/Na^+) collisions [167]. Spin-polarised hydrogen atoms have been photoassociated [168, 169] at 0.15 K. A combination of these techniques might make possible ion-molecule collision measurements with observable g/u symmetry breaking effects.

Other research groups interested in the problems of g/u symmetry breaking include (1) Tennyson and his co-workers at UCL, who have considered the astrophysical implications of g/u mixing in the spectrum of water [170]; (2) Chapovsky (Russian Academy of Sciences) and (3) Hermans (Leiden University) are interested in nuclear spin conversion in polyatomic molecules (see for example [135] and references therein).

5.2.2 *Proposal for Further Experiments on Diatomic Molecular Ions*

Using an experiment similar to that described in Chapter four, with a conventional ion source, it would be possible to investigate further examples of g/u mixing in H_2^+, D_2^+ and $^3He_2^+$, $^{21}Ne_2^+$, $^{83}Kr_2^+$, $^{129}Xe_2^+$ and $^{131}Xe_2^+$ diatomic molecular ions in energy levels within ~300 GHz of their lowest dissociation limits. The heavier molecular ions suffer from having many more vibration-rotation levels, the total ion beam population will be distributed amongst these levels making observations of all spectra rather weak. The 300 GHz (10 cm^{-1}) limit below dissociation is set both by the physics of the problem and by the available technology. Such experiments would investigate molecular ions in levels similar to those that may be investigated using observations of photoassociation in a Bose-Einstein condensates that are able to produce

ultracold molecules in states near dissociation [159] [156] [158]. Our technique would enable us to study similar states in molecular ions. The g/u mixing rapidly decreases in size (apart from cases of accidental degeneracy) away from a degenerate dissociation limit; available microwave and millimetre wave sources are ideally suited for studying in this frequency range, and the technique of electric field dissociation allows *only* those levels within this energy range of dissociation to be probed. It would be possible to measure frequencies of the stronger pure rotation and rotation-vibration transitions which are forbidden in the absence of the hyperfine interactions, along with the additional hyperfine structure in allowed transitions that occurs as a result of this g/u mixing. Relative intensities could also be measured.

5.2.3 *Relation to Other Work*

The interactions of atoms just above the dissociation limit are of crucial importance to a proper understanding of ultra-low energy scattering and photoassociation spectroscopy. This research probes the same energy regime of the molecular potential, but from below where each state is associated with a known rotational angular momentum. The effects of the weak couplings arising from the interaction between the valence electron and the nuclear spins will be investigated. The preliminary experiment has shown the feasibility of this work in light systems.

5.2.4 *Experiment*

A schematic diagram of our preliminary experiment was given in figure 4.1. This apparatus no longer exists, and further experiments would require either a similar purpose built instrument or else a modification of a commercially available mass spectrometer. The mass spectrometer would need to have a sufficiently large field free region to enable incorporation of a microwave cell and an electric field dissociation lens.

In addition to an ion-beam passing through a microwave cell and electric field dissociation lens, sources of radiation would also be required. It was crucial to the unambiguous identification of the transition in H_2^+ that double irradiation

(double resonance) measurements were made. The selected ions passed through a microwave cell in which radiation from two microwave synthesisers (S1, S2), amplified by amplifiers (A1, A2), was propagated. At resonance, population was transferred from one stable state to another and the upper state was subsequently fragmented using an electric-field dissociation lens. The fragment ions were selected with an electrostatic analyser (ESA) and detected with an electron multiplier (PMT) against an almost zero background. A plot of fragment ion intensity against Doppler-shifted frequency gave the spectrum. In the experiments proposed here, two microwave sources would be needed to enable double-resonance measurements which allow the determination of relative parity and relative rotational quantum numbers of the levels. Without the use of two sources measured spectra would probably be unassignable unless very high level theoretical predictions were available.

Zeeman splitting measurements might prove essential for experimental determination of the angular momentum quantum numbers of states involved in the transitions [171]. Without Zeeman measurements to help deduce the angular momentum quantum numbers, the spectra might be assignable, but assignments would be totally dependent upon theory (as were the measurements in H_2^+). A magnetic field suitable for Zeeman measurements can be made using a solenoid wrapped around the microwave cell. Others have employed both a simple wire-wound solenoid [172] and a water-cooled high-field solenoid [104, 171]. Using a solenoid wound with copper pipe (to allow water cooling) it should be possible to generate a 0.1 T field within a magnetization volume of 100 cm^3 using a current of 250 Amperes.

Measurement of *relative* intensities should be possible to an accuracy of about 10%. By construction of a suitable electric-field dissociation lens, the fraction of the ion beam in each of the levels involved in a transition should be directly measurable. It might also be possible to determine the *absolute* transition rates directly from knowledge of the radiation density and population density within the microwave cell. In addition, in favourable cases Rabi oscillations might be observed that would enable a direct measurement of the transition amplitude (see for example [103] and references therein).

5.2.5 *Programme and Methodology*

The energy-level structures of H_2^+ and D_2^+ and to a lesser extent, He_2^+, are known to high accuracy [93] [97, 104]. A clearly desirable extension to this work would be similar measurements in He_2^+ but only the $^3He_2^+$ isotope has a nuclear spin that could lead to g/u symmetry breaking effects. Nevertheless, earlier work on the structure of $^4He_2^+$ [173] near dissociation would provide an excellent starting point for an exploration of the odd isotope $^3He_2^+$.

5.3. Further Experiments

5.3.1 *Further Experiments on H_2^+*

While energy shifts due to g/u mixing have been evaluated for all the relevant high-lying levels [97], the hyperfine induced dipole moments have been calculated only for the v = 19 levels of the X state [92]. Analogous calculations would be needed for the v = 0 levels of the A state, as the induced transitions (v, N) = (0,0) → (0,1) and (0,1) → (0,2) are likely to have the largest induced dipole moments.

5.3.2 *Further Experiments on D_2^+*

Here the levels of interest are v = 26 and 27 in the X state and v = 0 and 1 in the A state. Energy shifts have been calculated and hyperfine-induced dipole moments are available [123], the evaluation was analogous to that for H_2^+. The influence of g/u symmetry breaking on frequencies and transition intensities in the spectrum of D_2^+ was considered by Moss [97] and Gerdova [123]. Moss calculated the effect of symmetry breaking on “allowed” electric dipole transitions, and Gerdova extended this work to calculations of intensities of electric dipole “forbidden” transitions in D_2^+. Consideration of table 5.2 below shows that the obvious candidates for observation with our technique would be, for example, the (27,1)-(27,0) transition at 9.7 GHz (for G = 1/2) and the (27,2)-(27,1) transition at 16.3 GHz (for G = 1/2). These could be observed using “x-

band" and "ku-band" waveguides respectively which have ideal operating ranges for these transitions.

The results of Gerdova's calculations are summarized below (adapted from tables 1, 2 and 3 of reference [123], reproduced with permission).

v',N'	v'',N''	Total dipole μ/ea_o	Hyperfine shift (cm^{-1})	Transition (cm^{-1})	Transition (GHZ)	Total dipole μ/ea_o	Hyperfine shift (cm^{-1})	Transition (cm^{-1})	Transition (GHZ)
		G = 1/2				G = 3/2			
27,0	26,1	0.005023	0.00361	9.9197	297.4	0.003971	–0.00733	9.9087	297.1
27,0	25,1	0.004640	0.00361	63.2356	1895.8	0.003668	–0.00733	63.2247	1895.4
27,0	24,1	0.001008	0.00362	186.4144	5588.6	0.000797	–0.00734	186.4035	5588.2
27,0	23,1	0.000202	0.00363	382.6142	11470.5	0.000160	–0.00734	382.6032	11470.2
27,0	22,1	0.000040	0.00364	649.7937	19480.3	0.000032	–0.00735	649.7827	19480.0
27,0	21,1	0.000008	0.00366	985.2739	29537.8	0.000006	–0.00736	985.2629	29537.4
27,1	27,0	0.141256	–0.00367	0.3228	9.7	0.111673	0.00732	0.3338	10.0
27,1	26,0	0.007708	–0.00370	11.4563	343.5	0.006094	0.00727	11.4673	343.8
27,1	25,0	0.005036	–0.00370	66.3384	1988.8	0.003981	0.00727	66.3494	1989.1
27,1	24,0	0.001076	–0.00370	191.0640	5728.0	0.000851	0.00729	191.0750	5728.3
27,1	23,0	0.000072	–0.00370	388.6815	11652.4	0.000057	0.00730	388.6925	11652.7
27,1	22,0	0.000043	–0.00370	657.1709	19701.5	0.000034	0.00732	657.1819	19701.8
27,1	21,0	0.000009	–0.00370	993.8759	29795.6	0.000007	0.00735	993.8870	29796.0
27,1	26,2	0.003661	–0.00370	7.9271	237.6	0.002894	0.00727	7.9380	238.0
27,1	25,2	0.005463	–0.00370	58.0981	1741.7	0.004319	0.00727	58.1091	1742.1
27,1	24,2	0.001178	–0.00370	178.1682	5341.3	0.000931	0.00729	178.1792	5341.7
27,1	23,2	0.000234	–0.00370	371.5239	11138.0	0.000185	0.00730	371.5349	11138.3
27,1	22,2	0.000046	–0.00370	636.0788	19069.2	0.000037	0.00732	636.0899	19069.5
27,1	21,2	0.000009	–0.00370	969.1064	29053.1	0.000007	0.00735	969.1175	29053.4
27,2	27,1	0.013672	0.00362	0.5445	16.3	0.010809	–0.00734	0.5336	16.0
27,2	26,1	0.008184	0.00356	10.7870	323.4	0.006470	–0.00735	10.7761	323.1
27,2	25,1	0.004692	0.00356	64.1029	1921.8	0.003709	–0.00735	64.0920	1921.4
27,2	24,1	0.000969	0.00357	187.2817	5614.6	0.000766	–0.00736	187.2708	5614.2
27,2	23,1	0.000190	0.00358	383.4815	11496.5	0.000150	–0.00736	383.4706	11496.2
27,2	22,1	0.000037	0.00359	650.6610	19506.3	0.000030	–0.00737	650.6501	19506.0
27,2	21,1	0.000007	0.00361	986.1412	29563.8	0.000006	–0.00738	986.1303	29563.4
27,2	26,3	0.010981	0.00356	5.3239	159.6	0.008681	–0.00735	5.3130	159.3
27,2	25,3	0.005660	0.00356	50.7411	1521.2	0.004475	–0.00735	50.7302	1520.9
27,2	24,3	0.001145	0.00357	166.1080	4979.8	0.000905	–0.00736	166.0971	4979.5
27,2	23,3	0.000221	0.00358	355.1755	10647.9	0.000175	–0.00736	355.1645	10647.6
27,2	22,3	0.000043	0.00359	615.7809	18460.6	0.000034	–0.00737	615.7700	18460.3
27,2	21,3	0.000008	0.00360	945.1223	28334.1	0.000007	–0.00737	945.1113	28333.7

Table 5.2

Summary of calculations by Gerdova [123] for D_2^+ in the ground electronic state ($1s\sigma_g$) showing forbidden $\Delta G = 0$ rotation and rotation–vibration transitions *(v″, N″)* - (*v′, N′)*; the total electric dipole transition moments (μ^a); the total hyperfine shifts (which include electronic g/u symmetry-breaking contributions); the transition energies in wavenumber

and frequencies in GHz. *(Adapted from Chemical Physics Letters, Vol. 385, Irina Gerdova, "Intensities of electric dipole forbidden rotation and rotation–vibration transitions in D_2^+", Pages456-461, Copyright (2004), with permission from Elsevier B. V.)*

[a] μ given in units of ea_0; 1 $ea_0 \approx 2.54175$ D

5.3.3 *Possible Experiments on $^3He_2^+$*

Accurate potential curves are available [173] [174] which reproduced observations of near-dissociation transitions in $^4He_2^+$ within 200 MHz after scaling was applied to improve agreement between theory and experiment [175]. In order to further confirm the accuracy of these potentials, a comparison was made of data calculated using them for $^3He^4He^+$ with previously measured transitions [176], this is shown in table 5.3. The comparison shown is for a purely ab-initio potential without scaling applied.

$^3He^4He^+$ transitions in the ground (X) state – experimental vs calculated values		
v'',J'' - v',J'	Experimental values (MHz)	Calculated (LEVEL) values (MHz)
(1,2)-(0,1)	1781.8394	1781.7034
(1,4)-(0,3)	1810.7172	1810.5814
(1,5)-(0,4)	1824.2118	1824.0748
(1,6)-(0,5)	1837.0549	1836.9166
(1,7)-(0,6)	1849.2293	1849.0904
(1,8)-(0,7)	1860.7190	1860.5798
(1,10)-(0,9)	1881.5800	1881.4404
(1,11)-(0,10)	1890.9155	1890.7799
(1,12)-(0,11)	1899.5091	1899.3713

Table 5.3

$^3He^4He^+$ transitions in the ground (X) state; comparison of observed values [176] to calculated values using Cencek's unpublished X-state potential [174].

Excellent agreement was obtained. Using these potentials we have simulated the near-dissociation spectra of $^{3}He^{4}He^{+}$ in the ground (X) state, and $^{3}He^{3}He^{+}$ in the ground (X) and first excited electronic (A) state, obtaining 11 transitions, in the absence of hyperfine structure, at frequencies between 15 GHz and 77 GHz as shown in tables 5.4 – 5.6.

Calculated values of electric dipole allowed pure-rotation transitions in the ground (X) state of heteronuclear $^{3}He^{4}He^{+}$			
v'',J'' - v',J'	E(upper) cm^{-1}	Calculated (LEVEL) values (cm^{-1})	Calculated (LEVEL) values (MHz)
(22,1)-(22,0)	-0.079	0.0279	836.42
(21,4)-(21,3)	4.02	2.0622	61 823.20
(21,3)-(21,2)	-1.666	1.9242	57 686.06
(21,2)-(21,1)	-3.595	1.4203	42 579.52
(21,1)-(21,0)	-5.016	0.7397	22 175.65

Table 5.4

Calculated values of electric dipole allowed pure-rotation transitions in the ground (X) state of heteronuclear $^{3}He^{4}He^{+}$ using the unpublished ground state potential calculated by Cencek. All transitions terminate in levels < 6 cm^{-1} below the dissociation limit and could be observed using microwave ion / beam techniques.

Calculated values of “Forbidden” pure-rotation transitions in the ground (X) state of $^{3}He^{3}He^{+}$			
v'',J'' - v',J'	E(upper) cm^{-1}	Calculated (LEVEL) values (cm^{-1})	Calculated (LEVEL) values (MHz)
(20,3)-(20,2)	0.358	1.0575	31 703.05
(20,2)-(20,1)	-0.679	0.9662	28 965.95
(20,1)-(20,0)	-1.630	0.5188	15 553.23
(19,6)-(19,5)	4.025	5.9968	179 779.54
(19,5)-(19,4)	-1.959	6.3559	190 545.09

Table 5.5

Calculated values of “Forbidden” pure-rotation transitions in the ground (X) state of $^{3}He^{3}He^{+}$ using the unpublished ground state potential calculated by Cencek. All transitions terminate in levels < 2 cm^{-1} below the dissociation limit and could be observed using microwave ion / beam techniques.

Calculated values of “Forbidden” pure-rotation transitions in the first excited electronic state (A) of $^3He^3He^+$			
v'',J'' - v',J'	E(upper) cm^{-1}	Calculated (LEVEL) values (cm^{-1})	Calculated (LEVEL) values (MHz)
(0,1)-(0,0)	-6.251	0.7670	22 994.08
(0,2)-(0,1)	-4.756	1.5128	45 352.60
(0,3)-(0,2)	-2.622	2.1522	64 521.33
(0,4)-(0,3)	-0.044	2.5685	77 001.69
(1,1)-(1,0)	-0.135	0.1989	5 962.87

Table 5.6

Calculated values of “Forbidden” pure-rotation transitions in the first excited electronic state (A) of $^3He^3He^+$ using the first excited state potential of Carrington *et al.* [173]. All transitions terminate in levels < 7 cm-1 below the dissociation limit. All transitions could be observed using microwave ion / beam techniques.

The transitions shown in tables 5.4 – 5.6 were all selected according to various criteria. These were:

- They are all pure rotation transitions
- The upper and lower states both lie very close to the dissociation limit (and so the effect of g/u mixing is greater)
- The upper bound level needs to be close to dissociation (within a few cm^{-1}) so they can be dissociated with electric field dissociation
- The transition frequency needs to be accessible with an appropriate combination of microwave synthesizer (and frequency doubler where necessary) and suitable waveguide

All of the 11 transitions identified above which lie between 15 and 77 GHz could be searched for using WR-62, WR-42 and WR-28 waveguide (also called “Ku band”, “K band” and “Ka band” respectively) – these have dimensions and cut-off frequency as shown below in table 5.7.

Waveguide designation		Operational frequency (GHz)	Cut-off frequency (GHz)	Internal dimensions (mm)
EIA WR-	Industrial			
137	C	5.85 – 8.20	4.29	34.84 x 15.80
90	X	8.20 – 12.4	6.56	22.86 x 10.16
62	Ku	12.4 – 18.0	9.49	15.80 x 7.90
42	K	18.0 – 26.5	14.1	10.67 x 4.32
28	Ka	26.5 – 40.0	21.1	7.11 x 3.56

Table 5.7

Data for standard rectangular microwave waveguide [149].

However, it is apparent from the data in table 5.7 that as the operational frequency range of the waveguides increase, the internal dimensions decrease which, in turn, causes attenuation of the ion beam. Previous studies [177] have found <10% ion beam attenuation using WR-90 waveguide, but approximately 50% attenuation using WR-28 waveguide and so choice of waveguide becomes a compromise since for a particular transition it is preferable to use a waveguide with an operational frequency range which includes the transition rest frequency thus avoiding the added complexity which occurs when higher $TE_{m,n}$ modes are propagated (see chapter 4, section 4.6.1 for greater detail).

The theory of the g/u mixing is very similar to that for D_2^+ [178, 179]. The stronger hyperfine splitting in ^{3}He, 8.665 GHz, than in H (711.4 MHz [142]) and the smaller energy spacings (15 GHz rather than 42 GHz) should enhance the breakdown of g/u symmetry. Determination of the hyperfine-induced dipole moment, requires values of the A-X transition dipole moment, which is available [178], and then of hyperfine induced couplings between bound levels and between bound levels and the continuum states.

^{3}He is an expensive and limited resource and to reduce costs and preserve the resource a closed cycle He re-circulating system should be used between the pumping system and the ion source [176]. This would require the use of He-leak-tight rotary pumps and good filtration of the gas before it is returned to the ion source.

5.4 Conclusion

Despite the inherent experimental challenges involved the observation of the v = 1, N = 0 level of the first excited electronic state ($2p\sigma_u$) of H_2^+ should be possible with a careful design of experiment; provided those difficulties identified earlier in this chapter are addressed. It is clear also that there are many candidates suitable for the observation of g/u symmetry-breaking using the ion-beam/microwave techniques described earlier in this work, many of which could be observed using the experimental set-up as described in chapters 2 and 4.

However, it is apparent that most of the groups currently working in this area are using very different instrumentation to that which was available in 1999. Examples of this are Bielsa et al. (2007) [180] who developed 50 mW continuous-wave quantum cascade laser (QCL) in the 9.2 μm range, phase locked to a single-mode CO_2 laser with a tuneable frequency offset; and Bakalov et al. (2011) [181] who analysed the effects of an external magnetic field on the ro-vibrational, rotational and radiofrequency transitions of the HD^+ molecular ion; and Borodin et al. (2012) [157] who have demonstrated rotational excitation of molecular ions that are sympathetically cooled by laser-cooled atomic ions to a temperature as low as approximately 10 mK. The advance in instrumentation has been accompanied by improvements in the precision of calculations (see for example Karr et al., 2011, [22]).

In the final chapter I discuss the contents of this work and summarise the conclusions drawn.

Chapter 6: In Conclusion

In Chapter one I set the scene for theory and measurements described in chapters three and four by giving a brief review of the theory of the hydrogen molecular cation. The Born-Oppenheimer and Adiabatic solutions were discussed in mathematical detail while the application of more sophisticated theoretical techniques was described qualitatively. The hydrogen molecular cation is (arguably) the simplest molecule, and is an example of the quantum mechanical three body problem. As was discussed experimental transition frequencies can now be reproduced by theory to within a few ppm in favourable cases. To achieve these high levels of accuracy requires non-adiabatic approaches, together with the inclusion of both relativistic and radiative corrections.

In Chapter two I described techniques of ion beam / laser and ion beam / microwave spectroscopy, including an assessment of the theoretical signal to noise ratios possible in an experiment of this type. Two methods of detection were discussed, predissociation arising from the unusual nature of diatomic dication potential energy curves, and electric field dissociation of singly charged molecular ions. Modifications to the apparatus that were made to obtain the microwave spectra described in chapter four were described in detail. Parts of this chapter were previously published as [100, 101].

The theory of hyperfine induced g/u symmetry breaking was discussed in Chapter three. It was seen that a simple perturbation treatment using only the Fermi-contact part of the Hamiltonian gave excellent agreement with hyperfine induced shifts and splittings that were observed in both H_2^+ and D_2^+ by Carrington and his co-workers. The application of the theory to the calculation of the intensity of electric dipole “forbidden” transitions was discussed, including the necessity of including terms arising from mixing with the continuum wavefunctions of the first excited electronic state. The influence of the newly

found (1,0) level of the first excited state ($2p\sigma_u$) on the perturbation expressions was discussed, but shown in the following chapter to be insignificant. Parts of this chapter were previously published as [98].

Chapter four discussed our measurements in both single and double resonance of a pure-rotation transition (19,0)-(19,1) in the ground electronic state. The observations were achieved by modifying our ion-beam system to allow the inclusion of a microwave cell and electric field dissociation lens (as described at the end of chapter one). Further searches for a similar transition (0,0)-(0,1) in the $2p\sigma_u$ state were unsuccessful due to time limits imposed by the necessity of returning borrowed apparatus. Parts of this chapter were previously published as [93, 98].

Finally, in Chapter five, I discussed how with the levels of sensitivity achieved we could have applied the apparatus described in this thesis to the observation of microwave transitions in (1) a transition to the newly discovered (1,0) level of the $2p\sigma_u$ state of H_2^+ and (2) g/u symmetry breaking pure-rotation transitions in D_2^+ and (3) g/u symmetry breaking pure-rotation transitions in $^3He_2^+$.

The field of spectroscopy of ions near to their dissociation limits is (admittedly) a minority interest. Nevertheless, the measurements of transitions close to dissociation have given surprising and valuable insights into simple molecular processes.

References

[1] E. Teller and H. L. Sahlin, "Chapter 2: The hydrogen molecular ion and the general theory of electron structure," in *Physical Chemistry: An Advanced Treatise*. vol. V, H. Eyring, Ed., ed New York: Academic, 1972, pp. 35-124.

[2] A. Carrington and R. A. Kennedy, "Chapter 26: Spectroscopy and Structure of the Hydrogen Molecular Ion," in *Gas Phase Ion Chemistry: Vol 3 Ions and Light*, M. T. Bowers, Ed., ed London: Academic, 1984, pp. 393-442.

[3] A. Carrington, I. R. McNab, and C. A. Montgomerie, "Spectroscopy of the hydrogen molecular ion," *Journal of Physics B: Atomic, Molecular and Optical Physics,* vol. 22, p. 3551, 1989.

[4] C. A. Leach and R. E. Moss, "Spectroscopy And Quantum-Mechanics Of The Hydrogen Molecular Cation - A Test Of Molecular Quantum-Mechanics," *Annual Review of Physical Chemistry,* vol. 46, p. 55, 1995.

[5] B. Roth, J. Koelemeij, S. Schiller, L. Hilico, J. P. Karr, V. Korobov*, et al.*, "Precision Spectroscopy of Molecular Hydrogen Ions: Towards Frequency Metrology of Particle Masses," in *Precision Physics of Simple Atoms and Molecules*. vol. 745, S. G. Karshenboim, Ed., 1st ed: Springer, 2008, pp. 205-232.

[6] W. Wing, G. Ruff, W. Lamb, and J. Spezeski, "Observation of the Infrared Spectrum of the Hydrogen Molecular Ion HD^+," *Physical Review Letters,* vol. 36, pp. 1488-1491, 1976.

[7] P. Blythe, B. Roth, U. Fröhlich, H. Wenz, and S. Schiller, "Production of Ultracold Trapped Molecular Hydrogen Ions," *Physical Review Letters,* vol. 95, p. 183002, 2005.

[8] B. Roth, J. Koelemeij, H. Daerr, and S. Schiller, "Rovibrational spectroscopy of trapped molecular hydrogen ions at millikelvin temperatures," *Physical Review A,* vol. 74, p. 04501(R), 2006.

[9] H. Li, J. Wu, B.-L. Zhou, J.-M. Zhu, and Z.-C. Yan, "Calculations of energies of the hydrogen molecular ion," *Physical Review A,* vol. 75, p. 012504, 2007.

[10] J. Koelemeij, B. Roth, A. Wicht, I. Ernsting, and S. Schiller, "Vibrational Spectroscopy of HD^+ with 2-ppb Accuracy," *Physical Review Letters,* vol. 98, p. 173002, 2007.

[11] J.-P. Karr, F. Bielsa, A. Douillet, J. Pedregosa Gutierrez, V. Korobov, and L. Hilico, "Vibrational spectroscopy of H_2^+: Hyperfine structure of two-photon transitions," *Physical Review A,* vol. 77, p. 063410, 2008.

[12] J.-P. Karr, V. Korobov, and L. Hilico, "Vibrational spectroscopy of H_2^+: Precise evaluation of the Zeeman effect," *Physical Review A,* vol. 77, p. 062507, 2008.

[13] V. Korobov, L. Hilico, and J. P. Karr, "Relativistic corrections of $m\alpha^6(m/M)$ order to the hyperfine structure of the H_2^+ molecular ion," *Physical Review A,* vol. 79, p. 012501, 2009.

[14] J. C. J. Koelemeij, D. W. E. Noom, D. Jong, M. A. Haddad, and W. Ubachs, "Observation of the $v'=8 \leftarrow v=0$ vibrational overtone in cold trapped HD^+," *Applied Physics B,* vol. 107, pp. 1075-1085, 2012.

[15] L. Hilico, N. Billy, B. Gremaud, and D. Delande, "Ab initio calculation of the J = 0 and J = 1 states of the H_2^+ , D_2^+ and HD^+ molecular ions," *Eur. Phys. J. D,* vol. 12, pp. 449-466, 2000.

[16] T. C. Scott, M. Aubert-Frécon, and J. Grotendorst, "New approach for the electronic energies of the hydrogen molecular ion," *Chemical Physics,* vol. 324, pp. 323-338, 2006.

[17] D. Bakalov, V. Korobov, and S. Schiller, "High-Precision Calculation of the Hyperfine Structure of the HD^+ Ion," *Physical Review Letters,* vol. 97, p. 243001, 2006.

[18] J. P. Karr and L. Hilico, "High accuracy results for the energy levels of the molecular ions H_2^+ D_2^+ and HD^+, up to J = 2," *Journal of Physics B: Atomic, Molecular and Optical Physics,* vol. 39, pp. 2095-2105, 2006.

[19] V. Korobov, "Bethe logarithm for the hydrogen molecular ion H_2^+," *Physical Review A,* vol. 73, p. 024502, 2006.

[20] V. Korobov, L. Hilico, and J. P. Karr, "Hyperfine structure in the hydrogen molecular ion," *Physical Review A,* vol. 74, p. 040502(R), 2006.

[21] C. Fabri, G. Czako, G. Tasi, and A. G. Csaszar, "Adiabatic Jacobi corrections on the vibrational energy levels of H_2^+ isotopologues," *J Chem Phys,* vol. 130, p. 134314, 2009.

[22] J. P. Karr, L. Hilico, and V. I. Korobov, "Theoretical progress in the H_2^+molecular ion: towards electron to proton mass ratio determination.," *Canadian Journal of Physics,* vol. 89, p. 103, 2011.

[23] A. Ishikawa, H. Nakashima, and H. Nakatsuji, "Accurate solutions of the Schrödinger and Dirac equations of , HD^+, and HT^+: With and without Born–Oppenheimer approximation and under magnetic field," *Chemical Physics,* vol. 401, p. 62, 2012.

[24] Q. L. Tian, L. Y. Tang, Z. X. Zhong, Z. C. Yan, and T. Y. Shi, "Oscillator strengths between low-lying ro-vibrational states of hydrogen molecular ions," *J Chem Phys,* vol. 137, p. 024311, 2012.

[25] R. Moss and I. A. Sadler, "A transformed hamiltonian theory for HD^+ near dissociation " *Mol. Phys.,* vol. 64, p. 165, 1988.

[26] R. E. Moss and L. Valenzano, "Relativistic corrections for the vibration-rotation levels of the ground electronic state of the hydrogen molecular cation H_2^+," *Molecular Physics,* vol. 101, p. 2635, 2003.

[27] G. Jaffé, "Zur Theorie des Wasserstoffmolekülions," *Z. Phys.,* vol. 87, p. 535, 1934.

[28] E. A. Hylleraas, "Über die Elektronenterme des Wasserstoffmoleküls," *Z. Phys.,* vol. 71, p. 739, 1931.

[29] G. Herzberg, "Molecular Spectra and Molecular Structure Volume 1 - Spectra of Diatomic Molecules." vol. 1, 2 ed Malabar, Florida: Krieger, 1989, pp. 226-236.

[30] G. Hunter and H. O. Pritchard, "Born—Oppenheimer Separation for Three-Particle Systems. II. Two-Center Wavefunctions," *The Journal of Chemical Physics,* vol. 46, p. 2146, 1967.

[31] G. Hunter and H. O. Pritchard, "Born—Oppenheimer Separation for Three-Particle Systems. III. Applications," *The Journal of Chemical Physics,* vol. 46, p. 2153, 1967.

[32] J. W. Cooley, "An Improved Eigenvalue Corrector Formula for Solving the Schrödinger Equation for Central Fields," *Mathematics of Computation,* vol. 15, pp. 363-374, 1961.

[33] R. J. Le Roy, "LEVEL 8.0: A Computer Program for Solving the Radial Schrödinger Equation for Bound and Quasibound Levels," University of Waterloo Waterloo, Ontario, Chemical Physics Research Report CP-663, 2007.

[34] M. Born and K. Huang, *Dynamical theory of crystal lattices*. Oxford, Eng.: Clarendon, 1954.

[35] G. Hunter, A. W. Yau, and H. O. Pritchard, "Rotation-vibration level energies of the hydrogen and deuterium molecule-ions," *Atomic Data and Nuclear Data Tables,* vol. 14, pp. 11-20, 1974.

[36] C. A. Coulson, "II.—The Van der Waals Force between a Proton and a Hydrogen Atom," *Proceedings of the Royal Society (Edinburgh) Section A,* vol. 61, pp. 20-25, 1941.

[37] J. P. Davis and W. R. Thorson, "Very low energy scattering in HH^+ and HD^+," *Canadian Journal of Physics,* vol. 56, pp. 996-1020, 1978/08/01 1978.

[38] A. Carrington, J. Buttenshaw, and P. G. Roberts, "Observation of vibration-rotation transitions in the HD^+ ion," *Molecular Physics,* vol. 38, pp. 1711-1715, 1979.

[39] A. Carrington and J. Buttenshaw, "Vibration-rotation spectroscopy of the HD^+ ion near the dissociation limit. 1. Experimental methods and measurements of the v=18-16 band," *Molecular Physics,* vol. 44, pp. 267-285, 1981.

[40] A. Carrington, J. Buttenshaw, and R. A. Kennedy, "Vibration-rotation spectroscopy of the HD^+ ion," *Journal of Molecular Structure,* vol. 80, p. 47, 1982.

[41] A. Carrington, I. R. McNab, and C. A. Montgomerie, "Vibration-rotation spectroscopy of the HD^+ ion near the dissociation limit. 5. Direct measurement of the asymmetric electron-distribution in v = 21," *Molecular Physics,* vol. 64, pp. 983-995, Aug 1988.

[42] A. Carrington, I. R. McNab, and C. A. Montgomerie, "Laser excitation and electric field dissociation spectroscopy of the HD^+ ion," *Chemical Physics Letters,* vol. 151, pp. 258-262, 10/14/ 1988.

[43] A. Carrington, C. A. Leach, A. J. Marr, R. Moss, C. H. Pyne, M. R. Viant*, et al.*, "Spectroscopy of HD^+ in high angular momentum states," *Chemical Physics,* vol. 166, pp. 145-166, 1992.

[44] L. Wolniewicz and J. D. Poll, "The vibration-rotational energies of the hydrogen molecular ion HD^+," *Journal of Chemical Physics,* vol. 73, pp. 6225-6231, 1980.

[45] L. Wolniewicz and J. D. Poll, "On the vibration rotational energy-levels of the hydrogen molecular ion HD^+," *Canadian Journal of Physics,* vol. 63, pp. 1201-1204, 1985.

[46] L. Wolniewicz and J. D. Poll, "On the higher vibration rotational levels of HD^+ and H_2^+," *Molecular Physics,* vol. 59, pp. 953-964, Dec 1986.

[47] A. Carrington, J. Buttenshaw, and R. A. Kennedy, "Vibration-rotation spectroscopy of the HD^+ ion near the dissociation limit. 2. Measurements of the v=17-14 band.," *Molecular Physics,* vol. 48, pp. 775-780, 1983.

[48] A. Carrington and R. A. Kennedy, "Vibration-rotation spectroscopy of the HD^+ ion near the dissociation limit. 3. Measurements of the v = 17-15 and 20-17 bands - demonstration of an asymmetric electron-distribution.," *Molecular Physics,* vol. 56, pp. 935-975, Nov 1985.

[49] A. Carrington, I. R. McNab, and C. A. Montgomerie, "Vibration-rotation spectroscopy of the HD^+ ion near the dissociation limit. 4. Nuclear hyperfine-structure in the v = 18-16 band.," *Molecular Physics,* vol. 64, pp. 679-689, Jul 1988.

[50] A. Carrington, C. A. Leach, R. E. Moss, T. C. Steimle, M. R. Viant, and Y. D. West, "Microwave electronic spectroscopy, electric field dissociation and photofragmentation of the H_2^+ ion," *Journal of the Chemical Society, Faraday Transactions,* vol. 89, p. 603, 1993.

[51] G. Herzberg, "Molecular Spectra and Molecular Structure Volume 1 - Spectra of Diatomic Molecules." vol. 1, 2 ed Malabar, Florida: Krieger, 1989, p. 133.

[52] L.-Y. Peng, I. D. Williams, and J. F. McCann, "Dissociation of H_2^+ from a short, intense, infrared laser pulse: proton emission spectra and pulse calibration," *Journal of Physics B: Atomic, Molecular and Optical Physics,* vol. 38, p. 1727, 2005.

[53] G. K. Paramonov and O. Kuhn, "State-Selective Vibrational Excitation and Dissociation of H_2^+ by Strong Infrared Laser Pulses: Below-Resonant versus Resonant Laser Fields and Electron-Field Following," *Journal of Physical Chemistry A,* vol. 116, pp. 11388-11397, Nov 2012.

[54] A. Kiess, D. Pavicic, T. W. Hansch, and H. Figger, "HD^+ in a beam in intense pulsed laser fields: Dissociation and ionization with high-energy resolution of the fragments," *Physical Review A,* vol. 77, pp. 053401 1-14, May 2008.

[55] G. Fuchsel, J. C. Tremblay, T. Klamroth, and P. Saalfrank, "Quantum dynamical simulations of the femtosecond-laser-induced ultrafast desorption of H_2 and D_2 from Ru(0001)," *Chemphyschem,* vol. 14, 2013.

[56] J. Hiskes, "Dissociation of Molecular Ions by Electric and Magnetic Fields," *Physical Review,* vol. 122, pp. 1207-1217, 1961.

[57] H. Wind, "Field dissociation probabilities of H_2^+," *Nuclear Fusion,* vol. 6, p. 67, 1966.

[58] Y. D. West, "Spectroscopy and dissociation of the Hydrogen Ions," PhD Thesis, Department of Chemistry, University of Southampton, Southampton, 1992.

[59] C. A. Leach, M. S. Child, and D. E. Manolopoulos, "Electric field dissociation of H_2^+: close-coupled scattering calculations," *Molecular Physics,* vol. 97, pp. 11-24, 1999.

[60] Z. Mulyukov, "Part I. Break up of the hydrogen molecular ion by an electric field," University of Southern California, 2000.

[61] L. Wolniewicz and J. D. Poll, "*Ab initio* Nonadiabatic Vibrational Energies of the Hydrogen Molecule ion," *J. Mol. Spectrosc.,* vol. 72, pp. 264-274, 1978.

[62] A. Carrington, I. R. McNab, C. A. Montgomerie-Leach, and R. A. Kennedy, "Vibration-rotation spectroscopy of the HD+ion near the dissociation limit," *Molecular Physics,* vol. 72, pp. 735-762, 1991.

[63] R. E. Moss and I. A. Sadler, "Transformed hamiltonian theory for HD^+," *Molecular Physics,* vol. 66, pp. 591-603, 1989.

[64] L. Foldy, *Pure appl. Phys,* vol. 10, p. 1, 1962.

[65] R. E. Moss, "Advanced Molecular Quantum Mechanics; An Introduction to Relativistic Quantum Mechanics and the Quantum Theory Of Radiation," ed London: Chapman and Hall, 1973, pp. 149-151.

[66] R. E. Moss, "On the fully nonadiabatic dipole polarizability of H_2^+ (0,0)," *Chemical Physics Letters,* vol. 311, pp. 231-235, Sep 1999.

[67] R. E. Moss, "Nonadiabatic dipole polarizability of H_2^+ (0,1)," *Physical Review A,* vol. 61, Apr 2000.

[68] R. E. Moss and L. Valenzano, "Adiabatic and non-adiabatic corrections to properties of the hydrogen molecular cation and its isotopomers: dissociation energies and bond lengths," *Molecular Physics,* vol. 100, pp. 649-654, 2002.

[69] R. E. Moss and L. Valenzano, "The dipole polarizability of the hydrogen molecular cation HD^+ and other isotopomers," *Molecular Physics,* vol. 100, pp. 1527-1535, May 2002.

[70] J. Frey, *Personal communication to I.R. McNab*, 1985.

[71] J. M. Hutson, "Coupled channel bound state calculations: Calculating expectation values without wavefunctions," *Chemical Physics Letters,* vol. 151, pp. 565-569, 1988.

[72] D. Bishop and L. Cheung, "Calculation of transition frequencies for H_2^+ and its isotopes to spectroscopic accuracy," *Physical Review A,* vol. 16, pp. 640-645, 1977.

[73] D. M. Bishop and L. M. Cheung, "Natural Orbital Analysis of Nonadiabatic H_2^+ Wave Functions," *International Journal Of Quantum Chemistry,,* vol. XV, pp. 517-532, 1979.

[74] J. Carbonell, R. Lazauskas, D. Delande, L. Hilico, and S. Kiliç, "A new vibrational level of the H_2^+ molecular ion," *Europhys. Lett.,* vol. 64, pp. 316-322, 2003.

[75] B. Roth, J. Koelemeij, S. Schiller, L. Hilico, J. P. Karr, V. Korobov*, et al.*, "Precision Spectroscopy of Molecular Hydrogen Ions: Towards

Frequency Metrology of Particle Masses," in *Precision Physics of Simple Atomic Systems*, ed: Springer, 2006.

[76] T. K. Rebane and A. V. Filinsky, "Energies of symmetric three-particle Coulomb systems," *Physics of Atomic Nuclei,* vol. 60, pp. 1816-1822, Nov 1997.

[77] M. H. Howells and R. A. Kennedy, "Einstein A factors for the $2p\sigma_u$-$1s\sigma_g$ electronic spectrum of the H_2^+ ion," *Chemical Physics Letters,* vol. 184, p. 521, 1991.

[78] R. E. Moss, "Calculations for the vibration-rotation levels of H_2^+ in its ground and first excited electronic states," *Molecular Physics,* vol. 80, p. 1541, 1993.

[79] R. E. Moss, "The $2p\sigma_u$-$ls\sigma_g$ Electronic Spectrum of D_2^+," *J. Chem. Soc. Faraday Trans.,* vol. 89, p. 3851, 1993.

[80] R. E. Moss, "Calculations for vibration-rotation levels of HD^+, in particular for high N " *Mol. Phys.,* vol. 78, p. 371, 1993.

[81] R. Bukowski, B. Jeziorski, R. Moszynski, and W. Kolos, "Bethe Logarithm and Lamb Shift for The Hydrogen Molecular Ion," *International Journal of Quantum Chemistry,* vol. 42, p. 287, Apr 1992.

[82] D. M. Bishop and L. M. Cheung, "Accurate One- and Two-Electron Diatomic Molecular Calculations," in *Advances in Quantum Chemistry*. vol. Volume 12, L. Per-Olov, Ed., ed: Academic Press, 1980, pp. 1-42.

[83] H. Dehmelt and K. Jefferts, "Alignment of the H_2^+ Molecular Ion by Selective Photodissociation. I," *Physical Review,* vol. 125, pp. 1318-1322, 1962.

[84] J. Babb and A. Dalgarno, "Electron-nuclear coupling in the hyperfine structure of the hydrogen molecular ion," *Physical Review Letters,* vol. 66, p. 880, 1991.

[85] C. Richardson, K. Jefferts, and H. Dehmelt, "Alignment of the H_2^+ Molecular Ion by Selective Photodissociation. II. Experiments on the Radio-Frequency Spectrum," *Physical Review,* vol. 165, pp. 80-87, 1968.

[86] K. Jefferts, "Hyperfine Structure in the Molecular Ion H_2^+," *Physical Review Letters,* vol. 23, pp. 1476-1478, 1969.

[87] A. Carrington, I. R. McNab, and C. A. Montgomerie, "Microwave Electronic Spectrum Of The H_2^+ Ion," *Chemical Physics Letters,* vol. 160, p. 237, 1989.

[88] A. Carrington, I. R. McNab, C. A. Montgomerie, and J. M. Brown, "Microwave spectra of the HD^+ and D_2^+ ions at their dissociation limits," *Molecular Physics,* vol. 66, p. 1279, 1989.

[89] A. Carrington, I. R. McNab, C. A. Montgomerie, and R. A. Kennedy, "Electronic spectrum ($2p\sigma_u$-$1s\sigma_g$) of the D_2^+ ion," *Molecular Physics,* vol. 67, pp. 711-738, 1989.

[90] A. Carrington, C. A. Leach, A. J. Marr, R. E. Moss, C. H. Pyne, and T. C. Steimle, "Microwave spectra of the D_2^+ and HD^+ ions near their dissociation limits," *The Journal of Chemical Physics,* vol. 98, p. 5290, 1993.

[91] A. Carrington, C. A. Leach, and M. R. Viant, "Nuclear hyperfine structure in the electronic millimetre wave spectrum of H_2^+," *Chem. Phys. Lett.,* vol. 206, pp. 77-82, 1993.

[92] P. R. Bunker and R. E. Moss, "Forbidden electric dipole rotation and rotation–vibration transitions in H_2^+," *Chemical Physics Letters,* vol. 316, pp. 266-270, 2000.

[93] A. Critchley, A. Hughes, and I. McNab, "Direct Measurement of a Pure Rotation Transition in H_2^+," *Physical Review Letters,* vol. 86, p. 1725, 2001.

[94] R. P. McEachran, C. J. Veenstra, and M. Cohen, "Hyperfine structure in the hydrogen molecular ion," *Chemical Physics Letters,* vol. 59, p. 275, 1978.

[95] R. E. Moss, "Calculated transition frequencies for microwave and far-infrared electronic transitions of the hydrogen molecular ion," *Chemical Physics Letters,* vol. 171, p. 513, 1990.

[96] R. E. Moss, *preliminary reults*.

[97] R. Moss, "Electronic g/u symmetry breaking in H_2^+," *Chem. Phys. Lett.,* vol. 206, pp. 83-90, 1993.

[98] A. D. J. Critchley, A. N. Hughes, I. R. McNab, and R. E. Moss, "Energy shifts and forbidden transitions in H_2^+ due to electronic g/u symmetry breaking," *Molecular Physics,* vol. 101, p. 651, 2003.

[99] A. Carrington, D. I. Gammie, A. M. Shaw, and S. M. Taylor, "Millimetre-wave electronic spectrum of the D_2^+ ion," *Journal of the Chemical Society, Faraday Transactions,* vol. 91, p. 1887, 1995.

[100] R. Abusen, S. G. Cox, A. D. J. Critchley, A. N. Hughes, F. Kemp, I. R. McNab*, et al.*, "Coaxial ion beam/infrared laser beam spectrometer for investigating infrared spectra of doubly positively charged molecules (molecular dications)," *Review of Scientific Instruments,* vol. 73, p. 241, 2002.

[101] A. N. Hughes, F. Kemp, P. S. Kreynin, I. R. McNab, and S. Spoor, "Recent research developments in Ion Beam Spectroscopy," *Solicited review for "Recent Research Developments in Chemical Physics, Vol-4",* vol. 4, pp. 359-377, 2003.

[102] A. Carrington, "Review Lecture: Spectroscopy of Molecular Ion Beams," *Proceedings of the Royal Society of London. Series A, Mathematical and Physical Sciences,* vol. 367, pp. 433-449, 1979.

[103] S. G. Cox, A. D. J. Critchley, I. R. McNab, and F. E. Smith, "High-resolution spectroscopy of ion beams," *Meas. Sci. Technol.,* vol. 10, p. R101, 1999.

[104] S. G. Cox, PhD Thesis, Physics, University of Newcastle upon Tyne, Newcastle upon Tyne, 2001.

[105] *We follow the usual convention in mass spectrometry whereby the beam direction at any point in the apparatus is the x-direction, the z-direction is that of the first magnetic field, and the y-direction is perpendicular to both*.

[106] D. A. Dahl and J. E. Delmore, "SIMION," Idaho National Engineering Laboratory, Idaho Falls, 1988.

[107] H. Wollnik, *Optics of Charged Particles*. Orlando, California: Academic Press, 1987.

[108] A. Carrington and R. A. Kennedy, "Infrared predissociation spectrum of the H_3^+ ion," *The Journal of Chemical Physics,* vol. 81, p. 91, 1984.

[109] B. P. Cowan, "Classical Mechanics," ed London: Routledge & K. Paul, 1984, p. 13.

[110] W. Rindler, *Introduction to special relativity*. New York: Oxford University Press, 1982.

[111] C. Le Sech, "Determination of highly excited states of diatomic-molecular ions using exact H_2^+-like orbitals," *Physical Review A,* vol. 51, pp. R2668-R2671, 1995.

[112] R. C. Shiell, PhD Thesis, Physcis, University of Newcastle upon Tyne, Newcastle upon Tyne, 1995.

[113] A. Critchley, "The Structure of Free Radicals," PhD Thesis, Physics, University of Newcastle upon Tyne, 2000.

[114] A. Carrington, J. Buttenshaw, R. A. Kennedy, and T. P. Softley, "Observation of bound to quasi-bound vibration-rotation transitions in the HeH^+ ion," *Molecular Physics,* vol. 44, pp. 1233-1237, 1981.

[115] N. F. Barber, "Shape of an electron beam bent in a magnetic field," *Proc. Leeds Phil. Lit. Soc. Sci. Sec.,* vol. 2, pp. 427-434, 1933.

[116] S. L. Kaufman, "High-resolution laser spectroscopy in fast beams," *Optics Communications,* vol. 17, pp. 309-312, 1976.

[117] J. A. Betts, "Signal processing, modulation and noise," in *Science and technology series*, ed Kent: Hodder and Stoughton, 1970, p. 82.

[118] I. R. McNab and F. R. Bennett, "The infrared spectrum of HCl_2^+ and its isotopomers," *Chem. Phys. Lett.,* vol. 251, pp. 405-412, 1996.

[119] A. P. Thorne, "Spectrophysics," 2nd ed London: Chapman and Hall, 1988, p. 293.

[120] F. E. Smith, PhD Thesis, Physics, University of Newcastle upon Tyne, Newcastle upon Tyne, 2000.

[121] R. J. Le Roy, "LEVEL: A Computer Program for Solving the Radial Schrödinger Equation for Bound and Quasibound Levels.," University of Waterloo, Waterloo, Ontario, Chemical Physics Research Report CP-642, 2000.

[122] P. R. Bunker and P. Jensen, "Molecular Symmetry and Spectroscopy," P. B. Cavers, Ed., 2 ed Ottawa: NRC Research Press, 1998, pp. 455-457, 473-474, 637-641.

[123] I. V. Gerdova, "Intensities of electric dipole forbidden rotation and rotation–vibration transitions in D_2^+," *Chemical Physics Letters,* vol. 385, pp. 456-461, 2004.

[124] D. L. Huestis, "Atomic Molecular and Optical Physics Handbook," G. W. F. Drake, Ed., ed New York: American Institute of Physics, 1996, p. 394.

[125] Y. C. Minh, J. E. Dickens, W. M. Irvine, and D. McGonagle, "Measurements of the $H_2{}^{13}CO$ ortho/para ratio in cold dark molecular clouds," *Astronomy and Astrophysics,* vol. 298, pp. 213-218, 1995.

[126] G. Herzberg, "Molecular Spectra and Molecular Structure Volume 1 - Spectra of Diatomic Molecules." vol. 1, 2 ed Malabar, Florida: Krieger, 1989, p. 139.

[127] L. Farkas, *Ergebnisse d exakten Naturwissenschaften,* vol. 12, p. 163, 1933.

[128] M. Broyer, J. Vigue, and J. C. Lehmann, "Effective hyperfine Hamiltonian in homonuclear diatomic-molecules - application to b-state of molecular-iodine," *Journal De Physique,* vol. 39, pp. 591-609, 1978.

[129] J. C. Raich and R. H. Good, "Ortho-para transition in molecular hydrogen," *Astrophys. J.,* vol. 139, p. 1004, 1964.

[130] I. Ozier, P.-n. Yi, A. Khosla, and N. Ramsey, "Direct Observation of Ortho-Para Transitions in Methane," *Physical Review Letters,* vol. 24, pp. 642-646, 1970.

[131] P. R. Bunker and P. E. R. Jensen, "Spherical top molecules and the molecular symmetry group," *Molecular Physics,* vol. 97, pp. 255-264, 1999.

[132] J. Bordé, C. Bordé, C. Salomon, A. Van Lerberghe, M. Ouhayoun, and C. Cantrell, "Breakdown of the Point-Group Symmetry of Vibration-Rotation States and Optical Observation of Ground-State Octahedral Splittings of $^{32}SF_6$ Using Saturation Spectroscopy," *Physical Review Letters,* vol. 45, pp. 14-17, 1980.

[133] J. Pique, F. Hartmann, R. Bacis, S. Churassy, and J. Koffend, "Hyperfine-Induced Ungerade-Gerade Symmetry Breaking in a Homonuclear Diatomic Molecule near a Dissociation Limit: $^{127}I_2$ at the $^2P_{3/2}$-$^2P_{1/2}$ Limit," *Physical Review Letters,* vol. 52, pp. 267-270, 1984.

[134] M. Broyer, H. Weickenmeier, U. Diemer, and W. Demtröder, "Hyperfine interaction between the singlet and triplet ground states of Cs_2, a textbook example of gerade-ungerade symmetry breaking," *Chem. Phys. Lett.,* vol. 124, pp. 470-477, 1986.

[135] P. L. Chapovsky and L. J. F. Hermans, "Nuclear spin conversion in polyatomic molecules," *Annual Review of Physical Chemistry,* vol. 50, p. 315, 1999.

[136] R. E. Moss, *unpublished work*.

[137] P. R. Bunker and P. Jensen, "Molecular Symmetry and Spectroscopy," P. B. Cavers, Ed., 2 ed Ottawa: NRC Research Press, 1998c, p. 62.

[138] J. P. Pique, F. Hartmann, S. Churassy, and R. Bacis, "Hyperfine interactions in homonuclear diatomic-molecules and u-g perturbations 1. Theory," *Journal De Physique,* vol. 47, pp. 1909-1916, Nov 1986.

[139] P. R. Bunker and P. Jensen, "Molecular Symmetry and Spectroscopy," P. B. Cavers, Ed., 2 ed Ottawa: NRC Research Press, 1998b, p. 23.

[140] P. R. Bunker and P. Jensen, "Molecular Symmetry and Spectroscopy," P. B. Cavers, Ed., 2 ed Ottawa: NRC Research Press, 1998d, p. 683.

[141] A. Dalgarno, T. N. L. Patterson, and W. B. Somerville, "The Hyperfine Structure of the Hydrogen Molecular Ion," *Proceedings of the Royal Society of London. Series A, Mathematical and PhysicalSciences,,* vol. 259, pp. 100-109, 1960.

[142] R. A. Kennedy, *unpublished*.

[143] J. K. G. Watson, *private communication to I. R. McNab*.

[144] R. S. Mulliken, "Intensities of Electronic Transitions in Molecular Spectra II. Charge-Transfer Spectra," *The Journal of Chemical Physics,* vol. 7, p. 20, 1939.

[145] "NIST Chemistry WebBook, NIST Standard Reference Database Number 101," in *Computational Chemistry Comparison and Benchmark DataBase*, R. D. Johnson III, Ed., Release 15b, August 2011 ed Gaithersburg MD: National Institute of Standards and Technology, 2011.

[146] R. J. Le Roy, "Diatom potential curves and transition moment functions from continuum absorption coefficients: Br_2," *The Journal of Chemical Physics,* vol. 65, p. 1485, 1976.

[147] R. J. Le Roy, "Bound → continuum intensities — A computer program for calculating absorption coefficients, emission intensities or (golden rule) predissociation rates," *Computer Physics Communications,* vol. 52, pp. 383-395, 1989.

[148] R. J. Le Roy, "BCONT: A Computer Program for Calculating Bound→Continuum Transition Intensities for Diatomic Molecules," University of Waterloo, Waterloo, Ontario, Chemical Physics Research Report CP-329, 1988.

[149] C. D. E. Systems, *Waveguide Component Specifications and Design Handbook*, #7 ed. Exeter, NH, USA: Cobham Defense, 2011.

[150] J. A. Seeger, *Microwave Theory, Components and Devices*. New Jersey: Prentice Hall, 1986.

[151] J. C. Owrutsky, E. R. Keim, J. V. Coe, and R. J. Saykally, "Absolute IR Intensities of the v1 Bands of HN_2^+ and HCO^+ Determined by Direct Laser Absorption Spectroscopy in Fast Ion Beams," *J. Phys. Chem.,* vol. 93, p. 5960, 1989.

[152] P. J. Jewsbury, T. Ridley, K. P. Lawley, and R. J. Donovan, "Parity Mixing in the Valence States of I_2 Probed by Optical-Optical Double-Resonance Excitation of Ion-Pair: Characterization of a New Ion-Pair State, $H1_u(^3P_1)$, and a Valence State, $c1_g$," *Journal of Molecular Spectroscopy,* vol. 157, pp. 33-49, 1993.

[153] L. Li, S. Kasahara, M. H. Kabir, Y. Sahashi, M. Baba, and H. Katô, "Nonadiabatic g–u mixing of the $F\,^1\Sigma_g^+$ and $2^1\Sigma_u^+$ states of ^{6}Li ^{7}Li," *The Journal of Chemical Physics,* vol. 114, p. 10805, 2001.

[154] Y. Nakano, H. Ukeguchi, and T. Ishiwata, "Observation and analysis of the $2_g(^1D)$ ion-pair state of I_2: the g/u mixing between the $1_u(^1D)$ and $2_g(^1D)$ states," *J Chem Phys,* vol. 121, p. 1397, 2004.

[155] A. M. Sjodin, T. Ridley, K. P. Lawley, and R. J. Donovan, "Electric-field-induced g/u mixing of the $E0_g^+(^3P_2)$ and $D0_u^+(^3P_2)$ ion-pair states of jet-cooled I_2 observed using optical triple resonance," *J Chem Phys,* vol. 120, pp. 2740-5, Feb 8 2004.

[156] C. D. Hamley, E. M. Bookjans, G. Behin-Aein, P. Ahmadi, and M. S. Chapman, "Photoassociation spectroscopy of a spin-1 Bose-Einstein condensate," *Physical Review A,* vol. 79, p. 023401, 2009.

[157] J. Shen, A. Borodin, M. Hansen, and S. Schiller, "Observation of a rotational transition of trapped and sympathetically cooled molecular ions," *Physical Review A,* vol. 85, 2012.

[158] H. Saßmannshausen, F. Merkt, and J. Deiglmayr, "High-resolution spectroscopy of Rydberg states in an ultracold cesium gas," *Physical Review A,* vol. 87, 2013.

[159] R. Wynar, R. S. Freeland, D. J. Han, C. Ryu, and D. J. Heinzen, "Molecules in a Bose-Einstein Condensate," *Science,* vol. 287, p. 1016, 2000.

[160] Y. Saito, *private communication to I. R. McNab*, 2001.

[161] I. Mills, *Quantitites, Units and Symbols in Physical Chemistry*, 1 ed. Oxford: Blackwell Scientific Publications, 1988.

[162] G. Hunter and M. Kuriyan, "Proton Collisions with Hydrogen Atoms at Low Energies: Quantum Theory and Integrated Cross-Sections," *Proceedings of the Royal Society of London. Series A, Mathematical and Physical Sciences,* vol. 353, p. 575, 1977.

[163] P. S. Krstic and D. R. Schultz, "Elastic scattering and charge transfer in slow collisions: isotopes of H and H^+ colliding with isotopes of H and with He," *J. Phys. B: At. Mol. Opt. Phys.,* vol. 32, p. 3485, 1999.

[164] J. Weiner, V. S. Bagnato, S. Zilio, and P. S. Julienne, "Experiments and theory in cold and ultracold collisions," *Reviews of Modern Physics,* vol. 71, p. 1, 1999.

[165] T. C. Killian, S. Kulin, S. D. Bergeson, L. A. Orozco, C. Orzel, and S. L. Rolston, "Creation of an Ultracold Neutral Plasma," *Physical Review Letters,* vol. 83, p. 4776, 1999.

[166] T. C. Killian, M. J. Lim, S. Kulin, R. Dumke, S. D. Bergeson, and S. L. Rolston, "Formation of Rydberg Atoms in an Expanding Ultracold Neutral Plasma," *Physical Review Letters,* vol. 86, p. 3759, 2001.

[167] R. Côté and A. Dalgarno, "Ultracold atom-ion collisions," *Physical Review A,* vol. 62, p. 012709, 2000.

[168] A. P. Mosk, M. W. Reynolds, T. W. Hijmans, and J. T. M. Walraven, "Photoassociation of Spin-Polarized Hydrogen," *Physical Review Letters,* vol. 82, p. 307, 1999.

[169] P. E. Siska, "Cold and ultracold ion-neutral inelastic collisions: Spin–orbit relaxation in $He+Ne^+$," *The Journal of Chemical Physics,* vol. 115, p. 4527, 2001.

[170] L. Lodi and J. Tennyson, "A line list of allowed and forbidden rotational transition intensities for water," *Journal of Quantitative Spectroscopy and Radiative Transfer,* vol. 109, p. 1219, 2008.

[171] S. G. Cox and I. R. McNab, "Zeeman measurements of a hyperfine resolved infrared transition of $D^{35}Cl_2^+$," *J. Phys. B: At. Mol. Opt. Phys.,* vol. 35, p. L237, 2002.

[172] J. S. Campbell and W. V. Houston, "A new determination of e/m from the Zeeman effect," *Phys. Rev.,* vol. 39, p. 601, 1932.

[173] A. Carrington, C. H. Pyne, and P. J. Knowles, "Microwave electronic spectrum of the He_2^+ ion," *The Journal of Chemical Physics,* vol. 102, p. 5979, 1995.

[174] W. Cencek, *private communication to I. R. McNab*, 2003.

[175] F. Kemp, "Spectroscopy of Molecular Ions (Including Dications)," PhD, Physics, University of Newcastle upon Tyne, 2004.

[176] N. Yu and W. H. Wing, "Observation of the infrared spectrum of the helium molecular ion $(^3He\ ^4He)^+$," *Physical Review Letters,* vol. 59, p. 2055, 1987.

[177] M. R. Viant, "The investigation of long-range atom-ion interactions by microwave and millimeter wave spectroscopy.," PhD, Chemical Physics, University of Southampton, 1994.

[178] F. X. Gadea and I. Paidarová, "Ab initio calculations for Ar_2^+, He_2^+ and He_3^+, of interest for the modelling of ionic rare-gas clusters," *Chemical Physics,* vol. 209, p. 281, 1996.

[179] C. Johann, S. H. Patil, K. T. Tang, and J. P. Toennies, "Asymptotic theory for the $^2\sum_u$ Van der Waals potentials of alkali dimer cations," *Chemical Physics Letters,* vol. 295, p. 158, 1998.

[180] F. Bielsa, A. Douillet, T. Valenzuela, J. P. Karr, and L. Hilico, "Narrow-line phase-locked quantum cascade laser in the 9.2 μm range," *Optics Letters,* vol. 32, pp. 1641-1643, 2007.

[181] D. Bakalov, V. I. Korobov, and S. Schiller, "Magnetic field effects in the transitions of the HD^+molecular ion and precision spectroscopy," *Journal of Physics B: Atomic, Molecular and Optical Physics,* vol. 44, p. 025003, 2011.